NTIS HC $8.00

CALIFORNIA INSTITUTE OF TECHNOLOGY

DANIEL AND FLORENCE GUGGENHEIM JET PROPULSION CENTER

(NASA-CR-129198) SOME CONSIDERATIONS IN THE COMBUSTION OF AP/COMPOSITE PROPELLANTS
R.N. Kumar (California Inst. of Tech.)
Aug. 1972 120 p CSCL 21B G3/33
N73-11973
Unclas
47521

SOME CONSIDERATIONS IN THE COMBUSTION OF AP/COMPOSITE PROPELLANTS

R. N. Kumar

This work was performed for the Jet Propulsion Laboratory, California Institute of Technology, sponsored by the National Aeronautics and Space Administration under Contract NAS7-100.

Reproduced by
NATIONAL TECHNICAL
INFORMATION SERVICE
US Department of Commerce
Springfield, VA. 22151

August 1972

SOME CONSIDERATIONS IN THE COMBUSTION OF AP/COMPOSITE PROPELLANTS

by

R. N. Kumar

This work was supported by NASA under the Jet Propulsion Laboratory
Contract NAS 7-100

JPL/Caltech W.O. 61496

Approved: F. E. C. Culick
F. E. C. Culick

August 1972

Daniel and Florence Guggenheim Jet Propulsion Center
California Institute of Technology
Pasadena, California

ABSTRACT

This report presents some theoretical studies on the time-independent and oscillatory combustion of nonmetallized AP/composite propellants. The study has for its aim a coherent and unified interpretation of the voluminous data available from experiments related to propellant combustion. Three fundamental hypotheses are introduced: the extent of propellant degradation at the vaporization step has to be specified through a scientific criterion; the condensed-phase degradation reaction of ammonium perchlorate to a vaporizable state is the overall rate-limiting step; gas-phase combustion rate is controlled by the mixing rate of fuel and oxidizer vapors. In the treatment of oscillatory combustion, the assumption of quasi-steady fluctuations in the gas phase is used to supplement these hypotheses. In comparison with experimental data, this study predicts several of the observations including a few that have remained inconsistent with previous theoretical results.

As a prelude to propellant combustion studies, the behavior of AP is pursued in some detail. Theoretical predictions of the linear regression rates of AP, including explicitly the condensed-phase Arrhenius degradation term, are seen to match well with experimental hot plate data. Based on available experimental evidence of the existence of a melt layer on the surface of self-deflagrating AP, it is assumed that pressure-dependent condensed-phase degradation in the melt layer controls the deflagration rate. The results obtained, by specifying the extent of degradation (at the vaporization step) through the vapor pressure equilibrium criterion, are found to predict the linear regression rate, the pressure index n, and the initial temperature sensitivity close to experimental data. The pressure index n is revealed as a composite quantity incorporating the component effects of condensed-phase degradation rate sensitivity to pressure and the vapor pressure effect.

The analysis is generalized to the combustion of composite propellants, where the site of the rate-limiting degradation reaction of AP is assumed to be a thin layer on the AP particles in the propellant. The case of surface reactions in a melt layer augmenting subsurface reactions is also considered with a view to include propellants with readily melting binders. The temperature at the wall (i.e., the interface plane between the condensed phase and the vapor phase) is required to be specified through proper matching with the gas-phase

energetics. Although a complete solution to the gas phase has remained elusive because of our lack of understanding of the non-laminar fluid dynamics encountered, two plausible models are analyzed: constant wall temperature, and uniform combustion in the gas phase. It is shown that either of these models, used in conjunction with the condensed phase analysis, yields results (linear regression rate versus pressure, flame standoff distance, etc.) close to experimental trends, thereby de-emphasizing the importance of gas-phase details in the combustion of propellants.

The response function of composite propellants, including explicitly the pressure-dependent degradation term in the condensed phase, is theoretically derived. The method of inner and outer expansions with the reduced activation temperature parameter $\theta_a \chi \equiv (E/\mathcal{R}\bar{T}_w) \cdot (1 - T_o/\bar{T}_w)$ as the singular perturbation parameter has been applied to the problem of oscillatory combustion. It is seen that greater difficulties are associated with the specification of the boundary conditions than with the actual solution procedure. Two physical situations are considered. In one case, the condensed-phase reactions are treated as taking place wholly in the subsurface region; in the other, surface reactions in a melt layer augment the subsurface degradation reactions. In both cases, the theoretical expression for the response function has the wall temperature fluctuation (T'_w) as an unknown quantity. Two models are considered for the gas phase in order to determine the complex amplitude of the wall temperature fluctuations. In one model, the "flame" temperature fluctuations are related to chamber pressure fluctuations through the isentropic relation. (It is shown that this assumption, however, does <u>not</u> lead to isentropic fluctuations at the <u>wall.</u>) In the other model, the gas phase combustion processes are assumed to be uniform even during oscillatory combustion. The response functions, so derived, exhibit dependence on mean chamber pressure; strongly so with the model of adiabatic fluctuations in the gas phase and weakly for the case of uniform combustion. For the models of no melt layer and non-oscillating melt layers, the theoretical response functions are seen to approach large values at low frequencies (as observed in some experiments) with the adiabatic assumption for the gas phase fluctuations. The proper limit (i.e., the steady-state pressure index n) is, however, reached at zero frequency when it is recognized that very slow changes in the gas phase are isothermal

and not adiabatic. It is also seen that a "zero-n" propellant can exhibit fairly strong instability behavior.

Thus, it is seen that many of the apparently diverse experimental observations are all consistent within the framework of the present theoretical developments. It is, therefore, concluded that the results obtained so far are sufficiently encouraging to warrant further research on similar lines.

TABLE OF CONTENTS

TABLE OF CONTENTS (cont'd.)

NOMENCLATURE

A	constant in the uniform combustion law, equation (72) [gm. cm.$^{-3}$ sec.$^{-1}$ atm.$^{-1}$]
a	mean size of the oxidizer particles in the composite propellant [cm.]
B	pre-exponential factor in the Arrhenius law for thermal degradation [sec.$^{-1}$]
C_i	constants (with i = 1, 2, 3, . . .) used as shorthand notations to simplify the algebra [dimensionless]
C_{Li}	constants (with i = 1, 2, 3, . . .) used as shorthand notations to simplify the algebra in the treatment of liquid layers on composite propellants [dimensionless]
c	specific heat [cal. gm.$^{-1}$ ^{o}C^{-1}]
D	heat of degradation of the solid, i. e., heat required to convert one gram of the polymer or crystal into one gram of the individual repeating units [cal. gm.$^{-1}$]
$\mathcal{D}$	mutual diffusion coefficient for the oxidizer and fuel gases [cm.^{2} sec.$^{-1}$]
E	activation energy for thermal degradation [cal. mole^{-1}]
FSV	statistical mean fragment size vaporizing [dimensionless]
FSSL	statistical mean fragment size at the solid-liquid interface [dimensionless]
h	normalized heat of degradation [dimensionless]
k	coefficient of thermal conductivity [cal. cm.$^{-1}$ sec.$^{-1}$ ^{o}C^{-1}]
L	thickness of the surface melt layer in composite propellant combustion [cm.]
ℓ	thickness of the surface melt layer in the self-deflagration of AP single crystals [cm.]
M	molecular weight [gm. (gm. mole)$^{-1}$]

NOMENCLATURE (cont'd.)

m	mass flux of combustion gases [gm. cm.$^{-2}$ sec.$^{-1}$]
m_i	mole fraction of species i [dimensionless]
$\dot{m}'''$	gas phase combustion rate during uniform combustion [gm. cm.$^{-3}$ sec.$^{-1}$]
N	fractional number of backbone bonds referred to the number in the undegraded state [dimensionless]
n	empirical index of pressure in the steady burning rate law for propellants [dimensionless]
P	pressure [atm.]
p	normalized temperature gradient [dimensionless]
Q	heat released by combustion gases upon complete combustion [cal. gm.$^{-1}$]
R	Reynolds number for the gas phase processes [dimensionless]
R_i	constants (with i = 1, 2, 3, . . .) used for shorthand notations [dimensionless]
$\mathfrak{R}$	universal gas constant [cal. mole^{-1} ^{o}C^{-1}]
$\mathfrak{R}$	complex (pressure) response function [dimensionless]
r	linear regression rate [cm. sec.$^{-1}$]
S	normalized heat release rate in the gas phase (defined in equation 73) [dimensionless]
T	temperature [^{o}K]
t	time coordinate [sec.]
U_i	shorthand notations (with i = 1, 2, 3, . . .) used in the section on uniform combustion model for the gas phase [dimensionless]
u	gas (mass flow) velocity above the burning propellant [cm. sec.$^{-1}$]
v	volume fraction of oxidizer in a composite propellant [dimensionless]

NOMENCLATURE (cont'd.)

W	normalized temperature difference between the flame zone and the wall [dimensionless]
X, x	distance coordinate [cm.]
y	normalized distance coordinate [dimensionless]
Z_i	shorthand notations (with $i = 1, 2$) used in the treatment of oscillatory combustion [dimensionless]
α	empirical constant in the FSV rule [atm.$^{\beta}$]
β	empirical index of pressure in the FSV rule [dimensionless]
γ	ratio of specific heats of combustion gases [dimensionless]
δ	empirical constant in the FSV equation [$^{o}K^{-1}$]
ϵ	a small parameter used in the expansions; any first order quantity; $r'/\overline{r}$ [dimensionless]
ζ	normalized flame standoff distance [dimensionless]
η	normalized stretched temperature coordinate in the "inner" region in the asymptotic analysis of degradation reactions [dimensionless
θ_a	activation energy parameter, $\equiv E/\mathcal{R}T_w$ [dimensionless]
$\varkappa$	thermal diffusivity [cm.^{2} sec.$^{-1}$]
Λ_g	normalized mass burning rate in the gas phase [dimensionless]
λ	normalized time-independent regression rate eigenvalue [dimensionless]
$\tilde{\lambda}$	normalized time-dependent regression rate eigenvalue [dimensionless]
λ_1	complex root of the heat transfer equation [dimensionless]
$\tilde{\mu}$	normalized amplitude of pressure fluctuations [dimensionless]
ξ	normalized "inner" dependent variable in the asymptotic analysis of degradation reactions [dimensionless]

NOMENCLATURE (cont'd.)

ρ	density [gm. cm.$^{-3}$]
τ	normalized temperature [dimensionless]
Ψ	thickness of the surface melt layer on the oxidizer crystals in a composite propellant [cm.]
χ	normalized temperature parameter used in solid phase analysis, $\equiv (T_w - T_o)/T_w$ [dimensionless]
Ω	normalized frequency of fluctuations, $\equiv \omega\kappa/\bar{r}^2$ [dimensionless]
ω	frequency of fluctuations [sec.$^{-1}$]

Subscripts and superscripts

$(\ )_b$	plane of burning, i.e., flame zone
$(\ )_f$	freezing (of chemical reactions) plane in the solid; flame region in the gas
$(\ )_g$	gas
$(\ )_o$	deep solid (ambient) conditions
$(\ )_s$	solid
$(\ )_{SL}$	solid-liquid interface plane
$(\ )_{ss}$	subsurface region
$(\ )_w$	wall plane
$(\ )^o$	outer region in the asymptotic analysis
$\bar{(\ )}$	time-averaged part
$(\ )'$	fluctuating part
$\tilde{(\ )}$	time-dependent quantity
$\hat{(\ )}$	reference quantity

SOME CONSIDERATIONS IN THE COMBUSTION OF AP/COMPOSITE PROPELLANTS

I. INTRODUCTION

Solid propellant rockets are here to stay. It is the wish of researchers in the field to be able to say the same of propellant combustion theories. Continuing development of solid propellant rockets has therefore depended largely on experimental programs which have proved extremely useful so far as the technological application is concerned. However, the lack of quantitative correlations among the vast amount of experimental data has left the predictive design of rockets an unrealized ideal. Many deficiencies in our understanding that are adequately concealed by empiricism when one considers steady combustion are revealed badly when the propellant enters unsteady and oscillatory modes of combustion. Since it has not been possible at the present time to accurately predict whether a given propellant would burn in the steady mode or in the unsteady mode in the rocket chamber, the difficulties are easy to comprehend. Even a coherent and unified interpretation of experimental data has remained a challenging problem, so that the few isolated successes of theories have not been above scepticism. Thus, the need is felt for work at the fundamental level in an attempt to identify the core processes common to most, if not all, of the propellants in use. If successful at the primary task of coherently interpreting different experimental phenomena in terms of a few unifying concepts, the study could then work out the details and refinements necessary in the prediction of results of any specific experiment.

In the present work a study is made of ammonium perchlorate-based, non-metallized composite propellants. The objective is to identify the fundamental processes that are likely to be common in a variety of propellants and propellant applications. The motivation for the present work comes from the observation that under normal conditions the rate processes in the gas phase are likely to be much faster than those in the condensed phase. As elaborated on in Section II, the present work differs from those available in the literature in three important aspects. The chemical kinetic degradation reactions in the condensed phase are explicitly included in the analytical treatment. The importance of a scientific criterion in specifying the extent of propellant degradation before vaporization is stressed, and it is shown that the usual arbitrariness is removed by applying the vapor pressure equilibrium criterion at the propellant surface. Lastly, the gas phase chemical reactions are treated as wholly controlled by pressure-independent molecular mixing processes. It is found that the study predicts several of the features observed in AP/propellant combustion.

Although no fundamentally new concept is introduced, some of the thoughts are either relatively new to, or have not all been considered at the same time in, propellant combustion theories. Those aspects of the problem that have already received adequate treatment on similar lines are not pursued here. Also, no attempt is made to review the literature on propellant burning. Not only is the research field very active at the present time, but the literature on the subject is also very extensive, rendering it difficult to cite a few references in the limited space here. Nevertheless, the reader should find useful information on the general subject in the collection by Warren[27], on the work of the Princeton group in Steinz, Stang and Summerfield[11], on the detailed theoretical studies in Williams, Barrère, and Huang[28],

and of the Russian work in Bakhman and Belyaev[29] and Novikov, Pokhil, and Ryazantsev[30]. The monograph[31] by Price and Culick familiarizes the reader with the status of the problem in 1969, which has not changed much since then. After the present study was initiated, it was found that some of the thoughts run parallel to those of Willfred Schmidt, who has also been considering the importance of condensed phase reactions in his recent studies[19-21].

Since AP is a prominent constituent, its behavior by itself is studied in some detail in Section III. The condensed-phase degradation rate obtained from small-sample isothermal data and the fragment size of the AP particles leaving the wall obtained from a vapor pressure criterion are used to predict the overall linear regression rates of AP in different experiments. Very good agreement is found with hot-plate data and with single-crystal deflagration experiments. It is found that the pressure index n is actually a composite quantity incorporating both the effects of pressure-dependent chemical reactions and the vapor pressure effect on the fragment size vaporizing. It is also found that a power law for pressure dependence of regression rate is an approximate representation at best. The actual dependence is non-simple and involves at least one logarithmic variation. The effects of initial temperature variation on the linear regression rate are also predicted and are found to be close to experimental observations.

Time-independent burning of AP composites is studied in Section IV. The study is undertaken in the belief that a thorough understanding of the oscillatory combustion of composite propellants would be difficult in the absence of an understanding of the time-independent burning. Effects of burning rate catalysts and oxidizer particle size are explicitly included. The depolymerization reactions of fuel (binder) are also included. The general problem of gas phase details is formulated and a solution is written in terms of non-

dimensional groups, which are also recognized to be important similarity parameters. A completely self-contained solution to the gas phase has not been possible because of our lack of understanding of the gas phase fluid dynamics above the regressing surface of the propellant. In order to render the solution self-contained, two physical models are considered; constant wall temperature and uniform combustion in the gas phase. It is seen that either of the models can predict results close to experimental trends (both qualitatively and quantitatively). This reinforces the belief that precise details of the gas phase mechanics are not very important in determining the general trends, if the rate-limiting reactions occur in the condensed phase.

Oscillatory combustion of composite propellants is considered in Section V. Employing the method of "inner" and "outer" expansions, linearized analytical solutions are obtained for the response function, including explicitly the Arrhenius reaction rate term in the condensed phase. Two physical situations are considered. In one case, the condensed phase reactions are treated as taking place wholly in the subsurface region; in the other, surface reactions in a melt layer augment the subsurface degradation reactions. In both cases, the theoretical expression for the response function has the complex amplitude of wall temperature fluctuation as an unknown quantity. Two models are considered for the gas phase (treated quasi-statically) in order to determine the complex amplitude of the wall temperature fluctuations. In one model, the "flame" temperature fluctuations are related to chamber pressure fluctuations through the isentropic relation. (It is shown that this assumption, however, does not lead to isentropic fluctuations <u>at the wall.</u>) In the other model, the gas phase combustion processes are assumed to be uniform even during oscillatory combustion. The response functions exhibit dependence on mean

chamber pressure; strongly so with the model of adiabatic fluctuations in the gas phase and weakly for the case of uniform combustion. It is also seen that a "zero-n" propellant can exhibit fairly strong instability behavior.

The present study is not complete. However, the results obtained so far are thought to be encouraging. The basic conclusion at this stage is that it is possible to understand a variety of superficially different experimental phenomena within the broad framework of a few unifying concepts.

II. QUALITATIVE CONSIDERATIONS

2.1 Introduction

The fundamental physical structure of the present work is discussed in this section. It is also the aim here to anticipate, on physical grounds, the analytical results of subsequent sections. The models of condensed phase reactions, the concept of fragment size vaporizing (FSV), the gas phase processes, and a brief discussion on the numerical values of the thermophysical and thermochemical constants that are needed later are introduced separately.

2.2 Condensed Phase Details

In an attempt to trace the entire history of the oxidizer (or fuel) from the deep solid state to the product state, the condensed phase details arise in a natural way. Since many composite propellants are heavily loaded with ammonium perchlorate (80 per cent or higher), we study the AP behavior at first. In its unaffected state AP may be looked upon as a large "molecule" made up of the fundamental building blocks $-(NH_4C\ell O_4)-$. While the degradation of AP has been studied in detail[7, 12, 13] and is known to involve the production of ammonia (NH_3) and perchloric acid ($HC\ell O_4$), it is interesting to inquire into AP behavior prior to such a decomposition. It would seem logical to expect that in the sequence of decomposition reactions the first stage would be the scission of the weak bonds between the neighboring $-(NH_4C\ell O_4)-$ units, particularly when the rate of heating is very high, as in propellant applications. The large crystals degrade into smaller groups of $-(NH_4C\ell O_4)-$ and we ask ourselves whether the degradation of AP completely into single molecules of ($NH_4C\ell O_4$) and the decomposition to NH_3 and $HC\ell O_4$ are prerequisites for the oxidizer to leave the condensed

phase and enter the vapor phase. It would seem unlikely that such indeed is the case. Under certain conditions, pure AP has been known to sublime and leave the surface as pure AP.[14] In one extreme case, at very low (subatmospheric) pressures, macroscopic particles of AP have been observed[15] to get ejected from the surface (of a burning composite propellant) into the vapor phase. These observations suggest that in order to specify, as a function of chamber pressure and wall temperature, the actual state of the oxidizer leaving the surface, a scientific criterion is necessary. The problem then is almost identical with that associated with the combustion of any solid, like a polymer, for example. Specification of the size of AP at the surface requiring that the vapor pressure sum of all fragments leaving the surface at the wall temperature equal the chamber pressure appears to be a scientific criterion. This vapor pressure criterion is invoked in the present study.

The fragment size of AP leaving the wall, as a multiple of the fundamental unit $-(NH_4C\ell O_4)-$ will be designated the fragment size vaporizing, or FSV, for short. For a constant wall temperature, the FSV will be very large at low pressures and small at high pressures. At sufficiently high pressures, the fragment size specified by the vapor pressure criterion gets smaller than the fundamental unit ($NH_4C\ell O_4$). Decomposition into smaller molecules is anticipated in such cases. In any attempt to experimentally determine the actual fragment size at the wall, it should be remembered that the entire process of propellant regression is a nonequilibrium one and that rapid quenching of all reactions is necessary, immediately after the species enter the vapor phase, in order to study the species leaving the surface. That is, reactions (degradation, decomposition) in the vapor phase

could mask the identity of the species actually leaving the wall surface.

At the surface of a burning composite propellant, both fuel and oxidizer species are present. Thus, the necessity for a proper mixing rule arises in the generalization of the vapor pressure criterion to multicomponent equilibria. A detailed study would consider the energetics as well and include the relative strengths of bonds between the neighboring molecules in the fuel and oxidizer in the propellant, the mole fractions of fuel and oxidizer and separate wall temperatures, if the "two-temperature" concept[16] is a physical reality. The nature of the present work does not require a sophisticated treatment of these effects. A logical mixing rule in Section IV handles the problem adequately. For a thorough discussion of the vapor pressure criterion, the reader is referred to ref. 17.

In order to determine the numerical value of the FSV as a function of specified conditions, a study has been made of the vapor pressure data of hydrocarbons and a rule has been evolved in Appendix B to predict the FSV. The approximate nature of extrapolations to AP and polymer from hydrocarbon data is recognized, but it is felt that for a simple physical quantity like the vapor pressure, the chemical nature of the molecules is not crucially important. As a matter of fact, the experimental vapor pressures of hexane and methylmethacrylate monomer (identical molecular weights, 100) are very close over a range of temperature[1].

A non-integer value of FSV predicted by equation B-2 is to be understood as an average over all fragment sizes and not as the presence of breakdown products from the fundamental repeating units.

From the above discussion, there emerge the following three considerations which form the backbone of the rest of this study.

(i) The fragment size of vaporizing AP can be specified through vapor pressure equilibrium criterion.

(ii) The degradation of macroscopic crystals of AP into vaporizable fragments of AP is the fundamental rate-limiting reaction of interest.

(iii) Assuming that the AP degradation is brought about by reactive species, the degradation rate is taken as directly proportional to pressure.

It is seen that the above three considerations not only remove considerable arbitrariness in propellant combustion theory but also lead to results that are close to experimental trends both qualitatively and quantitatively.

2.3 Gas Phase Details

It is useful to have an order-of-magnitude estimate of the characteristic scales in the physical problem. Chemical kinetic rates in the gas phase may be inferred through measurements of aerodynamic flame speeds in experiments where the speed is known to be controlled by the chemical kinetic reaction rates, such as premixed laminar flames. At atmospheric pressures, typically the aerodynamic flame speeds of air/hydrocarbon mixtures are like 100 cm/sec. The characteristic length scale, which is the flame thickness, is of the order of 100μ. Hence, the characteristic chemical reaction time is like 10^{-4} sec. At high pressures, as in propellant applications, we expect the reaction time to be much smaller. If the reaction is bimolecular, the characteristic time at 10 atm. would be 10^{-5} sec.

The characteristic transport/mixing time in the burning of a composite propellant is at most of the order of the ratio of combustion zone standoff distance to the mean velocity of the gases leaving the propellant surface. Employing typical numbers we arrive at a time like 10^{-4} sec. for the mixing process. While these estimates are not conclusive, the general trend is in favor of transport/mixing control and not of chemical kinetic control. Another factor that greatly accelerates the chemical kinetic rates in propellants is that the oxidizers used are much more powerful than air. Perhaps the most direct support to the argument is provided by the observation that the actual high reaction-rate zone occupies a small fraction of the total "flame" standoff distance at conventional pressures.

Thus, we look for pressure-dependent mechanisms other than gas-phase chemical kinetics, leading to the examination of condensed phase details mentioned in II. 2. However, we do need a solution to the gas phase to completely specify the regression rate.

The gas phase details have received a great deal of attention over the years. Several models have been presented. Actually, when once the assumption is made that the gas phase is not rate controlling, any model that incorporates the essential heat transfer details will suffice. This is because the role of the gas phase above the burning propellant degenerates from an active control of general propellant behavior to one of supplying boundary conditions on the solid phase details.

The reactants burn in a non-premixed combustion zone in the gas phase except in the following two cases.

(i) Gas phase chemical-kinetic rates become very slow, because of very low pressures or special ingredients, so that molecular

mixing processes take the gases to a premixed state before combustion.

(ii) A thorough mixing of fuel and oxidizer takes place in a surface layer on the propellant before they enter the vapor phase.[18]

The details of the gas phase, as required in the solid phase analysis, are developed in Section IV. It is seen that the simplest model of the combustion zone (treated like a "black box") is adequate for our purposes. The question of laminar versus turbulent nature of the fluid process is discussed. The important parameters are identified. A formal solution is obtained, although a closure has not been possible, mainly because of our lack of understanding of transport and mixing processes in propellant burning.

2.4 Numerical Values of Constants

Although the number of fundamental quantities that are needed in the present study is not large, considerable uncertainty exists in the numerical values of even the few properties that find extensive use. The principal quantities are the thermal diffusivity of the propellant, the pre-exponential factor and the activation energy of the degradation reaction and the heat of degradation. Early in the present study it was decided to use a single set of values consistently through the work.

(i) Thermal Diffusivity, κ. A majority of polymers have a thermal diffusivity around 10^{-3} $cm^2/sec.$, although there are indications that the value decreases considerably at high temperatures. AP is crystalline, and one would expect its thermal conductivity to be much higher than that for an amorphous polymer. For a material like composite propellant grain, we would expect the thermal diffusivity to be between that for the base fuel and that for crystalline AP. The values used here are:

pure polymer base	10^{-3}
normal AP composites with heavy AP loading	1.1×10^{-3}
pure AP	1.5×10^{-3}

Whenever a specific propellant is considered, if the κ for that propellant is available, such a value is used in preference to the above table.

(ii) Fundamental Rate Data for Pure AP. The high temperature (isothermal) degradation values of ref. 7 (page 41) are used. The values of the smallest sample are used for obvious reasons.

$$B = 9.2 \times 10^{7} \text{ sec}^{-1},$$

$$E = 28.9 \text{ k cal/mole.}$$

(iii) Heat of Degradation, D. The heat of degradation is taken as approximately 585 cal/gm for AP.[13] The same value is used for AP-based composites also. It is also taken as endothermic. While the overall pyrolysis of AP may be exothermic, it is possible that the rate-limiting degradation reaction is endothermic. A simple bond-breaking degradation scheme would suggest endothermicity. Besides, the value of the linear regression rate of propellants is theoretically seen to be not a strong function of the heat of degradation (see later). Physically, this is because the bulk thermal sink contribution, namely $c(T_w - T_o)$, far overwhelms the degradation heat term under most conditions.

III. DEGRADATION AND DEFLAGRATION OF AMMONIUM PERCHLORATE

3.1 Postulated Model

The aim of the present section is the theoretical prediction of the linear regression rate of AP as a function of chamber pressure (or other experimentally determined conditions). We examine the model (Section 3.2 within the framework of a one-dimensional picture.

The overall model is depicted in fig. 1. We consider the steady-state degradation of a semi-infinite mass of AP (all transverse gradients zero). In the coordinate system used, the wall surface is held stationary. A plane parallel to the wall surface moves up with time and we follow the changes in this plane as it moves from $x = +\infty$ (deep solid) to $x = 0$ (wall). Its temperature increases from the deep solid value (T_o) to the wall temperature (T_w). The mean fragment size of the AP particles changes from a very large value ($\rightarrow\infty$) at $x = \infty$ to FSV at the wall ($x = 0$).

Following the numerous studies in the field, the degradation of AP is modeled as a first-order Arrhenius reaction. The pre-exponential factor is taken as directly proportional to the pressure in the molten state (see later) and independent of pressure in the solid.

In the analysis to follow, energy balance due to conduction, "convection," and heat of degradation are considered. Diffusion of small fragments through larger ones is neglected. That is, non-random velocities of individual fragments differing appreciably from the mean are not considered. For reasons that will be clear later, the cases of subsurface and surface reactions are treated spearately.

3.2 Analysis of Subsurface Reactions

Although we are interested at present in the steady state only, the full (time-dependent) equations are written down since these are needed later (Section V) in the analysis of oscillatory burning.

Governing Equations:

Energy:

$$k\frac{\partial^2 T}{\partial x^2} + c\rho r\frac{\partial T}{\partial x} - \rho c\frac{\partial T}{\partial t} = D\rho NB\cdot\exp(-E/\Re T) \qquad (1)$$

Bond Conservation:

$$-\frac{dN}{dt} = NB\cdot\exp(-E/\Re T) \qquad (2)$$

Boundary Conditions:

$$x = 0: \qquad T = T_w \;;\; x = \infty \;,\; T = T_o \qquad (3)$$

$$x = 0: \qquad N = N_w = 1 - \frac{1}{FSV} \;;\; x = \infty \;,\; N = 1 \qquad (4)$$

In the above equations, k stands for the coefficient of thermal conductivity (cal/cm. sec ^{o}C), T for absolute temperature (^{o}K), x for the coordinate into the solid (cm), c for the specific heat of the solid (cal/gm. ^{o}C), ρ for the density of the solid (gm/cm^3), t for the time coordinate (sec), D for the heat of degradation of the solid, i. e., heat required to convert one gram of crystalline AP into one gram of individual ($NH_4C\ell O_4$) molecules (cal/gm), N for the fractional number of backbone bonds referred to the number at infinity, B for the pre-exponential factor (sec^{-1}), E for the activation energy of degradation (cal/mole), and $\Re$ for the universal gas constant (cal/mole^{o}C). When the initial number of backbone bonds is very large, it is easy to see that the fractional number of bonds at the wall is essentially (1 - 1/FSV), an approximation that has been used here. (See Appendix B for details of FSV.)

Defining

$$y \equiv c\rho rx/k = rx/\nu$$

and

$$\tau \equiv (T-T_o)/(T_w-T_o)$$

and substituting them into equations (1) and (2), we get (now we consider only the time-independent case):

$$\frac{d^2\tau}{dy^2} + \frac{d\tau}{dy} = \frac{k D\rho NB \exp(-E/\Re T)}{(\rho cr)^2 (T_w-T_o)} \tag{5}$$

and

$$\frac{dN}{d\tau} \cdot \frac{d\tau}{dy} = \frac{kN\rho cB \cdot \exp(-E/\Re T)}{(\rho cr)^2} \quad . \tag{6}$$

The nondimensionalizations,

$$p \equiv d\tau/dy$$

$$h \equiv D/c(T_w-T_o)$$

and

$$\Lambda \equiv kB/\rho cr^2$$

transform equations (5), (6), (3), and (4) to

$$pp' + p = \Lambda hN \exp(-E/\Re T) \tag{7}$$

$$pN' = \Lambda N \exp(-E/\Re T) \tag{8}$$

with

$$\tau = 0 : \; p = 0 \; , \quad N = 1$$

and

$$\tau = 1 : \; p = p_w \; , \quad N = N_w \; ,$$

where a prime denotes $d/d\tau$.

The Value of p_w . At the wall interface, the balance of energy requires

$$\begin{bmatrix}\text{heat supplied into the material}\end{bmatrix} = \begin{bmatrix}\text{heat used in raising the temperature from } T_o \text{ to } T_w\end{bmatrix} + \begin{bmatrix}\text{heat used in backbone bond breaking}\end{bmatrix}$$

$$-k\frac{dT}{dx} = r\rho c(T_w - T_o) + D\rho r/FSV \quad .$$

Within the framework of the model, heats needed for phase changes need not be included explicitly.

In terms of nondimensional variables defined earlier, heat balance at the interface takes the form

$$p_w = -1 - \frac{h}{FSV} \quad . \tag{9}$$

The Value of N_w. We have already seen that (Appendix B)

$$N_w = 1 - \frac{1}{FSV} \quad . \tag{10}$$

Solutions

The close similarity between equations (7) and (8) may be exploited in a manner analogous to treatments of laminar flame propagation in premixed gases. Multiplying equation (8) by h and subtracting the resulting equation from equation (7), we get an equation that can be integrated in closed form, leading (after the use of boundary conditions) to

$$N = (p + \tau + h)/h \quad . \tag{11}$$

Substituting equation (11) into equation (7), we get

$$pp' + p = (h+p+\tau)\Lambda \exp(-E/\Re T) \tag{12}$$

$$\tau = 0 : \; p = 0 \; ; \qquad \tau = 1 : \; p = p_w \tag{13}$$

Thus, we have succeeded in reducing the initial system of third-order differential equations to a single first-order differential equation. The nonlinearity is retained.

Typically, the activation energy E has a value like 30 k cal/mole, while the maximum temperature (which is at the wall) is like 900 - 1000°K. Hence, $E/\Re T$ is at least 10 - 15. This implies that the R.H.S. of equation (12) falls to exponentially small values even at short distances from the wall.

Such a behavior is particularly suited for a matched asymptotic analysis. Essentially, we neglect the reaction term from equation (12) far from the wall and obtain the solution to the resulting linear equation. Next, we consider the region close to the wall where the reaction term is explicitly included but the temperature range of interest is only a first order quantity. That is, expansions in powers of a small parameter are possible in the familiar fashion. We match the solution near the wall region with that away from the wall and in the process determine the regression rate, r. All of the details are available in Appendix A (and can also be inferred from the very similar treatment of oscillatory case presented here in Section V). The end result is

$$\lambda \equiv \frac{\Lambda \exp(-\theta_a)}{\theta_a \chi} = (h+1)\ell n\left\{\frac{FSV}{FSV-1}\right\} - \frac{h}{FSV} \qquad (14)$$

where $\theta_a \equiv E/\Re T_w$ and $\chi \equiv (T_w - T_o)/T_w$.

In terms of dimensional variables,

$$r = \left\{\frac{\kappa B \exp(-\theta_a)}{\theta_a \chi \lambda}\right\}^{\frac{1}{2}} . \qquad (15)$$

Equation (15) represents the desired result which will find extensive applications hereafter.

3.3 Comparison with Experimental Results

Recalling that the derivation in Section 3.2 did not make provision for surface reactions, we should examine data from those experiments where there is little possibility of such surface reactions. The familiar hot-plate experiments seem to come under this category. However, there are indications that a criterion other than the vapor pressure criterion is needed. There is no clearly-defined equilibrium interface between a condensed phase and a vapor phase. It was seen[1] that a constant molecular weight of 900 appears to match experimental data very well for the polymer PMMA. It is possible that a mechanical strength criterion is more applicable for hot-plate experiments. That is, as the material degrades from within the deep solid, a plane is reached where the increasing temperature and decreasing physical strength force the material out of the surface. A molecular weight of 900 corresponds to an FSV like 7 - 8 for AP (fundamental molecular weight 117.5 gm/gm. mole), and a value of 8 is used in the present study. At these high values of FSV, 7 or 8 will not make more than about 7 per cent difference in the final regression rate, an error that is much smaller than the general levels of uncertainty in such experiments.

Presented in fig. 2 are the experimental data points collected by Powling[9] from many different sources. The theoretical prediction of equation (15) is also plotted. Good agreement is evident. The variation of regression rate with surface temperature is extremely well predicted. It is noted that because of the square root factor in equation (15), an overall activation energy of nearly 15 k cal/mole would be inferred by forcing through the hot-plate data an Arrhenius expression. Actually, such curve fit procedures grossly average the fundamental processes. The valid pro-

cedure is to use the isothermal Arrhenius parameters (obtained from experiments on very small samples of AP) in equation (15), as has been done here. As regards the quantitative agreement of equation (15) with experimental data, it is worth remembering that no more than fundamental thermochemical property values were needed for the prediction.

While the validity of the model is borne out by the hot-plate data, several inconsistencies arise when an attempt is made to generalize the above model to other cases -- notably self-deflagration flame-heated AP. The quantitative, and even qualitative, disagreements noted below lead to the developments in Section 3.4.

To examine the simplest case, let us consider first pure crystals of AP. There are clear evidences in the literature that the surface temperature is no more than 900 - 950^{o}K. In fig. 2 we note that at such wall temperatures, a regression rate around 0.1 cm/sec is expected. (Actually r would be less theoretically because the FSV at the high pressures encountered is much smaller than 8, a number that has been used in the prediction presented in fig. 2.) Typical values of r observed in AP self-deflagration flame-heated samples are like 0.5 to 1 cm/sec.[4] Thus, subsurface thermal degradation rate alone cannot account for the high regression rates observed in AP self-deflagration flame-heated samples. Secondly, the wall temperature in pure AP deflagration is known not to vary too much with regression rate. While this point has been the subject of much discussion in the past, perhaps the most carefully performed experiments that were recently made available by Maltzev[5] provide a very direct support. In any case, the near constancy of surface temperature over wide ranges of regression rate suggests that some mechanism that does not depend on

the temperature effect in the Arrhenius reaction term is in operation. It is readily supposed that the pressure-dependent pre-exponential factor is involved.

However, equation (15) predicts a pressure index n of less than 0.5 always (this point will be elaborated on shortly); observed values of n are like 0.7 to 0.8. While it may be possible to account for all of the inconsistencies retaining the subsurface reaction model (thus retaining equation (15)), it would require fairly complicated interrelated variations in the simple parameters. It is shown in Section 3.4 that a very much simpler picture is also capable of accounting for all of the observations.

3.4 Self-Deflagration Flame-Heated Single Crystals of AP

Let us make the simple postulate that surface degradation by reactive species aids subsurface thermal degradation in producing vaporizable fragments and that at high pressures completely overwhelms the subsurface contribution. The direct dependence of the pre-exponential factor on pressure, that was postulated earlier, may lead us, at first sight, to predict the pressure index n to be unity (since the wall temperature is known to be reasonably constant). However, the fragment size (FSV) goes down as the pressure increases at constant wall temperature, and the additional requirement on kinetic degradation rate at the surface keeps the pressure index below unity. We shall make a numerical calculation shortly, but before undertaking such a calculation, it is necessary to consider the physics of heterogeneous reactions in some detail.

We expect the heterogeneous catalytic degradation by reactive species to take place in a very thin (but finite thickness) layer on the surface.

It would seem physical to think of this surface degradation as taking place in a layer where the catalytic species and the AP mixed thoroughly on the microscopic scale. The observation of a "liquid" layer on the surface of deflagrating AP[4] lends credence to such a picture. A question may arise with regard to the rate limiting process. It is easily seen that the diffusion of the catalytic reactive species into the melt layer is a much faster process than the degradation reaction. Eyring notes (see ref. 6) that diffusion in liquids may be looked upon as a "chemical reaction" in which the weak bonds between neighboring molecules are broken by the diffusing species' energy. Such bonds have strengths that are obviously equal to the heat of vaporization of the liquid. The heat of vaporization of many such liquids is of the order of 5 kcal/mole. Usual activation energies of degradation are around 30 kcal/mole. Naturally, diffusion is much faster than degradation.

Thickness of such a liquid layer on a regressing surface is observed[7] to, and can be theoretically shown[8] to, decrease with increasing regression rates at a constant wall temperature.* Finally, at a high enough regression rate, the melt layer may occupy only a very small portion of the surface. (In the ideal, one-dimensional case, the liquid layer disappears completely.) When this happens, the degradation by the reactive species becomes very slow because diffusion through the solid is a much slower process than through a liquid. The process of degradation is now more likely to be completely controlled by subsurface thermal degradation. We thus expect a marked drop in the regression rate after such a point is reached. An exploratory calculation has indicated that the sudden dip observed in the AP regression rate (around 2000 psia) may be due to such a phenomenon.

*Also explained in Appendix C.

Now we are in a position to write the relevant equations.

The linear regression rate may be written

$$r = \begin{pmatrix}\text{degradation rate in the} \\ \text{melt layer of thickness } \ell\end{pmatrix} \div \begin{pmatrix}\text{the number of bonds to} \\ \text{be broken}\end{pmatrix}$$

$$r = \frac{\ell \bar{N} B \cdot \exp(-E/\Re T_w)}{\left\{1 - \frac{1}{FSSL}\right\} - \left\{1 - \frac{1}{FSV}\right\}} \quad . \tag{16}$$

Use has been made of the fact that, at any plane, the fractional number of bonds left is

$$1 - \frac{1}{\text{fragment size at that plane}}$$

and FSSL stands for the mean fragment size at the interface between the solid and the liquid layers.

Consistent with the general kinetics schemes of such reactions, B is taken as $B_o P$, where P is the pressure and B_o is the pressure-independent reference value of the pre-exponential factor.

Below 2000 psi, surface photographs of deflagrating AP crystals[7] suggest considerable activity in the melt layer. Bubbles from below seem to stir the layer. Consistent with this picture, we assume a uniformly mixed layer. The average number of bonds in the layer follows immediately as

$$\bar{N} = \frac{1 - \frac{1}{FSV} + 1 - \frac{1}{FSSL}}{2}$$

$$\bar{N} = 1 - \left(\frac{1}{FSV} + \frac{1}{FSSL}\right) \Big/ 2 \quad . \tag{17}$$

When the surface contribution to degradation rate in the melt layer far overwhelms the subsurface thermal contribution, FSSL is very large compared to FSV. Thus, equations (16) and (17) may be simplified to read

$$r = \ell \bar{N} \cdot FSV \cdot B \cdot \exp(-E/\Re T_w) \tag{18}$$

and

$$\bar{N} = 1 - \tfrac{1}{2} FSV \quad . \tag{19}$$

Combining equations (18) and (19) we get

$$r = \ell(FSV - \tfrac{1}{2})B_o(P/P_o)\exp(-E/\Re T_w) \quad . \tag{20}$$

Predictions of r through equation (20) are compared in fig. 3a for three assumed values of the melt layer thickness ℓ. Experimental data trend is also indicated.

Again we note the extremely reasonable prediction through very simple modeling. A constant value of melt layer thickness (between 5 μ and 8 μ) is seen to match experimental data quantitatively. However, since the melt-layer thickness ℓ decreases with increasing regression rate (increasing pressure) as shown in Appendix C, this agreement should be due to self-compensating effects of slight increase in wall temperature with pressure (see Maltzev[5]) and the decrease in the melt layer thickness.

3.5 Effects of Initial Temperature (T_o) Variation

Equation (15) predicts the steady-state regression rate as a function of the temperature at any plane and the mean size of the fragments at the same plane. Thus, we see through fig. 1b that we can predict the regression rate of single crystals of self-deflagration-flame heated AP if we use T_w and FSSL in eq. (15). (The value of FSSL may be obtained by equating the regression rates in eqs. (15) and (20). This point has been discussed in detail in Section 4, in connection with heterogeneous reactions in composite propellant burning.) Equation (15) predicts the dependence on the initial temperature T_o as $r \propto 1/\sqrt{\chi} \propto [T_w/(T_w - T_o)]^{\frac{1}{2}}$. The 5$\mu$ curve in fig. 3a is plotted in fig. 3b for three different values of T_o. The recent experimental data of Boggs and Zurn[26] are also presented. We note the very close agreement.

IV. TIME-INDEPENDENT BURNING OF COMPOSITE PROPELLANTS

4.1 Introduction

In this section an attempt is made to apply the hypotheses and principal conclusions from the previous sections to the problem of composite propellant burning. We continue to consider only those cases in which the chemical kinetic rates of combustion reactions in the gas phase are far greater than transport and mixing rates; the overall rate-controlling reactions (viz. fundamental degradation of AP) occur in the condensed phase. The concept of fragment size vaporizing (FSV) is generalized to include multicomponent vapor phase/condensed phase equilibrium. That is, the contribution of the binder species to the vapor pressure is explicitly included. In the process, it is required to include the degradation kinetics of the binder as well. Thus, the formulation of the problem is "complete." The influence of burning rate catalysts is examined in the light of the same model used for uncatalyzed propellants. The increased reaction rate in a surface layer accounts for both the increased regression rate and the pressure index n. The effect of oxidizer particle size is studied in the simplest possible manner. In the condensed phase, its effect is introduced as an increased surface area for the degradation of AP. In the gas phase, the effect is anticipated as affecting the spatial extent of the combustion zone, although a quantitative formulation has remained elusive at the present time. The regression rate is predicted (by a slightly modified form of equation 15) as a function of the chamber pressure and the wall temperature. The case of subsurface reactions only and the case of surface reactions augmenting subsurface reactions are treated separately.

In order to render the system self-determined, it is required to specify the wall temperature through gas phase energetics and fluid mechanics. For this purpose, the familiar one-dimensional gas phase model is invoked. Significant dimensionless groups are evolved and the basic relation among them is obtained through a formal solution. In the absence of a thoroughly satisfactory theory for the gas phase details, a study is made of several ways in which the system may be closed. Procedures that have been usually successful in determining functional relations in a physical problem have limited success here. This is because of the extreme inconsistency in the magnitudes of wall-temperature variation effects in the pyrolysis law (strong exponential) and fluid-dynamic heat transfer (weak logarithmic). For the purposes of further calculations here, it is seen that the assumption of constant wall temperature leads to results sufficiently close to reality.

4.2 Rate-Controlling Reactions in the Subsurface Region

We start with the assumption that the rate-controlling reaction (AP degradation) occurs in a thin layer on the surface of AP crystals in the solid. The propellant material is represented as homogeneous for the purposes of heat transfer calculations. That is, a quantity like temperature is assumed to have a meaningful and unambiguous interpretation at any plane. The process of heat conduction is assumed to be adequately represented by Fourier's law with a properly averaged material property of thermal conductivity. The rest of the analysis will be very similar to that for pure AP (Section 3.2) except for a detail noted below.

When we consider the differential element dx in the analysis, and write the reaction rate in that element, we have to properly consider the

actual volume in the differential element in which degradation reactions are taking place. As a first approximation, an unimodal distribution of spherical AP particles in the solid is assumed. The diameter of AP particles is a . If the reactions take place in a layer of thickness ψ on the surface of AP particles, the volume of AP undergoing degradation reaction per particle is $\pi a^2 \psi$. The physical volume of an AP particle is $\pi a^3/6$. If v is the volume fraction of AP loading in the propellant, the volume fraction of AP undergoing degradation is

$$\frac{6\psi v}{a},$$

so that the reaction rate in the layer of thickness dx is modified by this factor. We may now absorb this factor into an "effective" pre-exponential factor in the reaction term

$$B_{eff} = B \cdot \left(\frac{6\psi v}{a}\right) . \tag{21}$$

Recognizing that the rest of the analysis is identical with that for a homogeneous solid, we substitute equation (21) into equation (15) and obtain

$$r = \left\{\left(\frac{6\psi v}{a}\right) \frac{\varkappa B \cdot \exp(-E/RT_w)}{(E/RT_w)\chi \cdot \lambda}\right\}^{\frac{1}{2}} . \tag{22}$$

It is worth remembering that the coefficient B is directly proportional to pressure. The value of the interfacial layer thickness ψ has to be specified from considerations external to the analysis. At this stage we leave it as a parameter. Given a valid prediction method for the fragment size vaporizing (FSV) for the composite propellant, equation (22) may be evaluated at any desired experimentally-determined condition.

Fragment Size Vaporizing. The vapor pressure criterion is directly applicable, irrespective of the nature of the vapor species. That is, given

the chamber pressure and the wall temperature, the rule in Appendix B may be used to predict the FSV as in other cases. It is only when one asks for the value of the wall value of AP fragment size in the burning composite propellant that careful interpretation becomes necessary. The statistical mean fragment size has to include averaging over the binder species also.

If m_1 gms. of binder (of mean molecular weight $M_1 \cdot FSV_1$) and m_2 gms. of AP fragments (of mean molecular weight $117.5 \times FSV_2$) are present in the vapor phase at the wall, the mean molecular weight is

$$M = (m_1+m_2) \Big/ \left(\frac{m_1}{M_1 \cdot FSV_1} + \frac{m_2}{117.5 \times FSV_2} \right) . \qquad (23)$$

Under the basic assumption of a plane wall surface (i. e., uniform consumption rate of fuel and oxidizer), the weights m_1 and m_2 are fixed by the initial mixture ratio in propellant formulation.

The assumption of uniform regression rate also furnishes another relation between FSV_1 (fuel) and FSV_2 (AP). The regression rate for the binder alone has to equal the regression rate for AP alone (and both have to equal the regression rate for the propellant). The regression rate of binder alone has been the subject of an extensive study in the past[1,8] and is predicted by eq. (15) if the thermochemical constants used in equation (15) are those of the binder material, including the binder fragment size vaporizing at the wall.

That is,

$$r_{AP} = r_{binder} \qquad (24)$$

is the equation that removes the arbitrariness in the values of M_1 and M_2.

For a typical binder (CTPB) and typical numerical values of composite propellant characteristics, the predictions are presented in fig. 4.

4.3 Joint Rate Control by Subsurface and Surface Reactions

There are many cases of practical interest where the assumption of

subsurface reactions alone is insufficient to account for all of the observations. It is suggested that under certain circumstances surface reactions in a thin layer augment subsurface reactions. It is found that many of the experimental observations can be coherently interpreted.

The physical model is shown in fig. 1c. After the material reaches the plane SL in its travel from the deep solid region (∞) to the surface, the binder and the oxidizer mix thoroughly in a melt layer of thickness L. This well-stirred surface layer is at a constant temperature T_w. In case the propellant has burning rate catalysts added in it, the catalyst is taken as inactive in the subsurface region (below the plane SL) and active in the surface layer. Such a model is presented on physical grounds. The catalyst for its action has to mix well at the microscopic level, a process that is difficult to visualize in the solid, but seems natural in the melt layer.

Equation (22) is directly applicable at the solid-liquid interface plane SL. We have to use the value of the AP fragment size FSSL in the expression for the non-dimensional eigenvalue λ. However, for a quantitative determination of the value of FSSL we need another equation relating FSSL to the regression rate. We note that the regression rate determined by the melt layer reactions (i. e., without involving any detail below the plane SL) is simply given by equation (16). The value of the average number of bonds $\bar{N}$ is given by equation (17). That is, the regression rate is

$$r = \frac{L \cdot \left\{1 - \left(\frac{1}{FSV} + \frac{1}{FSSL}\right)/2\right\} [B \cdot \exp(-E/\mathcal{R}T_w)]}{\left\{\frac{1}{FSV} - \frac{1}{FSSL}\right\}} \quad . \qquad (25)$$

Obviously, the regression rate determined by the subsurface reactions (eq. 22) has to equal the regression rate determined by surface reactions (eq. 25). Equating the two regression rates, we solve for the unknowns

FSSL and r simultaneously. For the case of catalyzed propellants we need to use the appropriate value of the reaction rate expression within the square brackets, in eq. (25).

The numerical solution for a typical case is presented in fig. 5, where the thickness of the melt layer is determined. The regression rate is plotted as a function of pressure in fig. 6 for the same case.

Discussion. For a set wall temperature and chamber pressure, there are two distinct ways in which the surface degradation contribution can be enhanced. An increase in the melt layer thickness L is one, and an increase in the reaction rate $B \cdot \exp(-E/RT_w)$ is another. However, the ultimate effect of either is felt the same way in the regression rate (see equation 25). That is, curves of regression rate versus pressure with L as a parameter may be considered the same as curves with the surface degradation rate as a parameter (possibly through catalysts).

Figure 6 displays curves where the pressure index n is greater than 0.5. It is also seen that practically any value of n (within the fundamental range, that is 0 to approximately 0.8) it is possible when one considers the possibility of surface reactions. This provides a very direct explanation of the experimentally observed values of n with catalyzed propellants.

The variations of the melt layer thickness L with regression rate (pressure) will have to be taken into consideration in a more refined analysis. We can, however, anticipate the qualitative trends. Since it is known that the melt layer thickness decreases with increasing regression rate, the regression rate versus pressure curve is likely to be of the shape shown by the broken line in fig. 6. We recall that propellants with binders that melt readily have been found[11] to exhibit such a decreasing n behavior.

4.4 Gas Phase Details

All along, it has been assumed that the wall temperature T_w can be prescribed from measurements or from calculations external to condensed phase analysis. In any combustion situation, however, the wall temperature is determined by the interaction of the solid phase with the general fluid dynamics and energetics of the gas phase. For premixed flames (pure AP, and double-base propellants) the full solution is available* in the literature and will not be pursued here. For non-premixed flames, as in the burning of composite propellants, the detailed solution to the gas phase depends on the assumptions we make regarding mixing and combustion. Several considerations are worth our thought before a theoretical analysis is undertaken.

For convenience, the gas phase is analyzed within the framework of a one-dimensional analysis. Under the basic assumption of chemical kinetic rates being far higher than mixing or diffusion rates, the main combustion reactions may be taken as occurring in a region that is standing off a distance X^* from the propellant surface.[22] Physically, the concept of flame standoff distance is as (un)realistic as the concept of a plane wall at the surface of the regressing propellant. However, in the analysis, the former concept is as useful as the latter. The overall model is depicted in fig. 1, which is also found in the current literature.

Now we turn our attention to the mechanistic details. It is difficult to characterize the gas phase above a burning composite as either laminar or turbulent. For double-base propellants (and for composites having very small oxidizer particles) there appears to be little room for doubt regarding the existence of laminar flow, simply from Reynolds number

*See refs. 16, 22, 32.

considerations. For normal composite propellants, photographs of the combustion region reveal that the gas phase is far from being laminar. There are present "spots" which give rise to transport and mixing on a scale far larger than molecular. However, the flow field may not merit the use of the word "turbulent" in that the origin of the large-scale spottiness has little to do with classical Tollmien-Schlichting instability. Moreover, and this is an important consideration, it is difficult to conceive of an exchange mechanism which would establish the standard turbulent energy spectrum that incorporates proven features such as, for example, Kolmogorov and Heisenberg limits. These thoughts render inapplicable a host of useful empirical rules that fluid dynamicists have evolved on flows that are truly turbulent. The point to note is that we cannot assume the flow to be turbulent simply because it is not laminar.

In an attempt to avoid these complications, if one examines a single crystal of oxidizer and details of gas evolution and flow, the simple laminar diffusion flame analysis may be utilized. However, the parameter

$$\frac{\bar{u}\,X^*}{\mathcal{D}} = \frac{\text{(mean velocity of gas flow)}\cdot\text{(flame standoff distance)}}{\text{(coefficient of interdiffusion of fuel and oxidizer gas)}}$$

has a value usually less than 5 so that the classical Burke-Schumann[33] model without consideration of axial diffusion is of limited validity. For the purposes of steady-state heat transfer calculations, it is sufficient to work with the non-dimensional flame standoff distance $\zeta \equiv \bar{u}X^*/\mathcal{D}$ as a parameter in the analysis. A more detailed study, required in the case of oscillatory burning, is deferred to Section V.

Analysis of Gas Phase Energetics. As already stated, the solution depends on the assumptions we make regarding combustion in the gas phase. In the absence of a complete understanding of the physical processes, two limiting cases are considered.

Case (i). The familiar flame-sheet approximation; no combustion until the gases have traversed a distance X^* from the surface, and complete combustion in a short distance after X^*.

Case (ii). Uniform combustion at a constant rate $\dot{m}'''$ ($gm/cm^3 sec$) starting from the solid-gas interface plane $(\ )_w$.

Physically, case (i) is probably a close approximation when the "delay" in combustion could be due to one or more of the following reasons. An "ignition" temperature has to be exceeded before combustion can commence. Due to macroscale coarseness of gas phase mixing, a certain distance has to elapse before the molecular mixing (needed for chemical reactions) can be attained. Even if molecular mixing started at the wall, certain stoichiometric proportion has to be reached for combustion to initiate and sustain itself.

Case (ii) is probably a satisfactory representation when the mixing process controls combustion as in the familiar concept of "well stirred reactor." Under the basic assumption of molecular diffusive processes controlling mixing (and hence combustion), the reaction rate may be taken as directly proportional to the density of the gases. Since it is known that the combustion temperature does not vary appreciably with mean pressure, it is easily seen through the state equation that the reaction rate $\dot{m}'''$ is directly proportional to the pressure. The molecular mixing rate also depends on the interfacial area of contact between the fuel and oxidizer gases and on the ve-

locity gradient between them. These inertial processes could be affected by the mean velocity of flow. For the present, the interfacial area and velocity gradients are taken as independent of velocity (and hence independent of the mean pressure through the law $r = ap^n$) so that the overall reaction rate $\dot{m}'''$ is directly proportional to the first power of mean pressure.

Case (i) The Flame-Sheet Approximation

The energy equation applied to gas flow between the wall plane w(-) and the burning plane b(+) is

$$k \frac{d^2T}{dx^2} + \rho u c \frac{dT}{dx} = 0 \ , \tag{26a}$$

with the boundary conditions

$$x = 0 : \qquad T = T_b$$

and (26b)

$$x = x^* : \qquad T = T_w \ .$$

The solution to the above linear system is written readily as

$$T = T_b - \frac{T_b - T_w}{1 - \exp(-ux^*/\varkappa_g)} \cdot \{1 - \exp(-ux/\varkappa_g)\} \tag{27}$$

($\varkappa_g$ is the average thermal diffusivity for the gases, $\varkappa_g \equiv (k/\rho c)_g$).

Simple mass continuity gives

$$\rho_s r = \rho_g u \ .$$

This equation may be used to write equation (27) as

$$T = T_b - \frac{T_b - T_w}{1 - \exp(-\zeta)} \{1 - \exp(-rx/\varkappa)\} \ ,$$

with the nondimensional flame standoff distance

$$\zeta \equiv rx^*/\varkappa_s \ .$$

The temperature gradient at the wall is given by

$$-\left(\frac{dT}{dx}\right)_w = \frac{r}{\varkappa}(T_b - T_w)\frac{\exp(-\zeta)}{1-\exp(-\zeta)} \quad . \tag{28}$$

Defining

$$\tau \equiv (T-T_o)/(T_w-T_o) ,$$

$$y \equiv rx/\varkappa ,$$

and

$$W \equiv (T_b-T_w)/(T_w-T_o) ,$$

we write equation (28) as

$$-\left(\frac{d\tau}{dy}\right)_w = \frac{W}{\exp(\zeta)-1} \quad . \tag{29}$$

If Q (cal/gm) is the heat released by the gases upon complete combustion, the overall energy balance between the planes w(-) and b(+) gives

$$-k\left(\frac{dT}{dx}\right)_w = Q\rho r - \rho c r(T_b - T_w) \quad . \tag{30}$$

Equation (30) may be used to evaluate the flame temperature T_b through the equation preceding eq. (9), since the LHS of that equation has to equal the LHS of (30). A more convenient procedure is to regard T_b as determined from fundamental thermodynamics and leave eq. (30) out of consideration.

Equating the nondimensional wall temperature gradient as determined by solid phase details (eq. 9) to the same quantity as determined by the gas phase details (eq. 29), we write

$$\zeta = \ell n \left\{1 + \frac{W}{1 + h/FSV}\right\} \quad . \tag{31}$$

An examination of the fundamental processes from several viewpoints consistently leads to the same groups, W, $(1 + h/FSV)$, and $W/(1 + h/FSV)$. It is suggested that these four groups be regarded as fundamental similarity parameters in propellant burning, in the same class as the groups θ_a and

χ in solid phase analyses.

To have a feel for the variations in ζ with regression rate and pressure, fig. 7 was prepared. The curves are computed through eqs. (15) and (31) for the case of a composite propellant with typical, assumed values of the various parameters. The binder contribution to the vapor pressure was neglected since such details are thought unimportant in determining the ζ trends.

It is interesting to note that (at constant T_w or an increasing T_w) the physical flame standoff distance x^* is predicted to decrease with increasing pressure. (This is to be recognized from fig. 7, after noting that u/κ depends on pressure like p^n where n is the pressure index in the law $r \propto p^n$.) This decrease in x^* with pressure increase is directly supported by experiments[5]. While it is true that such a decrease in x^* is also predicted by most other contemporary gas-phase theories, the result depends on the gas-phase chemical kinetic reaction rate in those theories. In terms of a simple picture, the chemical reactions can be completed in a shorter distance at higher reaction rates (at higher pressures), whereas, in the present case we see that the result follows even when the gas-phase chemical reaction details are completely ignored from the analysis.

It may be seen from figs. 3 - 7 that the assumption of constant T_w leads to predictions that are sufficiently close to experimental data. Further discussions on the subject of wall temperature determination through gas-phase details may be found in Section V.4.

Case (ii) Uniform Combustion

The solution here requires, for numerical computations, the value of the reaction rate $\dot{m}'''$, which has been taken from the work of Culick and

Dehority[34]. Also, in order to preserve the similarity to that work for easy comparison, the coordinate system is now taken as, distance x measured positive from the wall plane in the streamwise sense (see fig. 1d).

The energy equation and boundary conditions are:

$$\left.\begin{aligned} & k_g \frac{d^2T}{dx^2} - \rho_g c_p u \frac{dT}{dx} = - Q\dot{m}''' \\ & x = 0 : \; T = T_w \\ & \left(\frac{dT}{dx}\right)_w = \rho_g uc(T_w - T_o) + \frac{D}{FSV} \rho_g u \\ & x = x^* : \; T = T_b \\ & \left(\frac{dT}{dx}\right)_b = 0 \end{aligned}\right\} \qquad (32)$$

The definitions

$$\left.\begin{aligned} \tau &\equiv (T-T_o)/(T_w-T_o) \\ y &\equiv (ux)/\nu_g \\ m &\equiv \rho_g u \\ \Lambda_g^2 &\equiv \frac{k_g}{m^2 c_p^2} \frac{Q\dot{m}'''}{(T_w-T_o)} \\ \zeta &\equiv (ux^*)/\nu_g \end{aligned}\right\} \qquad (33)$$

transform the system (32) to

$$\left.\begin{aligned} & \frac{d^2\tau}{dy^2} - \frac{d\tau}{dy} = - \Lambda_g^2 \\ & y = 0 : \; \tau = 1 \\ & \frac{d\tau}{dy} = 1 + \frac{h}{FSV} \\ & y = \zeta : \; \tau = 1 + W \\ & \frac{d\tau}{dy} = 0 \quad \text{(inapplicable if } \Lambda_g = 0) \end{aligned}\right\} \qquad (34)$$

The symbol ζ is not the same as used by Culick and Dehority[34]; ζ in ref. 34 would be exp(y) in the present notation.

The solution to the linear system (34) is written readily as

$$\tau = 1 + \Lambda_g^2\{y + \exp(-\zeta) - \exp(y-\zeta)\} \quad . \tag{35}$$

Recalling the earlier definition,

$$W \equiv (T_b - T_w)/(T_w - T_o) \quad ,$$

eq. (35) may be made to yield

$$\left(\frac{d\tau}{dy}\right)_w = \left(1 + \frac{h}{FSV}\right) = \Lambda_g^2\{1 - \exp(-\zeta)\} \tag{36}$$

and

$$\tau_{x=x^*} = (1+W) = 1 + \Lambda_g^2\{\zeta + \exp(-\zeta) - 1\} \quad . \tag{37}$$

In principle, the problem is completely solved. For any prescribed pressure (and hence $\dot{m}'''$) a trial value of wall temperature T_w is assumed. The mass burning rate, m , is computed through eq. (22) (or eq. 25, if that case is being considered). The value of Λ_g^2 is computed through eq. (33). The nondimensional distance ζ is computed from eq. (36). The heat release parameter W is now computed from eq. (37). However, the parameter W can also be computed from the overall energy balance equation (30) which is written in nondimensional form (after the use of earlier definitions) as

$$\left(1 + \frac{h}{FSV}\right) = \frac{Q}{c_p(T_w - T_o)} - W \quad . \tag{38}$$

The iterations are repeated until satisfactory agreement is found between the two independent values of W . The results are presented in fig. (4b) for a case where the binder details have been ignored in the condensed phase treatment. It is a straightforward procedure to include them (as done in fig. 4a), but the details were thought to be unimportant in the present context

where the aim is the elucidation of gas phase details; besides, the values of Q (or T_b) are not readily available even for the simplest of specific propellant compositions.

In fig. 4b the burning rate pressure index is seen to be 0.46. In comparison with predictions based on the assumption of constant wall temperature (see fig. 4a), the general behavior is seen to be not appreciably different quantitatively, or even qualitatively.

The variations in wall temperature and the flame standoff distance (strictly speaking, the plane of onset of zero temperature gradient) are plotted as a function of pressure in fig. 7b. Again, in comparison with predictions based on the assumption of constant wall temperature (see fig. 7a), the general behavior is seen not to be appreciably different.

It would appear that the actual model for the gas phase processes is not crucially important in determining the general trends so long as the overall rate controlling reactions occur in the condensed phase. Such a conclusion was anticipated earlier (Section II. 3) purely on physical grounds.

V. OSCILLATORY BURNING OF COMPOSITE PROPELLANTS

5.1 Introduction

The rôle of the propellant in pressure-coupled instability in rocket motors is thought, at the present time, to be well represented by the response function, defined as

$$\frac{\tilde{\mu}}{\tilde{\epsilon}} = \frac{r'}{\bar{r}} \cdot \frac{\bar{P}}{P'} \tag{39}$$

with the familiar nomenclature. It has been shown[23] that the numerous theoretical derivations of the response function are essentially identical, since the fundamental assumptions in the various analyses are identical.

On the experimental side, some doubts exist regarding proper processing of the measured variables to yield the real part of the response function. Direct measurements of the fluctuating regression rate are difficult, and the several different techniques that are in use have not proved conclusive. Secondly, measurements at low frequencies involve large combustion chambers so that the question of thermal inertia and equilibration has introduced some doubts regarding the acceptability of data in the low frequency regime. Nevertheless, some of the general trends in the experimental response functions are thought to be well understood. The response function is usually found to be dependent on the mean chamber pressure, contrary to theoretical predictions. In some experiments, the response function seems to assume very large values at low frequencies, while theoretical predictions, and even physical arguments, suggest that the response function must tend to the limit of the steady-state pressure index n, in the limit as frequency tends to zero. Reference 37 presents an excellent introductory treatment of the general problem of combustion instability.

Based on the present model of composite propellant combustion, theoretical derivations of the response function are undertaken in this section. The cases of subsurface reactions only and surface reactions augmenting subsurface reactions are treated separately, since a cursory examination of the voluminous experimental data on response functions indicates that such a classification of propellant burning may be an important one. The analytical solutions are derived in a manner very similar to the steady-state analyses in the previous sections. The theoretical response function is found to be a function of the mean chamber pressure. Within the framework of the adiabatic approximation for flame temperature fluctuations, the theoretical response functions (for the case of subsurface reactions only) are seen to approach large values at low frequencies. However, it is recognized that ultimately the adiabatic variations have to give way to isothermal ones, thus removing the inconsistency in the low frequency limit (at zero frequency).

In a second attempt to postulate a physically valid model for the gas phase processes under oscillatory combustion, uniform combustion is considered in the gas phase. The general trends in the response function are not found to be very different from the case of adiabatic approximation, although the mean pressure dependence is now found to be much weaker.

The theoretical response functions derived in the present study are qualitatively discussed at the end of Section 5.3. It would aid the reader to study the figures 8, 8b, 9, 10, and 10b after going over that discussion.

5.2 Subsurface Reactions with No Surface Reaction.

The real problem in the solution of the time dependent case, it turns out, is the specification of the proper boundary conditions on temperature gradients. The rest of the procedure is very similar to the time independent case discussed in Section III and needs no elaboration here.

We recall that the temperature change across the reaction zone is of the order of reciprocal activation energy parameter, i.e., $\sim 1/\theta_a$. In terms of physical distance, x, this reaction zone has a thickness $\sim \varkappa/r\theta_a$. Thus, we see that, so long as we restrict our attention to small amplitude ($\sim 1/\theta_a$) fluctuations, the effect of temperature variation across the reaction zone is a second order quantity and need not be included in a first order analysis. That is, if we visualize a (hypothetical) freezing layer below which chemical reaction rates are negligible compared to other processes, we can neglect the effects of mean temperature variations between the wall and the freezing layer on fluctuations of temperature.

It will be shown (see later) that phase differences in variables may be neglected across the reaction zone except at very high frequencies. This fact can be exploited to write the exact expression for the wall boundary condition.

We shall first use a coordinate frame of reference held fixed at the mean position of the fluctuating wall (or freezing layer). We obtain the outer solution, neglecting the reaction term. We then use this exact solution to write the temperature-gradient boundary conditions both at the freezing layer (the interface between the "inner" and "outer" regions) and on the wall. Having obtained the boundary conditions, we solve for the time-dependent regression rate in a manner analogous to the time-independent case. That is, we solve the full equation, including explicitly the Arrhenius reaction

rate term in the inner region.

Outer Region. In the outer region, where the reaction rate term is exponentially small, we may write equation (1) as

$$k \frac{\partial^2 T}{\partial x^2} + \rho c \bar{r} \frac{\partial T}{\partial x} - \rho c \frac{\partial T}{\partial t} = 0 \quad , \tag{40}$$

Taking $r = \bar{r} + r'$, and defining

$$\tau \equiv (T - T_o)/(\bar{T}_w - T_o) = (\bar{T} - T_o)/(\bar{T}_w - T_o) + T'/(\bar{T}_w - T_o) \equiv \bar{\tau} + \tau' \ ,$$

$$y \equiv x\bar{r}/\kappa \ ,$$

$$\Omega \equiv \frac{\omega \kappa}{\bar{r}^2} \ ,$$

and assuming harmonic fluctuations in τ', we separate equation (40) into

$$\frac{d^2 \bar{\tau}}{dy^2} + \frac{d\bar{\tau}}{dy} = 0 \tag{41}$$

and

$$\frac{d^2 \tau'}{dy^2} + \frac{d\tau'}{dy} - i\Omega \tau' = 0 \tag{42}$$

The solutions to equations (41) and (42) are, respectively,

$$\bar{\tau} = \exp(-y) \tag{43}$$

and

$$\tau' = \tau'_w \exp(-\lambda_1 y) \tag{44}$$

where

$$\lambda_1 = \tfrac{1}{2}(1 + a_1 + ib_1)$$

$$a_1 \equiv [(1 + 16\Omega^2)^{\frac{1}{2}} + 1]^{\frac{1}{2}} / \sqrt{2}$$

$$b_1 \equiv [(1 + 16\Omega^2)^{\frac{1}{2}} - 1]^{\frac{1}{2}} / \sqrt{2}$$

Since the position of the wall plane (and also of the freezing plane) is fluctuating in time, the coordinate there is $x_w = \int r' \, dt$, which may be written

$$y_w = -i \frac{1}{\Omega} \frac{r'}{\bar{r}} \quad . \tag{45}$$

Expanding the temperature in Taylor's series around the freezing layer, and using equations (43), (44), and (45), it is a matter of algebra[2] to arrive at

$$-\left(k \frac{\partial T'}{\partial x}\right) = \bar{r}\rho \left[\lambda_1 T'_f + \frac{T_f - T_o}{\lambda_1} \frac{r'}{\bar{r}}\right] \quad ,$$

which may be written in terms of nondimensional variables as

$$-\left(\frac{\partial \tau}{\partial y}\right)'_f = \lambda_1 \tau'_w + \frac{1}{\lambda_1} \frac{r'}{\bar{r}} \quad . \tag{46}$$

Equation (46) specifies the outer boundary condition at the inner edge. The inner solution, which will be derived shortly, will have to match (in its outer limit) with equation (46).

In order to examine the order of various terms, we write equation (1) in non-dimensional form as

$$\frac{\partial^2 \tau}{\partial y^2} + \frac{\partial \tau}{\partial y} - \Omega \frac{\partial \tau}{\partial (\omega t)} = \Lambda h N \exp(-E/\Re T) \quad . \tag{47}$$

In the linearization of the fluctuating part of the reaction term, there is the inherent assumption that $\theta_a \chi \tau'_w \sim \epsilon$,* which implies that $\tau'_w \sim \epsilon^2$. Now, examining the terms in equation (47) in the inner region, we see that

$$\Omega \frac{\partial \tau}{\partial (\omega t)}$$

is of the order $\Omega\epsilon^2$. Hence, the term may be neglected from the equation except when $\Omega \sim 1/\epsilon$ or higher. Excluding such high frequencies from consideration, we write equation (1) as

*The symbol ϵ denotes any (arbitrary) first-order quantity. Examples, $1/\theta_a\chi$, $P'/\bar{P}$, $r'/\bar{r}$, etc. ϵ^2 denotes, thus, any second-order quantity.

$$k\frac{d^2T}{dx^2} + \rho\bar{r}c\frac{dT}{dx} = D\rho NB\exp(-E/\Re T) \quad . \tag{48}$$

Physically, this tells us that the reaction zone is of such a small thickness that effectively the phases of various quantities of interest are left unaffected across this layer. Viewed in another light, the length scale associated with the oscillations ($\sim\bar{r}/\omega$) is far larger than the length scale associated with the degradation reaction ($\sim \varkappa/\theta_a\chi\bar{r}$). These observations introduce remarkable simplifications in the analysis to follow.

First, we may use the convenient wall-fixed coordinate system and closely follow the (already derived) steady-state solution, recognizing that the variables have an implicit time dependence and that new boundary conditions are to be used. Second, we write the wall boundary condition in analogy with equation (46) [see figure 1e] as

$$-\left(\frac{\partial\tau}{\partial y}\right)'_w = \lambda_1\tau'_w + \frac{1}{\lambda_1}\frac{r'}{\bar{r}}\left(1 + \frac{h}{FSV}\right) \quad . \tag{49}$$

Lastly, we may substitute in the inner region,

$$\frac{d}{d\tilde{y}} = \frac{1}{(1 + r'/\bar{r})}\frac{d}{dy} \tag{50}$$

where

$$\tilde{y} \equiv rx/\varkappa \quad .$$

(We recall that $r = \bar{r} + r'$.)

Boundary Conditions on Temperature Gradients.

Freezing layer $(\ )_f$:

$$\left(\frac{\partial\tau}{\partial y}\right)_f = \left(\frac{d\bar{\tau}}{dy}\right)_f + \left(\frac{\partial\tau}{\partial y}\right)'_w = -1 - \left(\lambda_1\tau'_w + \frac{1}{\lambda_1}\frac{r'}{\bar{r}}\right)$$

or

$$\left(\frac{d\tau}{d\tilde{y}}\right)_f = \frac{1}{1 + r'/\bar{r}}\left(\frac{\partial\tau}{\partial y}\right)_f = -1 - \lambda_1\tau'_w - \frac{1}{\lambda_1}\frac{r'}{\bar{r}} + \frac{r'}{\bar{r}} \quad .$$

The variable $\xi \left(\equiv \frac{d\tau}{d\tilde{y}} + \tau\right)$ is written

$$\xi^o = \xi_f = \bar{\xi}_f + \xi'_f = 1 + \tau'_w - 1 - \lambda_1 \tau'_w - \frac{r'}{\bar{r}} \left(1 - \frac{1}{\lambda_1}\right) = \tau'_w(1-\lambda_1) + \frac{r'}{\bar{r}} \left(1 - \frac{1}{\lambda_1}\right). \quad (51)$$

Wall $(\ )_w$:

$$\left(\frac{\partial \tau}{\partial y}\right)_w = \left(\frac{d\bar{\tau}}{dy}\right)_w + \left(\frac{\partial \tau}{\partial y}\right)'_w = -1 - \frac{h}{FSV} - \lambda_1 \tau'_w - \frac{r'}{\bar{r}} \left(1 + \frac{h}{FSV}\right)\frac{1}{\lambda_1}$$

or

$$\left(\frac{d\tau}{d\tilde{y}}\right)_w = \frac{1}{1 + r'/\bar{r}} \left(\frac{\partial \tau}{\partial y}\right)_w = \left[-\left(1 + \frac{h}{FSV}\right) - \lambda_1 \tau'_w - \frac{1}{\lambda_1} \frac{r'}{\bar{r}} \left(1 + \frac{h}{FSV}\right)\right] \left(1 - \frac{r'}{\bar{r}}\right)$$

$$= -\left(1 + \frac{h}{FSV}\right) - \lambda_1 \tau'_w - \frac{1}{\lambda_1} \frac{r'}{\bar{r}} \left(1 + \frac{h}{FSV}\right) + \frac{r'}{\bar{r}} \left(1 + \frac{h}{FSV}\right) . \quad (52)$$

Now we have

$$\xi_w = \bar{\xi}_w + \xi'_w = -\frac{h}{FSV} + \tau'_w(1-\lambda_1) + \frac{r'}{\bar{r}} \left(1 + \frac{h}{FSV}\right)\left(1 - \frac{1}{\lambda_1}\right) . \quad (53)$$

It is convenient to employ the shorthand notation

$$\xi_w = -\frac{h}{FSV} + \xi^o + \frac{h}{FSV} \left(1 - \frac{1}{\lambda_1}\right) \frac{r'}{\bar{r}} \quad (54)$$

which is nothing more than a substitution of equation (51) into equation (53).

Now we have all the information necessary to solve the time-dependent regression rate r .

At the very start we observe the satisfactory feature that the boundary conditions, eqs. (51) and (54), tend to the proper steady-state limit as the frequency $\omega \to 0$ (i.e., as $\lambda_1 \to 1$). In all of the analysis to follow, it is worth remembering that the variable T and the parameter D/c have been normalized with respect to the steady state quantity, $(\bar{T}_w - T_o)$.

The Solution. In the inner region, where the gradients get very large, we write equation (12) as

$$pp'+p \doteq (h+p+\tau)\Lambda \exp[-\theta_a\{1+\chi(1-\tau)\}] . \qquad (55)$$

Using the small parameter $\epsilon \equiv 1/\theta_a\chi$ to stretch the variables in the inner region, and defining the inner variables

$$\eta \equiv \frac{1-\tau}{\epsilon}$$

$$\xi \equiv p + \tau$$

and

$$\tilde{\lambda} \equiv \epsilon \Lambda \exp(-\theta_a) ,$$

we write equation (55) as

$$-(\xi - 1 + \epsilon\eta)\xi' = (h+\xi)\tilde{\lambda}\exp(-\eta) \qquad (56)$$

where a prime denotes $d/d\eta$.

Making the expansions

$$\xi = \xi_o+\epsilon\xi_1+\epsilon^2\xi_2+ \ldots$$

and

$$\tilde{\lambda} = \tilde{\lambda}_o+\epsilon\tilde{\lambda}_1+\epsilon^2\tilde{\lambda}_2+ \ldots$$

and substituting them into eq. (56), we get, to the lowest order, after dropping the subscript o,

$$\xi' - \xi'\xi = (h+\xi)\tilde{\lambda}\exp(-\eta) . \qquad (57)$$

To clearly display the integration we write equation (57) as

$$\frac{d\xi}{h+\xi} - \frac{\xi\, d\xi}{h+\xi} = \tilde{\lambda}\exp(-\eta)d\eta ,$$

which integrates to

$$\ell n(h+\xi)-[\xi-h\,\ell n(\xi+h)] = -\tilde{\lambda}\exp(-\eta) + [\text{constant}] , \qquad (58)$$

i. e.,

$$(h+1)\ell n(h+\xi)-\xi = -\tilde{\lambda}e^{-\eta} + [\text{constant}] . \qquad (59)$$

Kaplun's matching theorem requires

$$\xi \to \xi^o \quad \text{as} \quad \eta \to \infty ,$$

yielding

$$(h+1)\,\ell n\,(h+\xi^o) - \xi^o = [\text{constant}] \ ,$$

$$(h+1)\ell n\{h\left(1 + \frac{\xi^o}{h}\right)\} - \xi^o = [\text{constant}] \ ,$$

i.e.,

$$(h+1)\,\ell n\,h + (h+1)\,\ell n(1 + \xi^o/h) - \xi^o = [\text{constant}] \ .$$

Recognizing that $\xi^o \sim \epsilon$, we approximate the logarithmic terms and write

$$(h+1)\,\ell n\,h + (h+1)\,\xi^o/h - \xi^o = [\text{constant}]$$

$$(h+1)\,\ell n\,h + \xi^o/h = [\text{constant}] \ . \qquad (60)$$

Equation (60) may be substituted into equation (59) to yield

$$(h+1)\ell n(h+\xi) - \xi = -\tilde{\lambda}\, e^{-\eta} + (h+1)\ell n\,h + \xi^o/h$$

or

$$\tilde{\lambda}\, e^{-\eta} = (h+1)\,\ell n\,\frac{h}{h+\xi} + \xi + \xi^o/h \ .$$

On the wall,

$$\eta = 0 \qquad \text{and} \qquad \xi = \xi_w \ ;$$

hence,

$$\tilde{\lambda} = (h+1)\,\ell n\,\frac{h}{h+\xi_w} + \xi_w + \xi^o/h \ . \qquad (61)$$

After considerable algebra, detailed fully in Appendix A, we write equation (61) as

$$\tilde{\lambda} = (h+1)\ell n\left[\frac{FSV}{FSV-1}\right] - \frac{h}{FSV} - \frac{r'}{r}\left(1 - \frac{1}{\lambda_1}\right)\left[\frac{h+1}{h(FSV-1)} + \frac{h+1}{FSV-1} - \frac{h}{FSV}\right]$$

$$- \tau'_w(\lambda_1 - 1)\,\frac{h+1}{h(FSV-1)} \ . \qquad (62)$$

Fluctuations in wall temperature, and chamber pressure fluctuations, produce fluctuations in the value of FSV. Its effects are second order in the third and the fourth terms in equation (62) and have been neglected. It is

shown in Appendix B that FSV can be satisfactorily represented as

$$FSV = \alpha P^{-\beta} \cdot \exp(\delta T_w)$$

where α, β, and δ are constants.

After some algebra detailed in Appendix A, we write equation (62) as

$$\tilde{\lambda} = (h+1)\ell n \frac{\overline{FSV}}{\overline{FSV}-1} - \frac{h}{\overline{FSV}} + C_5 \frac{p'}{\bar{p}} - \frac{r'}{\bar{r}} \left(1 - \frac{1}{\lambda_1}\right) C_3 - \tau'_w \{C_4 + C_1(\lambda_1 - 1)\} \qquad (63)$$

where

$$C_1 \equiv \frac{h+1}{h(\overline{FSV}-1)}$$

$$C_2 \equiv \frac{h+1}{\overline{FSV}-1} - \frac{h}{\overline{FSV}}$$

$$C_3 \equiv C_1 + C_2$$

$$C_4 \equiv C_2 \delta \bar{T}_w \chi$$

$$C_5 \equiv C_2 \beta$$

We recall (equation 14) that under steady conditions

$$\lambda = (h+1)\ell n\left[\frac{FSV}{FSV-1}\right] - \frac{h}{FSV} \quad ,$$

which can be used to normalize the unsteady $\tilde{\lambda}$ (equation 63).

$$\frac{\tilde{\lambda}}{\lambda} = 1 - \frac{C_4}{\lambda} \tau'_w + \frac{C_5}{\lambda} \frac{p'}{\bar{p}} - \frac{r'}{\bar{r}} \left(1 - \frac{1}{\lambda_1}\right) \frac{C_3}{\lambda} - \tau'_w (\lambda_1 - 1) \frac{C_1}{\lambda} \quad . \qquad (64)$$

It is worthwhile to recall the original definitions,

$$\lambda \equiv \frac{\kappa B \exp(-\theta_a)}{\theta_a \chi r^2}$$

and

$$\tilde{\lambda} \equiv \frac{\kappa\, \bar{B}(1 + p'/\bar{p})\cdot \exp(-\bar{\theta}_a)\cdot (1+\bar{\theta}_a \bar{\chi}\tau'_w)}{\bar{\theta}_a(1+\bar{\chi}\tau'_w)\left[\bar{\chi}\{1+\tau'_w(1-\bar{\chi})\}\right](\bar{r}+r')^2} \quad .$$

The expressions for λ and $\tilde{\lambda}$ give, through equation (64),

$$\mathcal{R} \equiv \left(\frac{r'/\bar{r}}{p'/\bar{p}}\right) = \frac{1 - C_5/\lambda}{2 - (1-1/\lambda_1)C_3/\lambda - \dfrac{\tau'_w}{r'/\bar{r}}\left[\bar{\theta}_a\bar{\chi} + C_4/\lambda - 1 + (\lambda_1 - 1)C_1/\lambda\right]} \quad . \qquad (65)$$

Equation (65) is the desired expression for the response function. Given a relation between τ'_w and $r'/\bar{r}$, the problem may be considered "solved."

A Relation Between τ'_w and $r'/\bar{r}$. A valid procedure is needed for specifying the relation between τ'_w and $r'/\bar{r}$, external to the solid phase analysis. For a propellant regressing under the influence of its own gas phase reactions, it is logical to invoke the gas phase details to supply the relation between τ'_w and $r'/\bar{r}$. However, we recall that a thorough and complete solution to the gas phase has not been obtained yet even for the time-independent case. For the present, we shall be content with choosing any one of the several criteria that were evolved in an attempt to eliminate the arbitrariness in time-independent burning. The data in fig. 4a suggest that constant (mean) T_w is an adequate assumption, reasonably representative of many experimental measurements. From dimensional considerations we expect that $\zeta \equiv \bar{r}x^*/\kappa$ does not vary too much from its steady state value during unsteady combustion. It is assumed in this work that ζ is identically equal to its value during time-independent burning at the same mean pressure. The variations in the value of ζ with mean chamber pressure have, however, not been neglected.

The temperature and pressure fluctuations have to match the "far field" values just beyond the "flame sheet." Gas phase acoustic processes

in the main chamber are usually fast enough to be isentropic (but not so fast as to introduce effects of thermodynamic nonequilibrium!). A relation between the temperature and pressure fluctuations follows immediately as

$$\frac{T'_b}{\overline{T}_b} = \frac{\gamma - 1}{\gamma} \frac{p'}{\overline{p}} \quad . \tag{66}$$

Some caution is necessary in the use of this seemingly universal equation (66). When we consider the low frequency limit, $\omega \to 0$, the above equation is obviously not representative of reality. It is known that flame temperatures vary little with mean pressure in time-independent burning. For a very slow change, the process is more likely to be isothermal than adiabatic. A convenient way of handling this effect mathematically is to let $\gamma \to 1$, in eq. (66), as $\omega \to 0$. In an ideal analysis, the index z in the expression $T'/\overline{T} = \frac{z-1}{z} p'/\overline{p}$, will be written as a function of frequency such that $z \to 1$ as $\omega \to 0$ and $z \to \gamma$, sufficiently far away from $\omega = 0$. It is found that a very similar argument has been put forward by other researchers[3], who have actually presented $T'/\overline{T} = \text{fn}(p'/\overline{p}, \omega)$. However, both the gas-phase physical model they use and the analysis are thought to be too involved to be consistent with the present work, if we think of using the available[3] expression here. A simpler procedure for handling such effect is being considered at the present time.

The debatable assumption of isentropic fluctuations in the gas phase may be dispensed with if some other criterion can be invoked to evaluate the ratio $\tau'_w/(r'/\overline{r})$. In the calculations of time-independent regression rates (see IV. 4), the model of uniform combustion in the gas phase was invoked to dispense with assumptions regarding the value of wall temperature. As a generalization from the time-independent case, the same model of uniform

combustion in the gas phase can be used in the time-dependent case also. We thus have two different models for the gas phase (adiabatic and uniform combustion), both of which can be used (independently) with the same condensed phase model.

(a) Adiabatic Fluctuations in the Gas Phase

Except for the small intricacy at very low frequencies, eq. (66) is to be used in the analysis. As discussed by Krier, et al.[36], many experiments are available where the isentropic assumption is valid. Hence, the present analysis finds use even without any refinement.

Under the basic assumption of quasi-steady processes in the gas phase, we recall that the value of the wall temperature gradient is

$$-\left(\frac{d\tau}{d\tilde{y}}\right)_w = \frac{\frac{T_b - T_w}{\bar{T}_w - T_o}}{\exp(\zeta)-1} = \frac{\frac{\bar{T}_b - \bar{T}_w}{\bar{T}_w - T_o} + \frac{T'_b}{\bar{T}_w - T_o} - \frac{T'_w}{\bar{T}_w - T_o}}{\exp(\zeta) - 1}$$

$$= \frac{\bar{W} + \frac{T'_b}{\bar{T}_b} \cdot \frac{\bar{T}_w}{\bar{T}_w - T_o} \cdot \frac{\bar{T}_b}{\bar{T}_w} - \frac{T'_w}{\bar{T}_w - T_o}}{\exp(\zeta) - 1} \quad . \tag{67}$$

Recalling all of the assumptions and nomenclature, it is a simple exercise in algebra to write equation (67) as

$$-\left(\frac{d\tau}{d\tilde{y}}\right)_w = \left(1 + \frac{h}{FSV}\right)\left[1 + \frac{\gamma-1}{\gamma} \frac{\chi W+1}{\chi W} \frac{p'}{\bar{p}} - \frac{\tau'_w}{W}\right] \quad . \tag{68}$$

Equating equation (68) to the same temperature gradient evaluated through solid phase analysis (eq. 52), we have

$$\frac{\gamma-1}{\gamma} \frac{\chi W+1}{\chi W} \frac{p'}{\bar{p}} - \frac{\tau'_w}{W} = \frac{\lambda_1 \tau'_w}{1 + \frac{h}{FSV}} + \frac{r'}{\bar{r}}\left(1 - \frac{1}{\lambda_1}\right) \quad . \tag{69}$$

It is a matter of convenience to work with

$$C_7 \equiv (1 + \frac{h}{FSV})/2$$

$$C_8 \equiv \frac{\gamma-1}{\gamma}\frac{\chi W+1}{\chi}$$

$$R20 \equiv \left(1 - \frac{1}{\lambda_1}\right)$$

which simplify equation (69) to read

$$\frac{\tau'_w}{r'/\bar{r}} = \frac{\frac{C_8}{W}\frac{1}{\Re} - R20}{\frac{1}{W} + \frac{\lambda_1}{2C_7}} \qquad (70)$$

where $\Re = (r'/\bar{r})/(p'/\bar{p})$.

The value of $\tau'_w/(r'/\bar{r})$ predicted by equation (70) may be substituted into equation (65) to obtain a formal solution, i.e., an expression for the response function, $\Re$. For convenience again, we employ short hand notations:

$$R6 \equiv \{\theta_a\chi - 1 + C_4/\lambda + (\lambda_1 - 1)C_1/\lambda\}$$

$$R41 \equiv \frac{C_8/W}{\frac{1}{W} + \frac{\lambda_1}{2C_7}}$$

$$R42 \equiv \frac{R20}{\frac{1}{W} + \frac{\lambda_1}{2C_7}}$$

$$R43 \equiv 1 - \frac{C_3}{2\lambda} R20 + \frac{R42 \cdot R6}{2}$$

$$R44 \equiv \frac{R6 \cdot R41}{2}$$

It is to be recognized that the group $(1-C_5/\lambda)/2$ is the pressure index n for time-independent burning (under the assumption of constant mean T_w) .

Finally, the normalized response function is written

$$\frac{1}{n}\,\mathcal{R} = \frac{1 + R44/n}{R43} \quad . \tag{71}$$

Discussion

Before an attempt is made to compare the theoretical curves in fig. 8 with experimental data, the validity of the theory must be clearly understood.

The curves are not valid at low frequencies because the index γ (in $T'/\overline{T} = \frac{\gamma - 1}{\gamma}\, p'/\overline{p}$) approaches unity and does not retain the value of 1.25 that was used in preparing the graphs. The effect of this shift to isothermal changes at low frequencies is to converge all the curves to the ordinate unity as $\Omega \to 0$.

The curves are not valid at high frequencies ($\Omega \gtrsim 10$). In the singular perturbation analysis we excluded such high frequencies from consideration.

There is a third limitation which may not be readily obvious. The curves are not valid at high pressures, or to be more precise, when the length scale $\kappa/\overline{r}$ becomes smaller than the mean size of the oxidizer particles in the propellant. The length $\kappa/\overline{r}$ is the effective thermal depth in the solid. When this depth gets comparable to, or smaller than, the mean size of the oxidizer particles, the material cannot be considered homogeneous any more. When the assumption of homogeneous solid breaks down, so does our analysis.

There are several reported experiments[7, 10] that closely follow the trends predicted in fig. 8. The numerical values of the real part of the response function measured in experiments are close to those predicted in

fig. 8. The frequency scale appears to be shifted slightly toward the higher side in the experiments if we use a value of 1.1×10^{-3} cm^2/sec for the thermal diffusivity α, as we have been doing all along. A different value (but not unrealistically different) for the thermal diffusivity would remove this frequency position discrepancy.

We regard with satisfaction the existence of experimental data that agree with the theoretical predictions. We recognize that the ultimate aim is to predict the outcome of any experiment.

(b) Uniform Combustion in the Gas Phase

Under the basic assumption of quasi-steady processes in the gas phase, the solution to the gas phase energy equation is valid during time-dependent burning also.

The wall temperature gradient was seen to be (Sec. IV. 4)

$$p_w \equiv \left(\frac{d\tau}{dy}\right)_w = -\Lambda_g^2(1-e^{-\zeta}) = -\frac{k_g}{\rho^2 r^2 C_p^2}\,\frac{Q_f \dot{m}'''}{(\bar{T}_w - T_o)}\,(1-e^{-\zeta}) \ .$$

From ref. 31 it may be seen that the mass consumption rate of gaseous reactants can be represented as

$$\dot{m}''' = A \cdot P \qquad (72)$$

where P is the mean pressure and A is an appropriate constant.

Defining the nondimensional mean heat release rate as

$$S \equiv \left(\frac{k}{\rho c}\right)_s \cdot \frac{Q_f}{c(\bar{T}_w - T_o)} \cdot \frac{A \cdot \bar{P}}{\rho_s \bar{r}^2}\,(1-e^{-\zeta}) \quad , \qquad (73)$$

the wall temperature gradient during time-dependent burning is written

$$p_w = -S(1 + P'/\bar{P})(1 - 2r'/\bar{r}) \ . \qquad (74)$$

In the above equation, the assumption (as first introduced in subsection (a) before) is made that the nondimensional reaction distance ζ can be taken as constant during unsteady combustion. The variations in ζ with mean pressure have not been neglected.

It is easily verified that the nondimensional S defined in eq. (73) has to equal the steady-state nondimensional wall temperature gradient $(1 + h/FSV)$. Although it is a very straightforward procedure to consider either, the value of FSV used here is the full time-dependent value and not just the steady-state value. This point needs amplification. The heat release Q_f in the gas phase combustion is not strictly a constant; it depends on the initial endothermicity of the propellant vapors. A large value of FSV indicates a large number of bonds left unbroken in the vapor molecules and the (necessary) scission of the bonds acts like a heat sink on some of the energy release in the gas phase due to combustion. Hence, the net Q_f, which is what is implied in the formulation here, actually depends on FSV. Thus, during unsteady burning, the fluctuations in the value of FSV produce fluctuations in the value of Q_f. We may absorb such fluctuations in Q_f into the $(1 + h/FSV)$ term and leave Q_f as a constant in the definition of S (eq. 73).*

Purely from an analysis of the condensed phase, we had the wall temperature gradient (eq. 52) as

$$p_w = -\left(1 + \frac{h}{FSV}\right) - \lambda_1 \tau'_w - \left(1 + \frac{h}{FSV}\right)\frac{r'}{\bar{r}}\left(1 - \frac{1}{\lambda_1}\right) .$$

Equating the two separate evaluations of the wall temperature gradient, we get

$$\frac{P'}{\bar{P}} - 2\frac{r'}{\bar{r}} = \frac{\lambda_1 \tau'_w}{\left(1 + \frac{h}{FSV}\right)} - \left(1 - \frac{1}{\lambda_1}\right)\frac{r'}{\bar{r}} \qquad (75)$$

*See Section VI(iv) for a detailed discussion.

or

$$\frac{P'}{\bar{P}} - \frac{r'}{\bar{r}}\left(1 + \frac{1}{\lambda_1}\right) = \frac{\lambda_1}{1 + \frac{h}{FSV}}\,\tau'_w \quad . \tag{76}$$

Division of eq. (76) throughout by $r'/\bar{r}$, and substitution of the identity $\mathcal{R} \equiv (r'/\bar{r})/(P'/\bar{P})$ yields

$$\frac{1}{\mathcal{R}} - \left(1 + \frac{1}{\lambda_1}\right) = \frac{\lambda_1}{1 + \frac{h}{FSV}}\,\frac{\tau'_w}{(r'/\bar{r})}$$

or

$$\frac{\tau'_w}{(r'/\bar{r})} = \left(1 + \frac{h}{FSV}\right)\left[\frac{1}{\mathcal{R}} - \left(1 + \frac{1}{\lambda_1}\right)\right] \Big/ \lambda_1 \quad , \tag{77}$$

so that the problem is solved, in principle. Using the result (77) in eq. (65) and employing shorthand notations for convenience, it is a matter of algebra to arrive at

$$\mathcal{R} = \frac{U1 + U2}{U4 + U5} \tag{78}$$

with

$$\left.\begin{aligned} U1 &\equiv 1 - C_5/\lambda \\ U2 &\equiv R6\left(1 + \frac{h}{FSV}\right)\Big/\lambda_1 \\ U3 &\equiv 1 + 1/\lambda_1 \\ U4 &\equiv 2 - R20 \cdot C_3/\lambda \\ U5 &\equiv U2 \cdot U3 \end{aligned}\right\} \tag{79}$$

5.3 Surface Reactions Augmenting Subsurface Reactions

In close analogy with the steady burning case (see 4.3), the case of time-dependent combustion is treated here. The physical picture is the same as in fig. 1b. The only difference from the steady burning case is that the fluctuating part of the regression rates in the subsurface region and in the surface melt layer need not be equal to each other, as the steady part of the regression rate has to be. The difference between the fluctuating parts of the regression rate in the surface and subsurface regions shows up as fluctuations in the thickness of the melt layer.

To anticipate the analysis, the developments in Section 5.2 are carried over as exact representation of the propellant below the plane SL. The fragment size is thus FSSL and not FSV; also, the fluctuations in FSSL are not given by a perturbation of the vapor pressure rule B.2, but have to be determined through proper matching with the melt layer. The surface contribution in the melt layer is a linear perturbation of the expression for the regression rate (eq. 25). The resulting equations are solved simultaneously to obtain the response function. The relation between the wall temperature fluctuation and the pressure fluctuation has to be supplied from gas phase details, as in Section 5.2.

In the following analysis, the steady and fluctuating parts are written

surface melt layer thickness	$L = \bar{L} + L'$
fragment size vaporizing	$FSV = \overline{FSV} + FSV'$
fragment size at the solid-liquid interface	$FSSL = \overline{FSSL} + FSSL'$
fluctuating part of the regression rate due to subsurface reactions only	r'_{ss}

(80)

It is an exercise in algebra to write equation (62) [applied below the plane SL] as

$$\frac{r'_{ss}}{\bar{r}}\left\{2 - \frac{CL3}{\lambda}\left(1 - \frac{1}{\lambda_1}\right)\right\} = \frac{CL2}{\lambda}\frac{\overline{FSSL'}}{\overline{FSSL}} + \tau'_w\left\{(\lambda_1 - 1)\frac{CL1}{\lambda} + \theta_a\chi - 1\right\} + \frac{P'}{\bar{P}} \quad . \quad (81)$$

In the above expression the shorthand notations are:

$$CL1 \equiv \frac{h+1}{h(\overline{FSSL} - 1)}$$

$$CL2 \equiv \frac{h+1}{\overline{FSSL} - 1} - \frac{h}{\overline{FSSL}}$$

$$CL3 \equiv CL1 + CL2$$

$$\lambda = (h+1)\,\ell n\left\{\frac{\overline{FSSL}}{\overline{FSSL} - 1}\right\} - \frac{h}{\overline{FSSL}}$$

It should be remembered that λ_1 is the complex root of the unsteady equation (see 5.2) and that the above shorthand notations are all steady-state quantities only.

It is again an exercise in algebra to write the unsteady part of equation (25) as

$$\frac{r'}{\bar{r}} = Z2\frac{\overline{FSV'}}{\overline{FSV}} + Z3\frac{\overline{FSSL'}}{\overline{FSSL}} + \frac{L'}{\bar{L}} + \frac{P'}{\bar{P}} + \theta_a\chi\tau'_w \quad (82)$$

with

$$Z2 \equiv \frac{\overline{FSV}\cdot\overline{FSSL}(1 - 1/\overline{FSSL})}{2\cdot\overline{FSV}\cdot\overline{FSSL} - \overline{FSV} - \overline{FSSL}} + \frac{\overline{FSV}}{\overline{FSSL} - \overline{FSV}}$$

and

$$Z3 \equiv \frac{\overline{FSV}\cdot\overline{FSSL}(1 - 1/\overline{FSV})}{2\cdot\overline{FSV}\cdot\overline{FSSL} - \overline{FSV} - \overline{FSSL}} - \frac{\overline{FSSL}}{\overline{FSSL} - \overline{FSV}} \quad ,$$

both of which are shorthand notations for steady-state quantities.

Mass conservation in the melt layer gives

$$r'_{ss} - r' = \frac{dL'}{dt} \quad . \tag{83}$$

Assuming harmonic variations in L', equation (83) is written in non-dimensional form as

$$\frac{r'_{ss}}{\bar{r}} - \frac{r'}{\bar{r}} = i\frac{\Omega}{4}\frac{L'\bar{r}\bar{L}}{\bar{L}\kappa} = \lambda_1(\lambda_1-1)\frac{L'}{\bar{L}}\frac{\bar{r}\bar{L}}{\kappa}$$

or

$$\frac{L'}{\bar{L}} = \left(\frac{\kappa}{\bar{r}\bar{L}}\right)\cdot\left\{\frac{r'_{ss}}{\bar{r}} - \frac{r'}{\bar{r}}\right\}\frac{1}{\lambda_1(\lambda_1-1)} \quad . \tag{84}$$

The fluctuating part of FSV may be written through

$$FSV = \alpha P^{-\beta}\exp(\delta T_w) \ ,$$

as

$$\frac{FSV'}{\overline{FSV}} = C_4\tau'_w - C_5 P'/\bar{P} \quad . \tag{85}$$

Substituting the values of $FSV'/\overline{FSV}$ and $FSSL'/\overline{FSSL}$ from equations (85) and (81) into equation (82), we get

$$\frac{r'}{\bar{r}} = Z2(C_4\tau'_w - C_5 P'/\bar{P}) + \frac{\lambda}{CL2}\cdot Z3\left\{\frac{r'_{ss}}{\bar{r}}\left[2 - \frac{CL3}{\lambda}\left(1-\frac{1}{\lambda_1}\right)\right] - \tau'_w\left[(\lambda_1-1)\frac{CL1}{\lambda} + \theta_a\chi - 1\right] - \frac{P'}{\bar{P}}\right\}$$
$$+ \frac{L'}{\bar{L}} + \frac{P'}{\bar{P}} + \theta_a\chi\tau'_w \quad . \tag{86}$$

During the discussion on steady-state combustion, the quantity L was supplied from external considerations. Strictly speaking, it should be determined (from a knowledge of the melting behavior of the propellant) as a function of FSSL and FSV. In the unsteady case, the fluctuating part L' thus remains unknown. We can, however, consider two limiting cases to obtain a closed form solution.

(i) The melt layer thickness is constant even in unsteady combustion as in steady combustion. Now, $r'_{ss} = r'$ and $L' = 0$.

(ii) The subsurface regression rate fluctuation vanishes, i.e., $r'_{ss} = 0$. Now, all of the fluctuation in the regression rate is entirely due to the melt layer.

The physically real solution exists between these two limiting cases, probably closer to the second criterion.

Both the solutions will be discussed here.

(i) Case of $L' = 0$ ($r'_{ss} = r'$); (a) Adiabatic Fluctuations.

It is easily seen that the wall temperature fluctuation is related to the other fluctuations through equation (70). That is, the flame temperature fluctuations affect the entire energy balance exactly as discussed in Section 5.2 Equation (86) is written

$$\frac{\tau'_w}{r'/\bar{r}} = \frac{Z7}{Z4} + \frac{Z5}{Z4}\frac{1}{\Re} \tag{87}$$

where

$$\left.\begin{aligned} Z4 &\equiv Z2\cdot C_4 - \frac{\lambda}{CL2} Z3\left[(\lambda_1 - 1)\frac{CL1}{\lambda} + \theta_a\chi - 1\right] + \theta_a\chi \\ Z5 &\equiv Z2\cdot C_5 + \frac{\lambda}{CL2} Z3 - 1 \\ Z6 &\equiv \frac{\lambda}{CL2} Z3\left[2 - \frac{CL3}{\lambda}\left(1 - \frac{1}{\lambda_1}\right)\right] \\ Z7 &\equiv 1 - Z6 \end{aligned}\right\} \tag{88}$$

Equating the values of $\tau'_w/(r'/\bar{r})$ in equations (70) and (87), we have

$$\frac{\frac{C_8}{W}\frac{1}{\Re} - R20}{\frac{1}{W} + \frac{\lambda_1}{2C_7}} = \frac{Z7}{Z4} + \frac{Z5}{Z4}\frac{1}{\Re},$$

yielding, through the definitions,

$$\left.\begin{aligned} R30 &\equiv \frac{W}{C_8}\, R20 \\ R31 &\equiv \frac{Z7}{Z4}\left(\frac{1}{W} + \frac{\lambda_1}{2C_7}\right)\frac{W}{C_8} \\ R32 &\equiv \frac{Z5}{Z4}\,\frac{W}{C_8}\left(\frac{1}{W} + \frac{\lambda_1}{2C_7}\right) \end{aligned}\right\} \qquad (89)$$

$$\Re \equiv \frac{1 - R32}{R30 + R31} \qquad (90)$$

(i) Case of $L' = 0$ ($r'_{ss} = r'$); (b) Uniform Combustion.

From the earlier discussion on the model of uniform combustion in the gas phase (Section 5.2(b)) we have an expression for $\tau'_w/(r'/\bar{r})$ in equation (77). Equating the two independent expressions obtained for the same quantity (equations 77 and 87), we get

$$\frac{Z7}{Z4} + \frac{Z5}{Z4}\,\frac{1}{\Re} = \left(1 + \frac{h}{FSV}\right)\left[\frac{1}{\Re} - U3\right]/\lambda_1 \quad . \qquad (91)$$

Hence, the response function is

$$\Re = \frac{\left(1 + \frac{h}{FSV}\right)\cdot\frac{1}{\lambda_1} - \frac{Z5}{Z4}}{\left(1 + \frac{h}{FSV}\right)\cdot\frac{U3}{\lambda_1} + \frac{Z7}{Z4}} \quad . \qquad (92)$$

Case (ii) $r'_{ss}/\bar{r} = 0$ and $L'/\bar{L} \neq 0$; (a) Adiabatic Fluctuations.

Substituting the values of $FSV'/\overline{FSV}$ and $L'/\bar{L}$ into equation (82), we get

$$\frac{r'}{\bar{r}} = Z2\left[C_4\tau'_w - C_5\,\frac{P'}{\bar{P}}\right] - Z_3\left\{\tau'_w\left[(\lambda_1 - 1)\frac{CL1}{\lambda} + \theta_a\chi - 1\right] + \frac{P'}{\bar{P}}\right\}\frac{\lambda}{Z1}$$

$$-\left(\frac{\kappa}{\bar{L}\,\bar{r}}\right)\cdot\frac{1}{\lambda_1(\lambda_1 - 1)}\,\frac{r'}{\bar{r}} + \frac{P'}{\bar{P}} + \theta_a\chi\tau'_w \quad . \qquad (93)$$

Defining

$$\left.\begin{aligned} R531 &\equiv Z2\cdot C_4 - Z3\left\{(\lambda_1-1)\frac{CL1}{\lambda}+\theta_a\chi-1\right\}\frac{\lambda}{Z1}+\theta_a\chi \\ R532 &\equiv Z2\cdot C_5 - Z_3\frac{\lambda}{Z1}+1 \\ R533 &\equiv 1+\frac{\left(\frac{\kappa}{\bar{L}\bar{r}}\right)}{\lambda_1(\lambda_1-1)} \end{aligned}\right\} \qquad (94)$$

we write equation (93) as

$$R533\cdot\frac{r'}{\bar{r}} = R531\,\tau'_w - R532\,\frac{P'}{\bar{P}} \quad . \qquad (95)$$

From considerations of gas phase details only we can write (see Section 5.2) the wall temperature gradient as

$$-\left(\frac{d\tau}{d\tilde{y}}\right)_W = \left\{1+C_8\frac{P'}{\bar{P}}-\frac{\tau'_w}{\bar{W}}\right\}\left(1+\frac{h}{\overline{FSV}}\right) . \qquad (96)$$

Recalling that r'_{ss} is zero, we may write the temperature gradient at the plane SL as a simplified version of equation (52):

$$-\left(\frac{d\tau}{d\tilde{y}}\right)_{SL} = \left(1+\frac{h}{\overline{FSSL}}\right)+\lambda_1\tau'_w \quad . \qquad (97)$$

The difference between the heat transfer rates across the two planes SL and w has to be the sink term due to chemical reactions in the isothermal layer on the surface. In terms of nondimensional variables, the sink term is

$$h\left\{\frac{1}{\overline{FSV}}-\frac{1}{\overline{FSSL}}\right\} ,$$

which is valid regardless of whether the processes are steady or unsteady. This is both because we are considering a region of no phase lag and the normalization of the variable x into $\tilde{y}$ has the full time-dependent regression rate included in it.

Equating the difference between the equations (96) and (97) to the above expression, we get

$$\tau'_w \left\{ \frac{1+\frac{h}{\overline{FSV}}}{W} + \lambda_1 \right\} = \frac{P'}{\overline{P}} C_8 \left(1 + \frac{h}{\overline{FSV}} \right) . \tag{98}$$

Using the convenient notation

$$R534 \equiv \frac{C_8(1 + h/\overline{FSV})}{\left\{ \frac{1 + h/\overline{FSV}}{W} + \lambda_1 \right\}} ,$$

we combine equations (95) and (98) to write the response function as

$$\mathcal{R} = \frac{R531 \cdot R534}{R533} - \frac{R532}{R533} . \tag{99}$$

For representative values of the parameters, equations (90) and (99) have been plotted in figs. 9 and 10.

Case (ii) $r'_{ss}/\overline{r} = 0$ and $L'/\overline{L} \neq 0$; (b) Uniform Combustion.

The only difference between this case and that of adiabatic fluctuations (treated under (a)) is that the wall temperature gradient is given by equation (74) and not by equation (96). Now we get

$$\tau'_w = \frac{\left(1 + \frac{h}{\overline{FSV}}\right)}{\lambda_1} \frac{P'}{\overline{P}} - 2 \frac{\left(1 + \frac{h}{\overline{FSV}}\right)}{\lambda_1} \frac{r'}{\overline{r}} \tag{100}$$

in place of equation (98).

Using the convenient notation,

$$R535 \equiv \left(1 + \frac{h}{\overline{FSV}}\right) \Big/ \lambda_1 ,$$

we get

$$\tau'_w = R535 \frac{P'}{\overline{P}} - 2 \cdot R535 \frac{r'}{\overline{r}} . \tag{101}$$

Combining equations (95) and (101) to eliminate τ'_w, we get

$$\mathcal{R} = \frac{R535 - (R532/R531)}{(R533/R531) + 2 \cdot R535} . \tag{102}$$

Discussion on the Predicted Response Functions

Several features of the present study invite a discussion on the derived response functions in order to bring into sharp focus their distinct differences from the response functions of previous theories.

For our purposes here, the response functions of contemporary theories may be taken as adequately represented by

$$\Re = \frac{nB}{\lambda_1 + \frac{A}{\lambda_1} - (1+A) + B} , \qquad (103)$$

where A and B (not to be confused with the A and B of the nomenclature of the present report) are parameters related to the activation energy for the surface pyrolysis reaction. For any given n for a propellant, different curves are obtained by the choice of different values of A and B, a procedure that essentially implies having a flexible value of the activation energy for the pyrolysis reaction. In the present study, a single value of the activation energy (28.9 k cal/mole) has been used throughout. That is, the familiar A - B parametric representation of the response functions is outside the scope of the present work. The propellant is allowed to determine its own pressure index n through the reaction rate and the vapor pressure criterion, as contrasted with other theories where the pressure index n is specified as an empirical number from external considerations. The proper zero frequency ($\lambda_1 \to 1$) limit of $\Re$ (i.e., $\Re_{\lambda_1=1} = n$) is automatically reached in those theories, for the simple reason that this limit is used as one of the requirements on the response function in the derivations. In the present study, no such requirement is imposed, and hence some interesting observations can be made on the behavior of the response functions at very low frequencies. Two other features of the present calculations which were mentioned earlier are worth repetition.

The nature of the present theoretical analyses introduces a high frequency limit on the validity of the derived response functions. Since simplifications have been introduced by limiting our attention to moderate frequencies, the interpretation of the theoretical results above a non-dimensional frequency (Ω) of 10 is questionable.

For the purposes of heat transfer calculations, the assumption of a homogeneous solid has been made all through the present study. That is, the assumption of the characteristic linear dimension (effective thermal depth, $\kappa/\bar{r}$) associated with the heat transfer process in the solid being far larger than the characteristic linear scale (oxidizer particle size, a) associated with solid heterogeneity is inherent in all of the present theoretical derivations. Since the thermal diffusivity may be taken as a constant during the small variations in the wall temperature encountered, the assumption of homogeneous solid becomes questionable at high regression rates and hence at high pressures. This is an important consideration. Interestingly enough, results of unpublished experiments currently near completion have strongly indicated that the familiar stabilizing effect of high pressures on unstable burning propellants may be due to the fact that the propellant is taken beyond the homogeneous solid limit, so that the heat reservoir effect in the solid (i. e., the $C \cdot \Delta T$ "charge" - "discharge" effect) would lose its significance. Deprived of the mechanism introducing phase differences in heat-transfer related variables, the propellant would burn in a non-oscillatory manner above a certain "threshold" pressure.

Following the above general comments we now examine the specific cases presented in figs. 8, 8b, 9, 10, and 10b.

Figure 8: Deep Solid Reactions with No Surface Reactions; Adiabatic Fluctuations in the Gas Phase.

For this particular case, the results have already been discussed in Section 5.2. The essential point to note is that the "flame" temperature is assumed to vary with pressure according to the adiabatic law, an assumption that is difficult to justify at very low frequencies and is definitely incorrect at zero frequency (as revealed by thermochemical equilibrium calculations). The present analysis relates the wall temperature, and hence the regression rate through the pyrolysis law, to the flame temperature. Thus, increases in flame temperature that accompany a pressure increase lead to large increases in the regression rate. However, if the flame temperature does not vary at low frequencies, neither does the wall temperature, and hence we approach the steady-state pressure index n. The fact that no peaks are revealed in the curves at any frequency indicates that the values of the parameters used ($E/\mathcal{R}\bar{T}_w$, in particular) do not permit such a behavior. The mean pressure dependence of the response function is due to the vapor pressure equilibrium effect. When wall temperature fluctuations are present, the fragment size and the pyrolysis rate are not affected in the same manner as during time-independent combustion. This is essentially because of the phase differences (between the pressure and the wall temperature fluctuations), which are inoperative during time-independent variations in mean pressure. For example, if the flame temperature fluctuations vanish, the regression rate variations at low frequencies are affected by pressure variations exactly as during steady combustion, and hence the response function tends to the limit of steady-state pressure index n for all values of the mean pressure.

Figure 8b: Deep Solid Reactions with No Surface Reactions; Uniform Combustion in the Gas Phase.

This case provides a particularly interesting example in the wake of the discussions on the adiabatic case (fig. 8). For the case of quasi-steady uniform combustion in the gas phase, the gas-phase temperature variations accompanying pressure fluctuations are almost the same as those during time-independent combustion. However, at higher frequencies, the phase lag introduced by the condensed phase heat reservoir effect does not affect the pressure sensitivity in the reaction rate term and the vapor pressure term in the same way, so that the curves reveal a mean pressure dependence.

Figure 9: Surface Reactions in a Melt Layer of Constant Thickness Augment the Deep Solid Reactions; Adiabatic Fluctuations in the Gas Phase.

When the thickness of the melt layer on the surface does not vary during oscillatory burning, all of the oscillatory burning characteristics are controlled by the deep solid reaction behavior. Thus, we see that the results (i.e., frequency dependence of the response function) are likely to be close to the case of no surface reactions, as indeed they are in fig. 8b. The rest of the discussion on fig. 9 would be very similar to the one on fig. 8 and is not pursued here.

Figure 10: Surface Reactions in a Melt Layer of Fluctuating Thickness; Fluctuating Part of Regression Rate Associated with Deep Solid Reactions Vanish; Adiabatic Fluctuations in the Gas Phase.

The propellant studied is the one for which the time-independent characteristics were presented in figures 5 and 6. In the analysis (Section 5.3) it was assumed that the regression rate fluctuations resulted from variations in melt layer thickness only. That is, accompanying a pressure increase there

would always be present a decrease in the melt-layer thickness of a magnitude precisely requisite to balance out the regression rate variations (see eq. 83). If such variations occurred during time-independent combustion, the propellant would exhibit a zero pressure index, as shown in fig. 5. It would be a simple matter to consider an incomplete balance and thereby introduce non-zero values of the pressure index n. That is, a propellant with any n can be considered almost as easily. The zero-n case represents one interesting limit in the general class of propellants.

Turning our attention to the frequency dependence, we expect such propellants to be fairly unstable from physical considerations. The deep solid is homogeneous and gives rise to temperature fluctuations due to the heat reservoir effects. The surface reactions rates are hence subject to large fluctuations because of the strong Arrhenius term. It should be recalled that for the present case of constant-temperature melt layer, regression rate depends directly on the surface reaction rate and not on its square root. Visualizing the phenomenon in another way, the temperature fluctuations originating from the deep solid effects drive the Arrhenius rate term at the surface. The pressure dependence of the position of the peak on the frequency scale is also easily understood. With the existence of a melt layer on the surface, we have a new length scale in the problem, the thickness of the melt layer (ℓ). We thus form a natural frequency, r/ℓ. For a constant mean regression rate with the variation of mean pressure (i. e., the zero-n propellant) the melt layer thickness decreases with increasing pressure (see fig. 5). Hence, the natural frequency increases with increase of mean pressure. If we associate some "resonance-like" phenomenon with the peak in the response function, it would seem physical to expect such a peak to occur close to this natural frequency. This explains the shift towards higher frequencies of the peak with

increases in pressure.

Figure 10b: Surface Reactions in a Melt Layer of Fluctuating Thickness; Fluctuating Part of Regression Rate Associated with Deep Solid Reactions Vanish; Uniform Combustion in the Gas Phase.

For the case of a zero-n propellant considered here, the response function is not expected to differ appreciably from the one with adiabatic fluctuations in the gas phase. As can be seen, most of the discussions on the previous figure are independent of the nature of the temperature or pressure fluctuations in the gas phase. The broader peak observed in fig. 10b is probably due to much milder temperature fluctuations compared to the adiabatic case.

5.4 Further Considerations in Gas Phase Processes

Several aspects of the problem provide a strong motivation for the study of gas phase in detail. It was seen in Section IV that a completely self-contained solution to the time-independent combustion problem has not been possible because of our lack of understanding of gas phase details. In the present section we observed that our progress toward a solution to the oscillatory combustion case was also hindered by the same difficulty; more specifically, by our inability to write a general expression for the flame temperature fluctuation as a function of the pressure fluctuations and frequency. In many of the experiments on oscillatory combustion, the pressure fluctuations are seen not to grow indefinitely but to reach a limiting value, indicating the presence of nonlinear effects. However, the pressure fluctuations themselves are almost purely sinusoidal. Thus, the origin of the nonlinearity is not obvious. It has been shown recently that under typical conditions the rocket chamber cannot sustain nonlinear pressure oscillations so that the nonlinearities are associated with either the condensed phase or the gas phase combustion zone. The condensed phase behavior was seen (Secs. 5.2, 5.3) to be controlled strongly by the gas phase "flame region" through the relation $T_f' = \text{fn}(p', \omega, \dots)$. The above thoughts add to the fundamental interest intrinsic with the unconventional non-premixed "flame" by itself.

The variables of possible interest to the gas phase are

$$u\ ,\ a\ ,\ x^*\ ,\ \mathcal{D}\ ,\ T_b\ ,\ T_w\ ,\ T_o\ .$$

The rate of intermixing of fuel and oxidizer is incorporated into x^* and $\mathcal{D}$. Chemical kinetic rates were argued to be unimportant (Sections I and II).

From dimensional considerations we write

$$W = \frac{T_b - T_w}{T_w - T_o} = \text{fn}\left(\frac{ua}{\mathfrak{D}}, \frac{x^*}{a}\right) .$$

Since $\mathfrak{D} \sim \nu$, $ua/\mathfrak{D}$ may be considered as a Reynolds number, R. We thus have

$$W = \text{fn}\left(R, \frac{x^*}{a}\right) .$$

Except at very low values of R (low r and hence low p), molecular diffusive effects are not likely to be important. Hence, at sufficiently high burning rates,

$$W = \text{fn}\left(\frac{x^*}{a}\right)$$

independent of gas velocity. This is reminiscent of the classical experiments of Hawthorne, et al. on combusting turbulent jets where the brush length was a function of feed velocity in the low flow-rate regime only. At high flow rates, the brush length was independent of feed velocity. The added complication in the case of propellant combustion is that the "feed" velocity (u) is dependent on wall temperature (through the pyrolysis law) so that the group x*/a would be a constant only if W is constant. Intuitively one might expect for all propellants the existence of such an asymptotic limit at which both the wall temperature and the flame standoff distance become truly independent of regression rate. The numerical values of the limits, however, cannot be determined from dimensional considerations alone. A formal solution would require a quantitative knowledge of the mixing processes. We also recognize that equation (26) is no longer adequate to describe the flow, unless the property values, k, ρ, and c are averaged over macroscopic transport also.

During oscillatory combustion, the pressure waves in the far field (chamber) are acoustic. Thus, the temperature fluctuations are known as a function of the pressure fluctuations. This is valid up to the downstream end of the combustion zone, e (fig. 1). We need the amplitude of the temperature fluctuations at the upstream end of the combustion zone, b (fig. 1).

It is suggested that an experiment be performed to gain insight into the problem. To facilitate measurements, the composite propellant surface would be simulated by a perforated porous plate with provision for injection of fuel gas through the fine mesh and oxidizer gas through the perforations. The fraction of total surface area occupied by the perforations will simulate the oxidizer volume fraction in the propellant. The scaling rules for feed velocities are given by the foregoing dimensional considerations. The choice of gaseous fuel and oxidizer gases would control the flame temperature T_b. Measurements of wall temperature and the flame standoff distance at various pressures would complete the time-independent combustion studies.

The same apparatus could then be used to study the case of oscillatory burning. The same details as before would be studied with isentropic pressure disturbances in the main chamber. The coupling between the fluctuations of feed rate and the temperature and pressure is difficult to simulate precisely. However, we are mainly interested in the behavior of the acoustic wave across the nonlaminar combustion zone. The experiments are expected to shed light on an important facet of the general problem of composite propellant combustion.

VI. CONCLUDING REMARKS

Most of the significant developments have already been discussed in the previous sections. However, the following points call for special mention.

(i) From dimensional considerations one recognizes a natural regression rate $\hat{r} \equiv \kappa/a$ for all composite propellants. Interesting characteristics are anticipated for propellants operating in the vicinity of this natural regression rate. At values of $r < \hat{r}$, the propellant may be looked upon as homogeneous and hence deep solid reactions may be important. At values of $r > \hat{r}$, the thermal profile in the solid is too shallow to lend credence to the homogeneous - solid approximation. Surface reactions are expected to dominate the regression rate behavior. The present study indicates (Section IV) that the pressure index n should change by approximately a factor of two as one passes through the $r = \hat{r}$ point. Many propellants have been experimentally found to exhibit such a pronounced "break" in the r versus P curve (T-17, CIT-2 ... for example). If the oxidizer particle melts and mixes thoroughly with the readily melting binder, the particle size a loses its significance and hence there exists no natural regression rate. Such propellants are not expected to show a marked break in the r versus P curve.

(ii) If, by some means, the degradation of the oxidizer is suppressed in the subsurface region, the pressure index n is expected to be unusually high for a composite propellant. This offers a simple explanation for the high n obtained by Muzzy[25] when he coated the oxidizer particles with a passive layer. Also, the surface reactions, with little deep solid reactions, could give a very pronounced peaky response

function as shown through the present analysis (Section 5.3 and fig. 10). His experimental data[25] provide a strong support for the theoretical developments here.

(iii) One of the most important developments of the present work is the identification of the pressure index n as a composite quantity which reflects the combined influences of several different physical phenomena. Thus, a zero-n propellant can exhibit strong instability, if these different influences are not affected in a self-compensating way during oscillatory burning (Section 5.3 and fig. 10). This offers an explanation for the behavior of zero-n propellants whose tendency to oscillate has not been explained so far on the basis of existing theories which treat n as a simple entity completely characterizing the pressure sensitivity of a propellant both during steady and unsteady combustion. The identification of the different physical influences behind the composite entity n also shows how the response function can be dependent on mean chamber pressure, contrary to previous theoretical results, but in agreement with experimental data.

(iv) It should be recognized that the heat of combustion (Q, Q_f) is pressure dependent for a given propellant. As defined here, the heat of combustion represents the heat released in the gas phase by vapors leaving the propellant surface. The net heat release would depend on the initial endothermicity of the propellant vapors. The initial endothermicity depends on the number of unbroken bonds left in the fragments entering the vapor phase. The number of unbroken bonds is characterized by the fragment size vaporizing FSV. For vapors of a specific fragment size (which may be taken as the reference value), the heat of combustion would have a fixed value ($\hat{Q}$). For vapors of mean initial fragment size larger than this reference value, the heat of combustion would

be smaller than $\hat{Q}$, since the larger number of unbroken backbone bonds left in the fragments introduce a larger heat sink on the total heat release. The reference state is arbitrary and may be taken as unity FSV. Now, the heat of combustion of propellant vapors is,

$$Q_f = \hat{Q} - D(1 - \frac{1}{FSV}) \quad . \tag{104}$$

Recalling that the mean fragment size vaporizing (FSV) depends on the wall temperature and the chamber pressure through the vapor pressure equilibrium criterion, we see that the heat of combustion Q_f also depends on the wall temperature and the chamber pressure. During time-independent burning, such variations in Q_f are expected to slightly modify the results of the uniform combustion model in this report. Preliminary calculations have shown that the modifications are no more than a few per cent in r and hardly any at all in T_w. Likewise, during oscillatory burning, we expect fluctuations in the value of Q_f because of fluctuations in the value of FSV through equation (104). The response functions (employing the uniform combustion model) in the present report are expected to undergo slight modifications because of this variable value of Q_f. The results in the report have used a constant value of Q_f. Again, it is expected that the modifications would be minor; nevertheless, the variable Q_f case is anticipated to remove the small discrepancy in the zero frequency limit of the response function in fig. 8b. A variable Q_f was considered in a crude manner in Section 5.2 (page 55). A more rigorous procedure is under consideration.

(v) In the present report, a linear structure has been assumed for AP in order to relate the mean fragment size at any state (of degradation) to the number of unbroken backbone bonds in AP. This is a debatable assumption. A more accurate procedure would be to bring out this relationship through

the actual structure of partially degraded (but undecomposed) AP if the structure is accurately known. The results of such a refined procedure are, however, not expected to alter the present conclusions significantly, mainly because the concepts of FSV and vapor pressure equilibrium at the wall would not be affected, and most of the principal conclusions of the present report result more from the concepts of FSV and vapor pressure equilibrium than from the actual value of FSV as related to the degradation rate.

Salient Conclusions

(i) The assumption of condensed-phase degradation of AP being the rate-limiting step in the overall pyrolysis of AP leads to theoretical results that match well with experimental hot-plate data.

(ii) The hypothesis of pressure-dependent (condensed-phase) degradation of AP in a surface layer controlling the overall regression rates of AP/composite propellants leads to predictions in agreement with experimental data covering both single-crystal AP self-deflagration and composite propellant combustion.

(iii) The extent of degradation at the vaporization step can be specified through the vapor pressure equilibrium criterion.

(iv) The hypothesis of gas-phase combustion rate completely determined by pressure-independent diffusive-mixing processes leads to analytical results in agreement with experimental trends.

(v) The response function of a composite propellant can be theoretically derived through the method of inner and outer expansions including explicitly the non-linear (Arrhenius) degradation rate term in the condensed phase.

(vi) The response functions so derived exhibit dependence on mean chamber pressure, strongly so with the model of adiatatic fluctuations in the

gas phase and weakly with the model of uniform combustion in the gas phase.

(vii) A "zero-n" propellant can exhibit fairly strong instability behavior.

(viii) A few unifying concepts enable us to coherently interpret a host of superficially diverse data.

In conclusion, the author wishes to thank Professor Fred E. C. Culick for many helpful comments and encouragement, Mr. Warren L. Dowler for his interest in these studies and encouragement, and Mrs. Roberta I. Duffy for her excellent typing.

Literature Cited

1. Kumar, R. N. and Stickler, D. B., "Polymer Degradation Theory of Pressure-Sensitive Hybrid Combustion," XIII Symposium (International) on Combustion (1971), pp. 1059-1072.

2. Culick, F. E. C., "Some Problems in the Unsteady Burning of Solid Propellants," Naval Weapons Center, TP 4668 (Feb. 1969).

3. Krier, H., et al., "Entropy Waves Produced in Oscillatory Combustion of Solid Propellants," AIAA Paper 68-499 (1968).

4. Boggs, T. L., et al., "The Deflagration of Pure and Isomorphously Doped Ammonium Perchlorate," XIII Symposium (International) on Combustion (1971), pp. 995-1008.

5. Maltzev, V., "Certain Problems Related to Mechanism of Combustion of Condensed Systems (Double-Base and Mixed Propellants)," Institute of Chemical Physics, USSR Academy of Sciences, Moscow (Aug. 1971 - Feb. 1972). See also, Combustion and Flame, V. 13 (April 1969), p. 139.

6. Hirschfelder, J. O., et al., Molecular Theory of Gases and Liquids, John Wiley and Sons, New York (1954).

7. "Combustion of Solid Propellants and Low Frequency Combustion Instability," NOTS TP 4244 (June 1967).

8. Kumar N. R. Ramohalli, "Some Considerations in Hybrid Combustion," Ph. D. Thesis, Dept. of Aeronautics and Astronautics, Massachusetts Institute of Technology (June 1971).

9. Powling, J., "Experiments Relating to the Combustion of Ammonium Perchlorate-Based Propellants," XI Symposium (International) on Combustion (1967), pp. 447-456.

10. Horton, M. D. and Rice, D. W., "Effect of Compositional Variables upon Oscillating Combustion of Solid Rocket Propellants," Combustion and Flame, V. 8 (March 1964), pp. 21-28.

11. Steinz, J. A., et al., "The Burning Mechanism of Ammonium Perchlorate-Based Composite Solid Propellants," AMS Report 830, Princeton University (Feb. 1969).

12. Jacobs, P. W. M. and Whitehead, H. M., "Decomposition and Combustion of Ammonium Perchlorate," Chemical Reviews, V. 69 (1969), pp. 551-590.

13. Guirao, C. and Williams, F. A., "A Model for Ammonium Perchlorate Deflagration between 20 and 100 atm.," AIAA Journal, V. 9 (1971), pp. 1345-1356.

14. Kraeutle, K. J., "The Thermal Decomposition of Orthorhombic Ammonium Perchlorate Single Crystals," J. Phys. Chem., V. 74 (March 19, 1970), pp. 1350-1356.

15. Ohlemiller, T. J. and Summerfield, M., "Radiation Augmented Burning of a Solid Propellant," AMS Report No. 799, Princeton University (Nov. 1967).

16. Penner, S.S., Chemical Rocket Propulsion and Combustion Research, Gordon and Breach (1962).

17. Stickler, David B. and Kumar N. R. Ramohalli, "Polymer Degradation Rate Control of Hybrid Rocket Combustion," SPL Report 70-2, Massachusetts Institute of Technology (Sept. 1970).

18. Derr, R. L. and Boggs, T. L., "Role of Scanning Electron Microscopy in the Study of Solid Propellant Combustion: Part III. The Surface Structure and Profile Characteristics of Burning Composite Solid Propellants," Combustion Science and Technology, V. 1 (1970), pp. 369-384.

19. Schmidt, W. G., "The Effect of Solid Phase Reactions on the Ballistic Properties of Propellants," NASA CR-66757 (May 1969).

20. Schmidt, W. G., "The Effect of Solid Phase Reactions on the Ballistic Properties of Propellants," NASA CR-111940 (Sept. 1970).

21. Schmidt, W. G., "The Effect of Solid Phase Reactions on the Ballistic Properties of Propellants," Aerojet Solid Propulsion Co., Sacramento, Calif.

22. Beckstead, M., et al., "The Combustion of Solid Monopropellants and Composite Propellants," XIII Symposium (International) on Combustion (1971), pp. 1047-1056.

23. Culick, F. E. C., "A Review of Calculations for Unsteady Burning of a Solid Propellant," AIAA Journal, V. 6 (Dec. 1968), pp. 2241-2255.

24. Varney, A. M. and Strahle, W. C., "Thermal Decomposition Studies of Some Solid Propellant Binders," Combustion and Flame, V. 16 (Feb. 1971), pp. 1-7.

25. Muzzy, R. J., "Research on Combustion of Solid Propellants," UTC 2136 - TRS2 (11 October 1967).

26. Boggs, T. L. and Zurn, D. E., "The Temperature Sensitivity of the Deflagration Rates of Pure and Doped Ammonium Perchlorate," Combustion Science and Technology, V. 4 (Jan. 1972), pp. 227-232.

27. Warren, F. A., ed., "Solid Propellant Technology," AIAA Selected Reprint Series, Vol. X (Feb. 1970).

28. Williams, F. A., Barrère, M., and Huang, N. C., "Fundamental Aspects of Solid Propellant Rockets," Aerospace Research and Development of NATO, Technivision Services, London (1969).

29. Bakhman, N. N. and Belyaev, A. F., "Combustion of Heterogeneous Condensed Systems," Rocket Propulsion Establishment Translation 19, London (1967).

30. Novikov, S.S., Pokhil, P. F., and Ryazantsev, Yu. S., "Modern Ideas on the Mechanism of Combustion of Condensed Systems," A Review. Fizike Goreniya i Vzryva, V. 4, no. 4 (1968), pp. 469-481.

31. Price, E. W. and Culick, F. E. C., "Combustion of Solid Propellants," AIAA Professional Study Series,

32. Johnson, W. E. and Nachbar, W., "Deflagration Limits in the Steady Burning of a Monopropellant with Application to Ammonium Perchlorate," VIII Symposium (International) on Combustion (1962), pp. 678-689.

33. Burke, S. P. and Schumann, T. E. W., "Diffusion Flames," I Symposium on Combustion (1928), The Combustion Institute, published in 1965.

34. Culick, F. E. C. and Dehority, G. L., "An Elementary Calculation for the Burning Rate of Composite Solid Propellants," Combustion Science and Technology, V. 1 (1969), pp. 193-204.

35. Kirk-Othmer, Encyclopedia of Chemical Technology, Vol. 13, John Wiley and Sons, New York (1967), pp. 213-217.

36. Krier, H., et al., "Nonsteady Burning Phenomena of Solid Propellants: Theory and Experiments," AIAA Journal, V. 6 (1968), pp. 278-285.

37. Culick, F. E. C., "Research on Combustion Instability and Application to Solid Propellant Rocket Motors," AIAA Paper No. 71-753 (June 1971).

APPENDIX A. Details of Algebra

(i) Equation (62) from Equation (61)

We had

$$\tilde{\lambda} = (h+1)\ell n\left\{\frac{h}{h+\xi_w}\right\} + \xi_w + \frac{\xi^o}{h} \quad . \tag{61}$$

Using equation (54) to write ξ_w in terms of ξ^o, we write equation (61) as

$$\tilde{\lambda} = (h+1)\ell n\left[\frac{h}{h - \frac{h}{FSV} + \xi^o + \frac{h}{FSV}\frac{r'}{\bar{r}}\left(1 - \frac{1}{\lambda_1}\right)}\right] - \frac{h}{FSV} + \xi^o$$

$$+ \frac{h}{FSV}\frac{r'}{\bar{r}}\left(1 - \frac{1}{\lambda_1}\right) + \frac{\xi^o}{h} \tag{A1}$$

$$= (h+1)\ell n\left[\frac{1}{\frac{FSV-1}{FSV}\left\{1 + \frac{FSV}{FSV-1}\left[\frac{\xi^o}{h} + \frac{1}{FSV}\frac{r'}{\bar{r}}\left(1 - \frac{1}{\lambda_1}\right)\right]\right\}}\right]$$

$$- \frac{h}{FSV} + \xi^o + \frac{h}{FSV}\frac{r'}{\bar{r}}\left(1 - \frac{1}{\lambda_1}\right) + \frac{\xi^o}{h} \tag{A2}$$

Recognizing that

$$\frac{FSV}{FSV-1}\left[\frac{\xi^o}{h} + \frac{1}{FSV}\frac{r'}{\bar{r}}\left(1 - \frac{1}{\lambda_1}\right)\right] \sim \epsilon \quad ,$$

we may approximate the logarithmic term and write

$$= (h+1)\ell n\frac{FSV}{FSV-1} - (h+1)\frac{FSV}{FSV-1}\left[\frac{\xi^o}{h} + \frac{1}{FSV}\frac{r'}{\bar{r}}\left(1 - \frac{1}{\lambda_1}\right)\right]$$

$$- \frac{h}{FSV} + \xi^o + \frac{h}{FSV}\frac{r'}{\bar{r}}\left(1 - \frac{1}{\lambda_1}\right) + \frac{\xi^o}{h} \tag{A3}$$

Defining $\lambda \equiv (h+1)\ell n\left\{\frac{FSV}{FSV-1}\right\} - \frac{h}{FSV}$, where FSV has both the steady and the time-dependent components $\overline{FSV}$ and FSV', equation (A3) is written,

$$\tilde{\lambda} = \lambda - \xi^{o}\left\{ \frac{FSV}{h} \frac{h+1}{FSV-1} - 1 - \frac{1}{h} \right\} - \frac{r'}{\bar{r}} \left(1 - \frac{1}{\lambda_1}\right)\left[\frac{h+1}{FSV-1} - \frac{h}{FSV} \right]$$

$$= \lambda - \xi^{o}\left\{ \frac{FSV}{h} \frac{h+1}{FSV-1} - \frac{h+1}{h} \right\} - \frac{r'}{\bar{r}} \left(1 - \frac{1}{\lambda_1}\right)\left[\frac{h+1}{FSV-1} - \frac{h}{FSV} \right] \qquad (A4)$$

Substituting the value of ξ^{o} from equation (51) into equation (A4),

$$\tilde{\lambda} = \lambda - \left\{ \frac{r'}{\bar{r}} \left(1 - \frac{1}{\lambda_1}\right) - \tau'_w(\lambda_1 - 1) \right\}\left\{ \frac{FSV}{FSV-1} \frac{h+1}{h} - \frac{h+1}{h} \right\} - \frac{r'}{\bar{r}} \left(1 - \frac{1}{\lambda_1}\right)\left\{ \frac{h+1}{FSV-1} - \frac{h}{FSV} \right\}$$

$$= \lambda - \frac{r'}{\bar{r}} \left(1 - \frac{1}{\lambda_1}\right)\left\{ \frac{FSV}{h} \frac{h+1}{FSV-1} - \frac{h+1}{h} + \frac{h+1}{FSV-1} - \frac{h}{FSV} \right\}$$

$$- \tau'_w(\lambda_1 - 1)\left\{ \frac{FSV}{h} \frac{h+1}{FSV-1} - \frac{h+1}{h} \right\}$$

$$= \lambda - \frac{r'}{\bar{r}} \left(1 - \frac{1}{\lambda_1}\right)\left\{ \frac{(h+1)}{h(FSV-1)} + \frac{h+1}{FSV-1} - \frac{h}{FSV} \right\} - \tau'_w(\lambda_1 - 1)\left\{ \frac{(h+1)}{h(FSV-1)} \right\} \qquad (62)$$

(ii) Equation (63) from Equation (62)

$$\lambda = (h+1)\ln\left\{ \frac{FSV}{FSV-1} \right\} - \frac{h}{FSV} \quad .$$

During oscillatory combustion,

$$FSV = \overline{FSV} + FSV' \quad .$$

Hence,

$$\lambda = (h+1)\ln\left[\frac{\overline{FSV}\left(1 + \frac{FSV'}{FSV}\right)}{(\overline{FSV}-1)\left(1 + \frac{FSV'}{\overline{FSV}-1}\right)} \right] - \frac{h}{\overline{FSV} + FSV'}$$

$$= (h+1)\ln\left[\left\{ \frac{\overline{FSV}}{FSV-1} \right\} \cdot \left\{ 1 + \frac{FSV'}{\overline{FSV}} \right\} \cdot \left\{ 1 - \frac{FSV'}{\overline{FSV}-1} \right\} \right] - \frac{h}{\overline{FSV}\left(1 + \frac{FSV'}{\overline{FSV}}\right)} \quad .$$

Approximating the logarithmic term, as usual,

$$= (h+1)\ell n\left\{\frac{\overline{FSV}}{\overline{FSV}-1}\right\} - \frac{h}{\overline{FSV}} + (h+1)\frac{\overline{FSV'}}{\overline{FSV}} - \frac{h+1}{\overline{FSV}}\frac{\overline{FSV}\cdot\overline{FSV'}}{(\overline{FSV}-1)} + \frac{h}{\overline{FSV}}\frac{\overline{FSV'}}{\overline{FSV}}$$

$$= (h+1)\ell n\left\{\frac{\overline{FSV}}{\overline{FSV}-1}\right\} - \frac{h}{\overline{FSV}} + \frac{\overline{FSV'}}{\overline{FSV}}\left\{h+1-h\frac{\overline{FSV}}{\overline{FSV}-1} - \frac{\overline{FSV}}{\overline{FSV}-1} + \frac{h}{\overline{FSV}}\right\}$$

$$= (h+1)\ell n\left\{\frac{\overline{FSV}}{\overline{FSV}-1}\right\} - \frac{h}{\overline{FSV}} - \frac{\overline{FSV'}}{\overline{FSV}}\left\{\frac{h+1}{\overline{FSV}-1} - \frac{h}{\overline{FSV}}\right\} . \qquad (A5)$$

From Appendix B it is seen that a good representation of FSV is

$$FSV = \alpha P^{-\beta} \exp(\delta T_w)$$

where α, β, and δ are constants. It is easily seen that

$$\frac{\overline{FSV'}}{\overline{FSV}} = -\beta\frac{\overline{P'}}{\overline{P}} + \frac{\overline{T'_w}}{\overline{T}_w}\delta = -\beta\frac{\overline{P'}}{\overline{P}} + \frac{\overline{T'_w}}{\overline{T}_w - T_o}\frac{\overline{T}_w - T_o}{\overline{T}_w}\delta = -\beta\frac{\overline{P'}}{\overline{P}} + \tau'_w\delta\chi . \qquad (A6)$$

Substitution of equation (A5) into equation (62) and utilization of equation (A6) yields equation (63).

(iii) Solution of Equation (12)

The following solution obtained through the method of matched asymptotic expansions is reproduced from reference 1. It would aid the reader to go over the descriptive discussion of the solution method on page 17.

$$pp' + p = (h+p+\tau)\,\Lambda \exp(-E/\Re T) \qquad (12)$$

$$\tau = 0 : p = 0 ; \qquad \tau = 1 : p = p_w \qquad (13)$$

Outer solution

Away from the wall region, the exponentially small reaction rate term (R. H. S.) can be neglected from equation (12).

$$\frac{d^2\tau}{dy^2} + \frac{d\tau}{dy} = 0 \qquad (A7)$$

$$\tau = 0 : p = 0 \qquad (A8)$$

$p = -\tau$ is the solution to equations (A7) and (A8) to all orders. The solution cannot satisfy the hot boundary condition because equation (A7) is not valid near the hot boundary.

Inner solution

The large activation energy encountered in degradation reactions limits the temperature range of interest to very small values around the wall temperature. Hence, equation (12) may be approximated near the wall as

$$pp'+p \doteq (h+p+\tau)\Lambda \exp\{-\theta_a[1+\chi(1-\tau)]\} \quad . \tag{A9}$$

Since Λ is a very large number (it has B in it), it is convenient to define

$$\text{א} \equiv \Lambda \exp(-\theta_a)$$

and get

$$pp'+p = (h+p+\tau)\text{א} \exp\{-\theta_a\chi(1-\tau)\} \quad . \tag{A10}$$

Identifying the small parameter, $\epsilon \equiv 1/\theta_a\chi$, and defining the inner variables,

$$\eta \equiv (1-\tau)/\epsilon \quad , \quad \xi \equiv (p+\tau) \quad ,$$

along with a new nondimensional regression rate $\lambda \equiv \epsilon\text{א}$, we write equation (A10) as

$$-(\xi-1+\epsilon\eta)\xi' = (h+\xi)\lambda \exp(-\eta) \quad . \tag{A11}$$

Here, a prime denotes differentiation with respect to η.

At $\tau = 1$ (on the wall), $\eta = 0$

$$\eta = 0 \; : \; \xi_w = p_w+\tau_w = -1 - \frac{h}{FSV} + 1 = -\frac{h}{FSV} \quad . \tag{A12}$$

Making the expansions,

$$\xi = \xi_o + \epsilon\xi_1 + \epsilon^2\xi_2 + \epsilon^3\xi_3 + \ldots$$

$$\lambda = \lambda_o + \epsilon\lambda_1 + \epsilon^2\lambda_2 + \epsilon^3\lambda_3 + \ldots$$

and substituting these expansions into equation (A11), we get to zero order

(the subscript 0 has been dropped here),

$$\xi' - \xi'\xi = (h+\xi)\,\lambda \exp(-\eta) \quad . \tag{A13}$$

Equation (A13) is better written as

$$\frac{d\xi}{h+\xi} - \frac{\xi\, d\xi}{h+\xi} = \lambda \exp(-\eta) d\eta \quad , \tag{A14}$$

which integrates to

$$\ell n(h+\xi) - [\xi - h\,\ell n(\xi+h)] = -\lambda e^{-\eta} + (\text{a constant}) \quad . \tag{A15}$$

Kaplun's matching theorem requires

(inner limit of the outer solution) = (outer limit of the inner solution)

or

$$p^{\text{outer}}_{\tau\to 1} = p^{\text{inner}}_{\eta\to\infty} \quad ,$$

which gives $\xi = 0$ as $\eta \to \infty$, yielding through equation (A15) the value of the constant as

$$(h+1)\,\ell n\, h \quad .$$

Substituting this value into equation (A15), we get

$$(h+1)\ell n(h+\xi) - \xi = -\lambda \exp(-\eta) + (h+1)\ell n\, h \quad . \tag{A16}$$

Using the boundary condition on the wall, namely,

$$\xi = -\frac{h}{FSV} \quad \text{on} \quad \eta = 0 \quad ,$$

we get

$$\lambda = (h+1)\,\ell n\left\{\frac{FSV}{FSV-1}\right\} - \frac{h}{FSV} \quad , \tag{A17}$$

which was quoted earlier as equation (14).

APPENDIX B. The Fragment Size Vaporizing FSV

The importance of the statistical mean size (FSV) of fragments vaporizing from the wall cannot be overstated. Specification of FSV through a scientific procedure (which has often been taken as arbitrary in the older literature) was seen to hold the key to a host of problems in hybrid combustion. Throughout the present study we have had ample opportunities for recognizing the role of FSV in the deflagration of composites. We thus feel the need for a quick rule for evaluating the FSV as a function of wall temperature and chamber pressure.

After some study of API hydrocarbon vapor-pressure data, the following rule was evolved to predict the fragment weight as a function of interface temperature (^{o}K) and chamber pressure (atmospheres).

$$\mathfrak{m} = 32.8\, P^{-0.2615} \cdot \exp(3.67 \times 10^{-3} T_w) . \qquad (B1)$$

The equation has been evolved to slide rule accuracy and no minimum-error procedure has been employed. The equation has not been tested beyond the temperature range available in API charts (i.e., T = 1200^{o}F or 922^{o}K). However, the extremely smooth data trend within this range appears to justify extrapolations as have been necessitated on occasions in the application of the above rule to composite propellant burning.

For AP (molecular weight 117.5) the above rule takes the form

$$FSV = 0.2795\, P^{-0.2615} \exp(3.67 \times 10^{-3} T_w) . \qquad (B2)$$

It seems more than probable that the weak power law for pressure effect is an approximation for a logarithmic law (which may be evolved through more accurate curve fit procedures). Such a logarithmic law would also seem more physical. In any case, the rule has been found to possess very good accuracy.

C 2

Consider a linear chain of $(n_\infty + 1)$ elements (beads) having n_∞ bonds in the chain. We follow the degradation of this chain to smaller fragments. If n_b bonds are broken in the original chain, the number of fragments originating is $(n_b + 1)$. The mean size of the fragments, i.e., the number of elements in a fragment-chain is

$$FS = \frac{n_\infty + 1}{n_b + 1} \quad .$$

The number of bonds broken in the original chain is the original number n_∞ minus the total number of bonds n_r remaining now. Hence,

$$FS = \frac{n_\infty + 1}{n_\infty - n_r + 1} \quad .$$

If $n_\infty \sim 10^3$ we may neglect unity in comparison with n_∞, and write

$$FS = \frac{n_\infty}{n_\infty - n_r} = \frac{1}{1 - \frac{n_r}{n_\infty}} \quad .$$

Denoting by N the fractional number of bonds, n_r/n_∞, we get

$$N = 1 - \frac{1}{FSV} \quad . \qquad \text{(B3)}$$

APPENDIX C. THE MELT LAYER

To eliminate any arbitrariness associated with the useful concept of a melt layer on the surface of regressing AP, the following treatment is given as a first approximation. This treatment is an almost exact reproduction from ref. 8.

Although we normally use in it the wall values of temperature and fragment size, equation (14) is quite general and predicts the regression rate of any homogeneous material if the quantities, temperature and fragment size can be specified at a plane in the material. A parametric plot of equation (14) would look like fig. A-1. The higher the mean molecular weight (fragment size), the higher will be the regression rate. This is because a higher fragment size implies a smaller number of bonds to be broken from the deep solid value, and it can be accomplished at a higher rate. The important point to note is that the regression rate is the same for all planes in the material.

A clear discussion in the Encyclopedia of Chemical Technology[35] indicates a correlation of the following form between the molecular weight of a substance and its melting point:

$$\log M = A_o + B T_m .$$

Typical values of A_o and B are available[35] for families of molecules. In the degrading AP, the "molecular" weight at any plane is simply the product of fragment size at that plane and the molecular weight of the fundamental NH_4ClO_4 (117.5). Hence, the melting point vs. molecular weight correlation would be of the form indicated by the broken line in fig. A-1.

At a specified regression rate r_A let us follow the changes in a plane as the plane moves from the low-temperature interior to the high-temperature

surface. At an intermediate station 1 , the temperature is T_1 and the fragment size is FS_1 . At the intermediate station 2 , the fragment size is FS_2 and the temperature is T_2 . Now, as shown in fig. A-1, this also happens to be the melting point of a material of molecular size FS_2 . The AP melts at this temperature, and the rest of the travel of this plane till the wall, i. e., temperature T_3 , is through the melt layer. That is, the intercept 2 - 3 represents the melt layer. Now consider a higher regression rate r_B . We can see through the above arguments that the melt layer now represents a smaller intercept 2 - 3 at B than at A . At the limiting regression rate r_C , the melting point of the fragment size at the wall happens to exactly equal the wall temperature, so that the limiting condition of zero melt-layer thickness is reached. At a still higher regression rate r_D , the melt layer is imaginary because the melting point of the fragment size at the wall is higher than the wall temperature.

The temperature intercept 2 - 3 may be related to the physical thickness through the temperature profile solution to the energy equation.

Although the limiting case of vanishing melt layer is exactly valid, it should be carefully noted that the preceding arguments are not applicable in a rigorous manner to the postulated liquid layer invoked elsewhere in this report. This is because the melt layers have been taken as isothermal in those applications; that is, different from the temperature solution to the energy equation as used here in Appendix C. It is expected that the arguments would, however, be valid in an "average" manner, considering the very small thickness of the melt layers encountered.

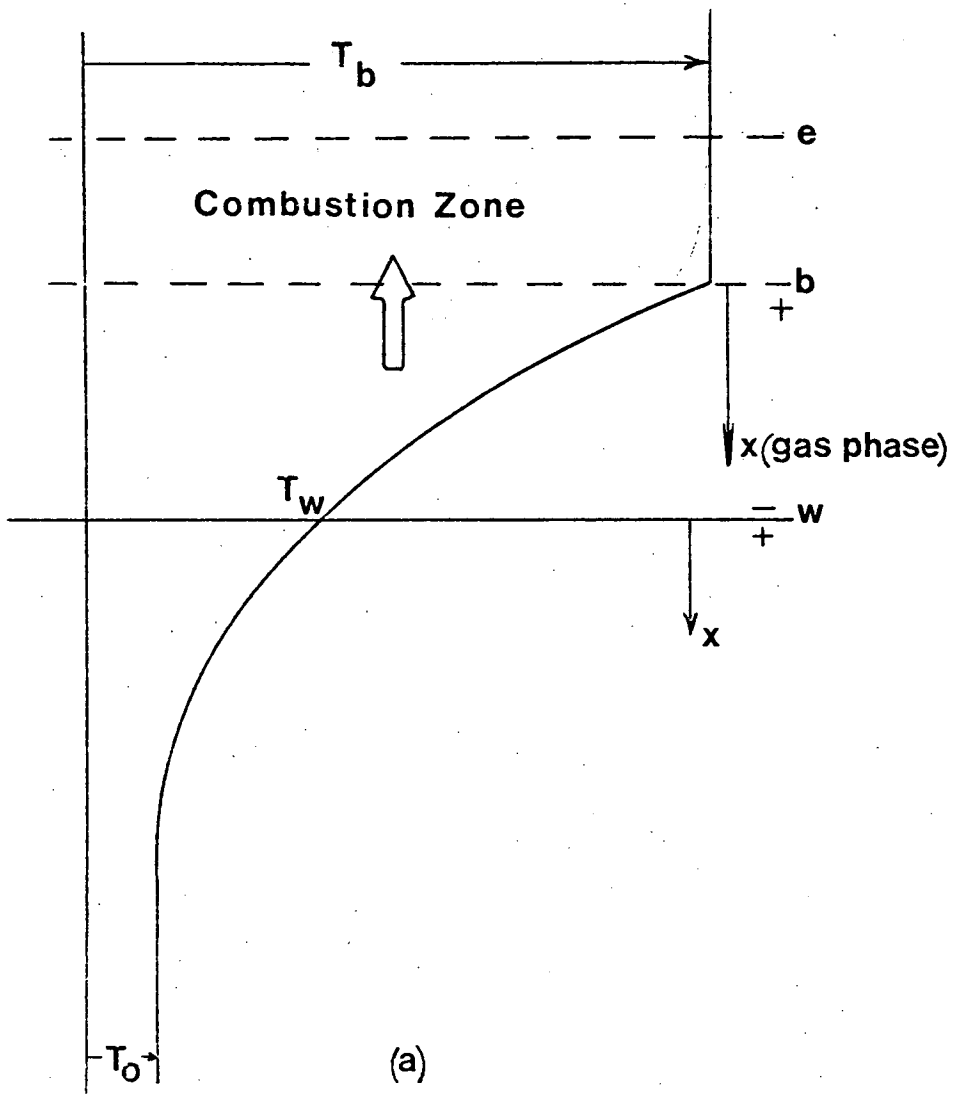
T_b
e
Combustion Zone
b
+
x(gas phase)
T_w
w
+
x
T_o
(a)

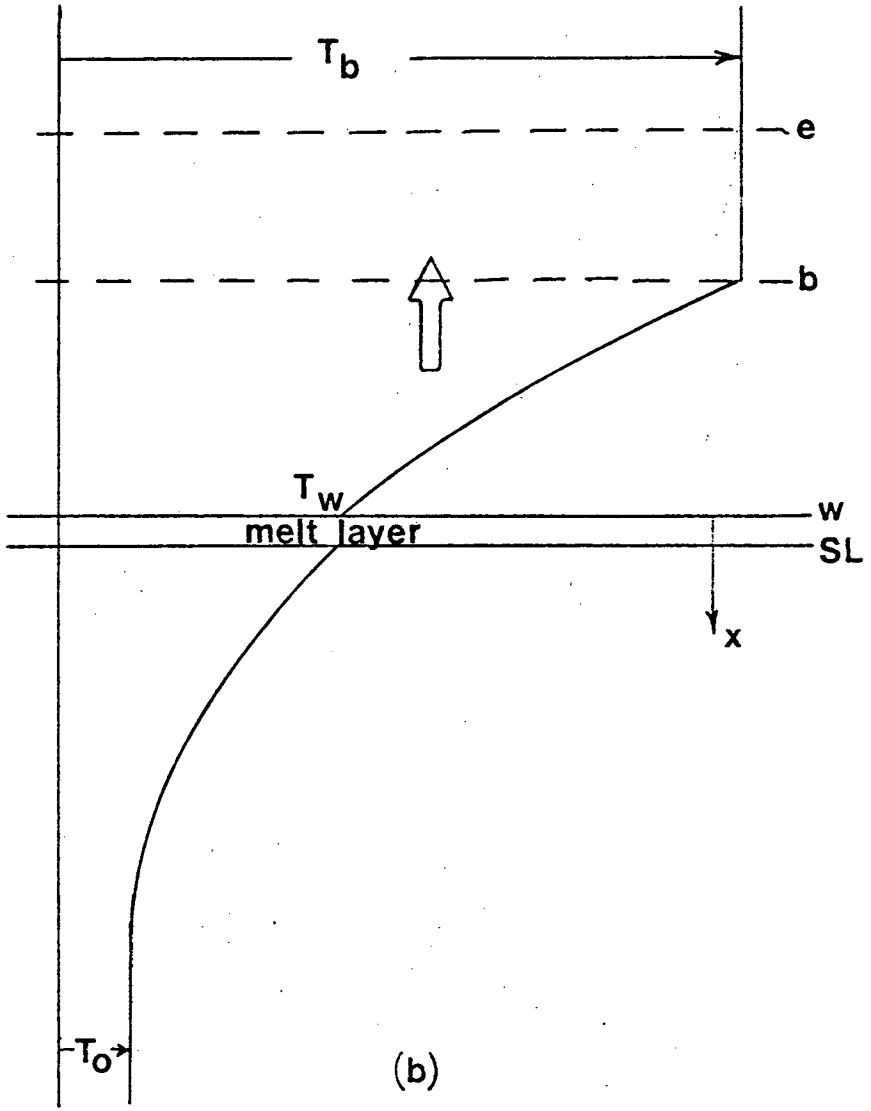
T_b
e
b
T_w
w
melt layer
SL
x
T_o
(b)

Fig·1

90

Figure 1(c). Details of the Postulated Model for Composite Propellant Combustion.

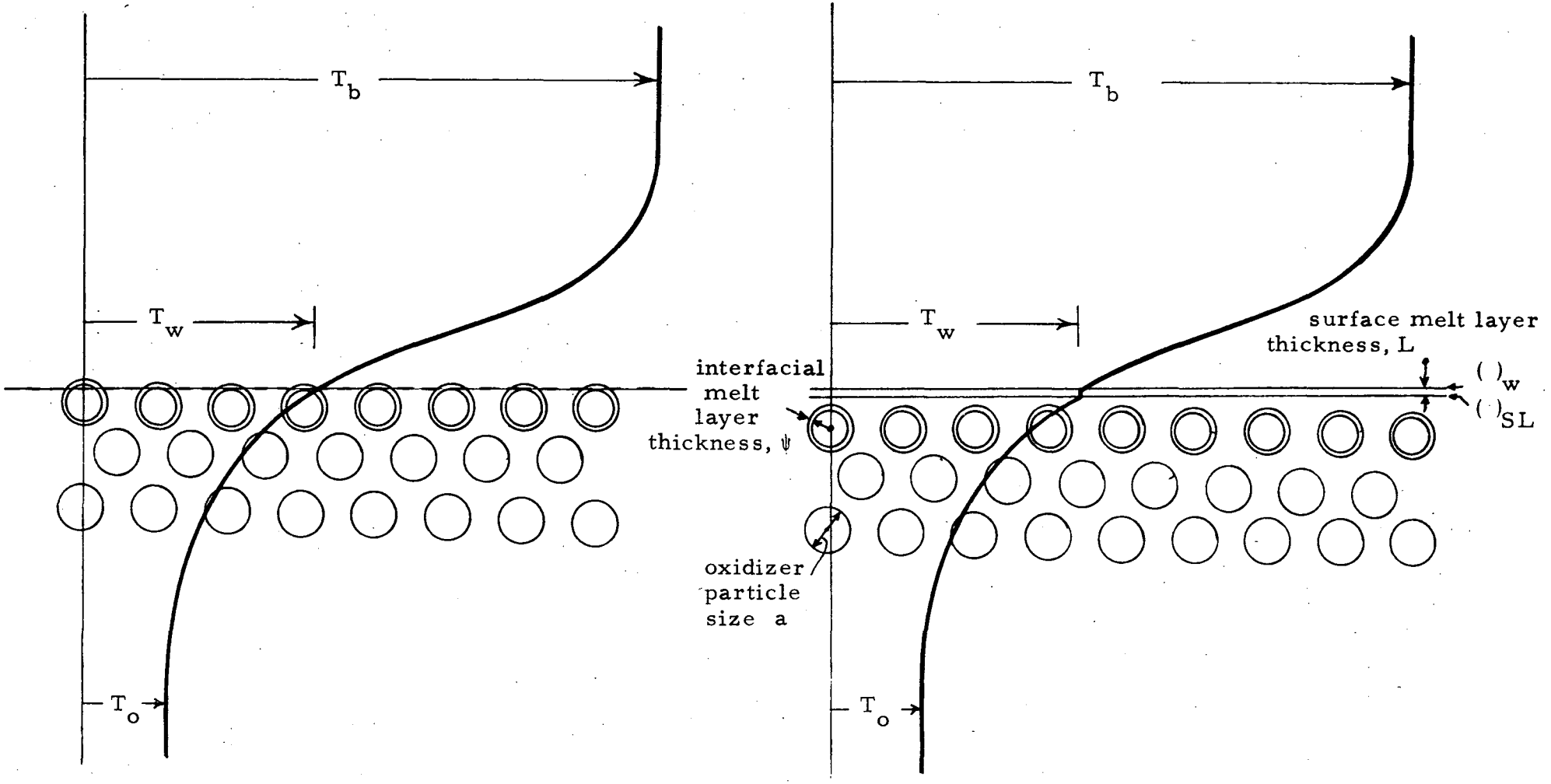

(a) Subsurface Reactions Only

(b) Surface Reactions in a Melt Layer Augmenting Subsurface Reactions.

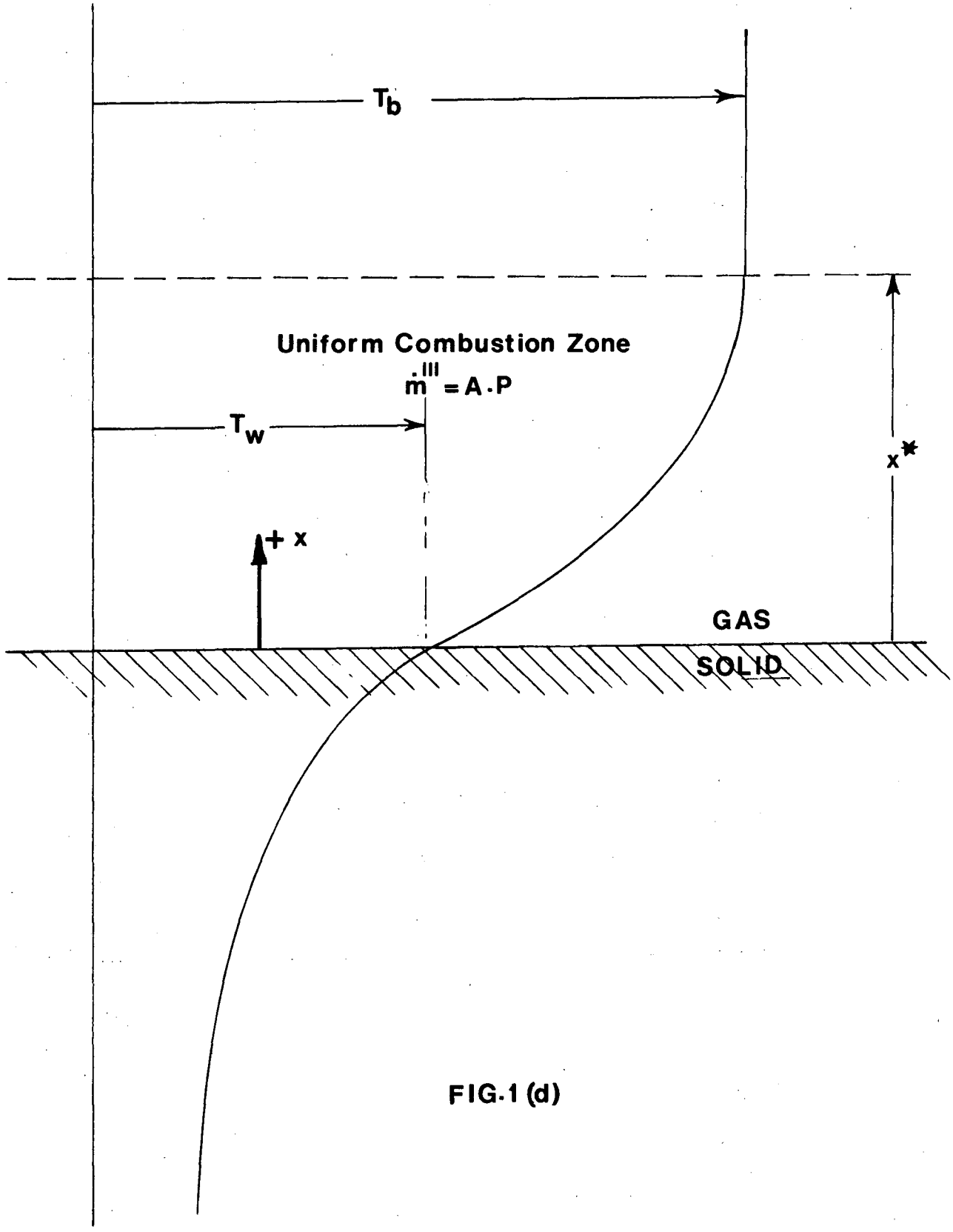

FIG.1 (d)

Figure 1(e). Temperature Gradients During Oscillatory Combustion

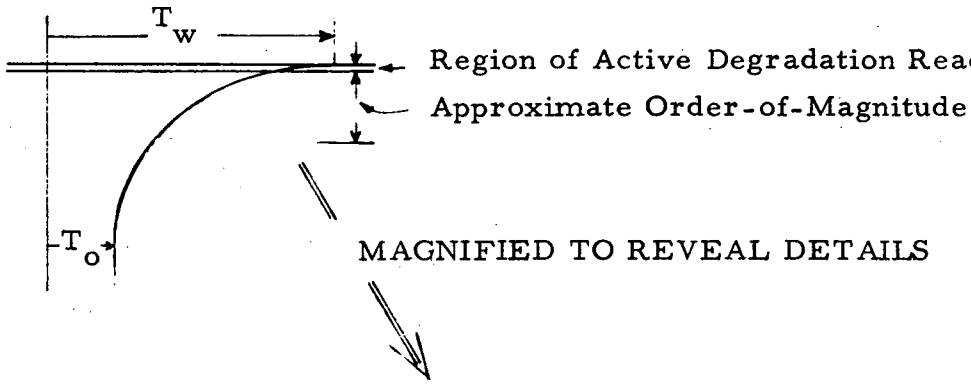

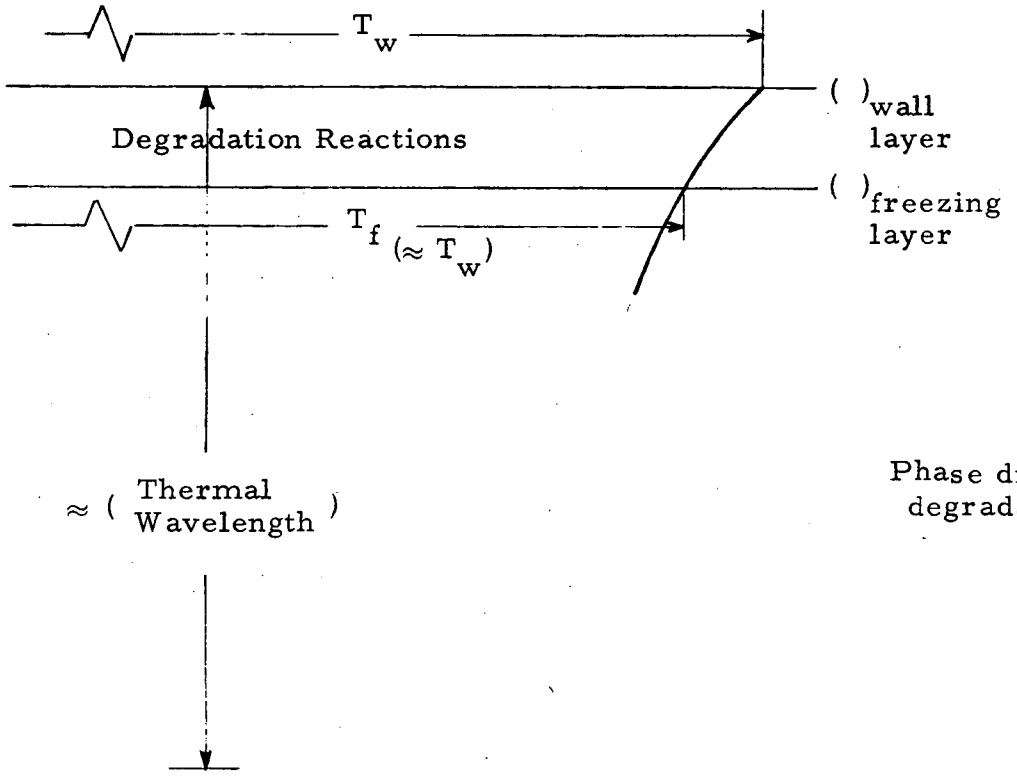

Normalized Steady Part	Temperature Gradient Oscillatory Part
$\left(1 + \frac{h}{FSV}\right)$	$\lambda_1 \tau'_w + \left(1 + \frac{h}{FSV}\right) \frac{1}{\lambda_1} \frac{r'}{\bar{r}}$
1	$\lambda_1 \tau'_w + \frac{1}{\lambda_1} \frac{r'}{\bar{r}}$

Phase differences may be neglected across the degradation zone.

93

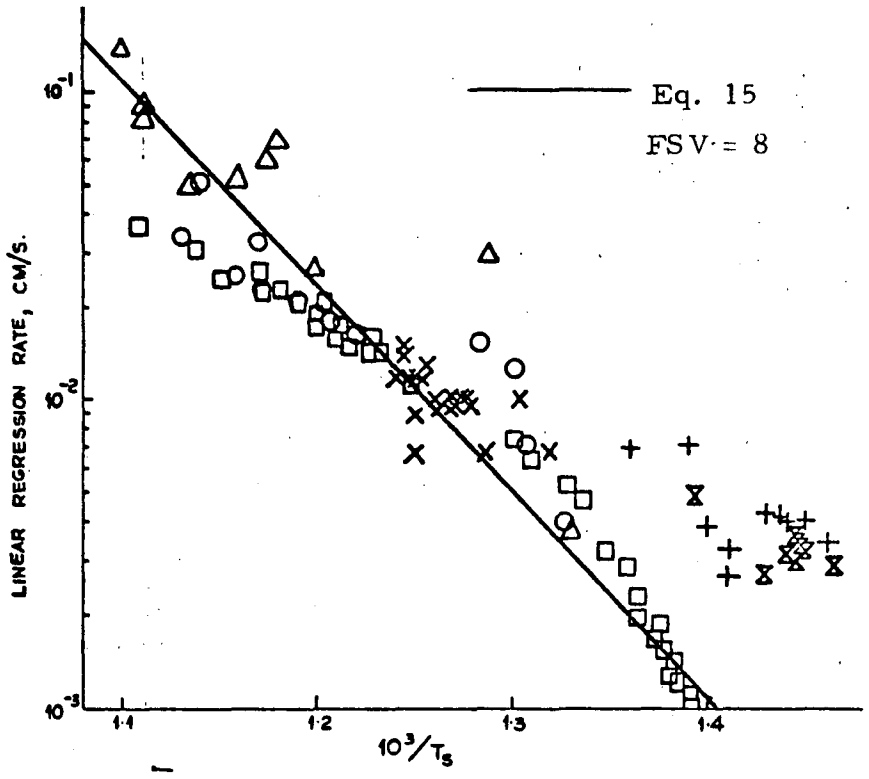

Linear pyrolysis of ammonium perchlorate. Hot-plate pyrolysis: △ Andersen and Chaiken (Ref. 7); ○ Coates (Ref. 8); □ ONERA (Ref. 1). Diffusion-flame pyrolysis (all from this work): × in 760 mm Hg of (H_2 + N_2) See Note 1; ⧖ in 30–35 mm Hg of (H_2 + N_2) see Note 1; + in 100–200 mm Hg of (CH_4 + N_2) see note 2.

Notes:
(1) 1-in. diameter disks of AP burning in counterflow of gas with infrared surface temperature measurement, see Ref. 3, Fig. 1b(c).
(2) Half-inch-square section rods, burning in parallel flow of (CH_4 + N_2); Ref. 18.

Fig. 2. Theoretical Predictions for AP and Comparisons with Hot Plate Data from Powling[9].

Fig. 3(a). Linear Regression Rate of Self Deflagration - Flame Heated AP. Prediction through eqn. (10) and comparison with experimental data[4]. (Assumed wall temperature, $T_w = 900^{\circ}K$)

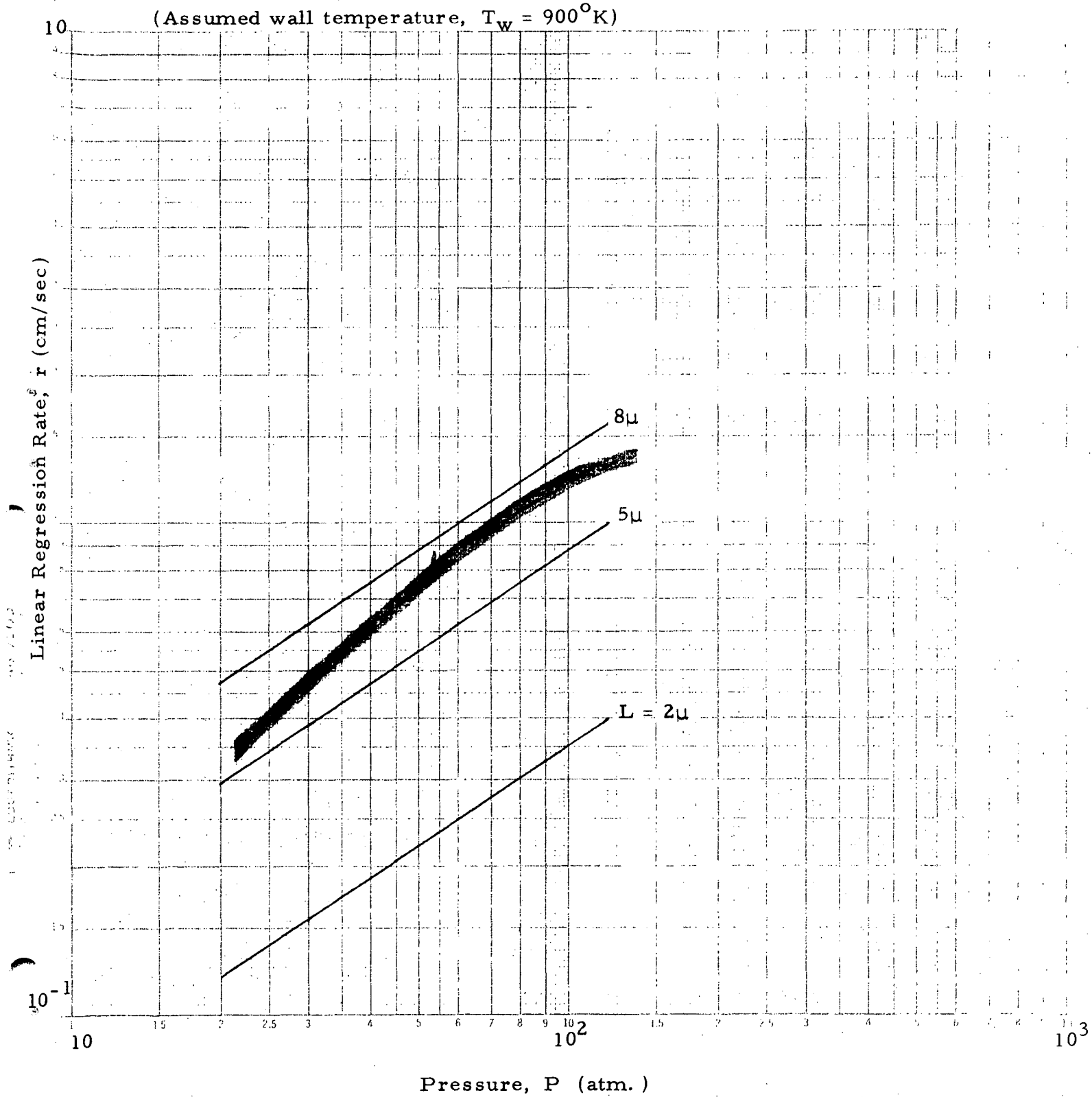

Fig. 3(b). Same as fig. 3(a); sensitivity to initial temperature, T_o. Comparison with experimental data[26].

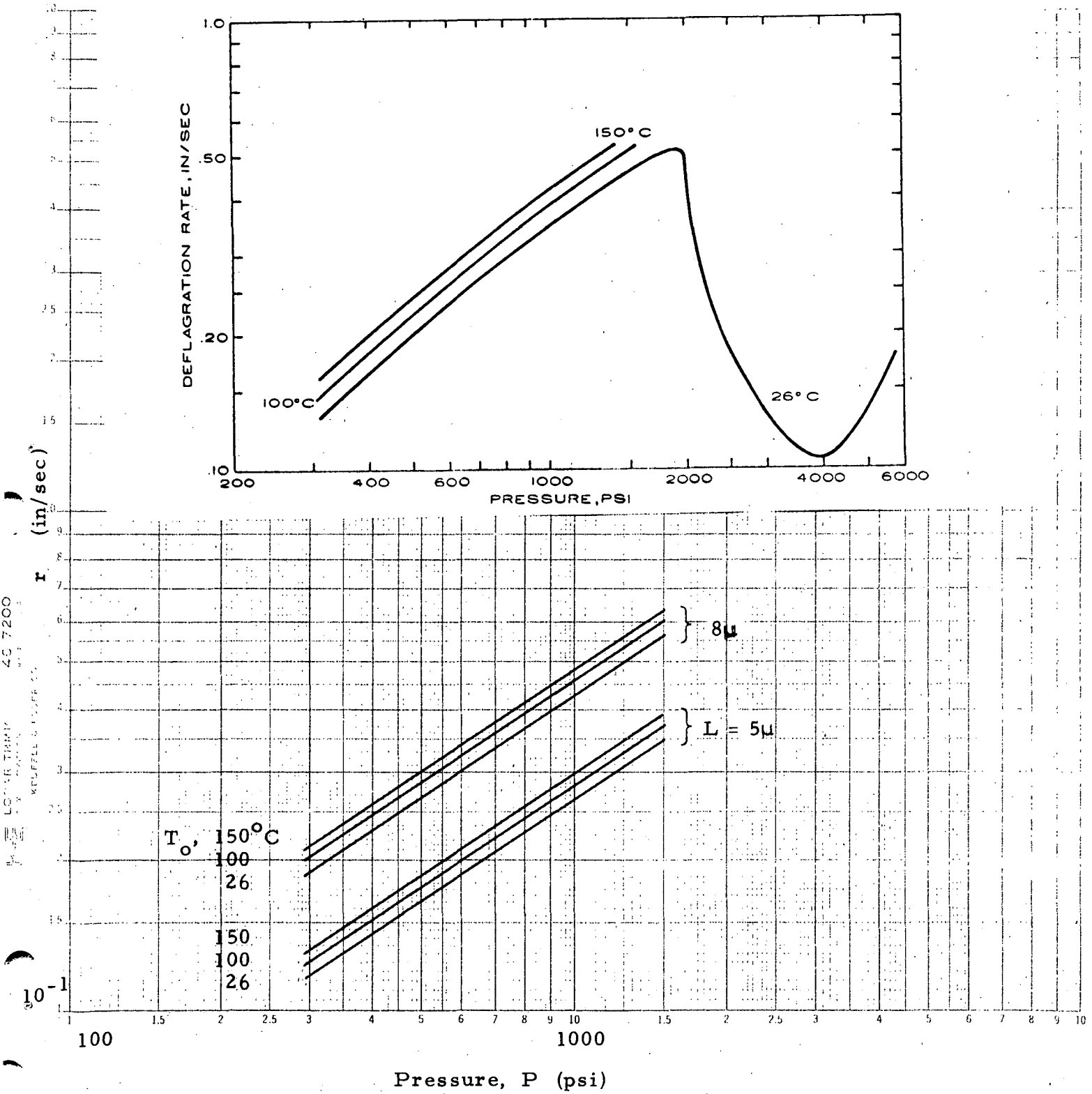

Theoretical Predictions for a Typical Composite Propellant
Considering Subsurface Reactions Only

Mass fractions: 0.75 AP, 0.25 CTPB (binder kinetics from ref. 24)
AP particle size, a: 90 μ
Interfacial reaction layer thickness, ψ: 5 μ

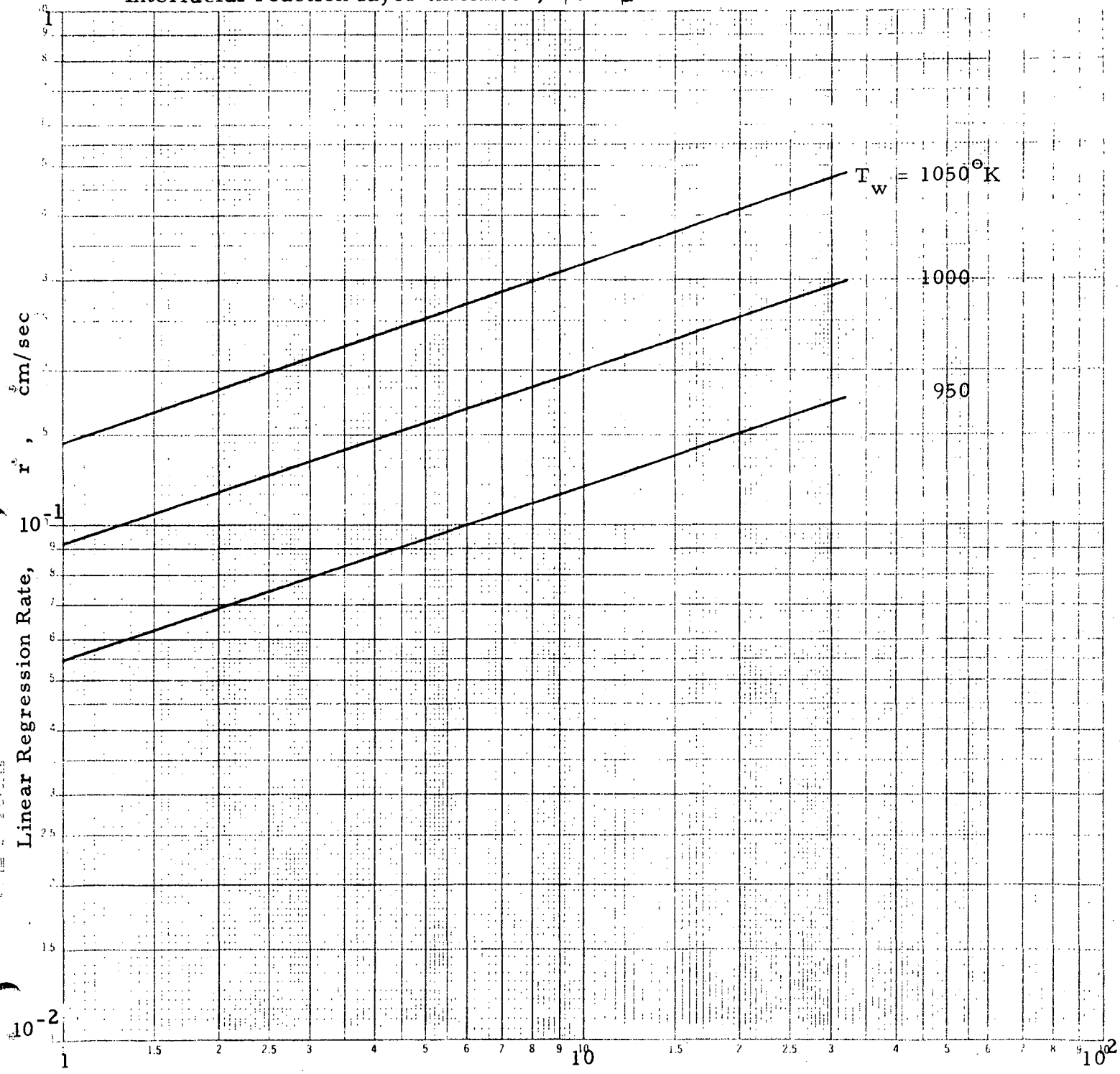

06/28/72 19:48:58

Figure 4(a).

Theoretical Predictions for a Typical Composite Propellant
Considering Subsurface Reactions Only

The Assumption of Uniform Combustion in the Gas Phase,

$\dot{m}''' = A \times P$ (gm/cm^{3}sec)

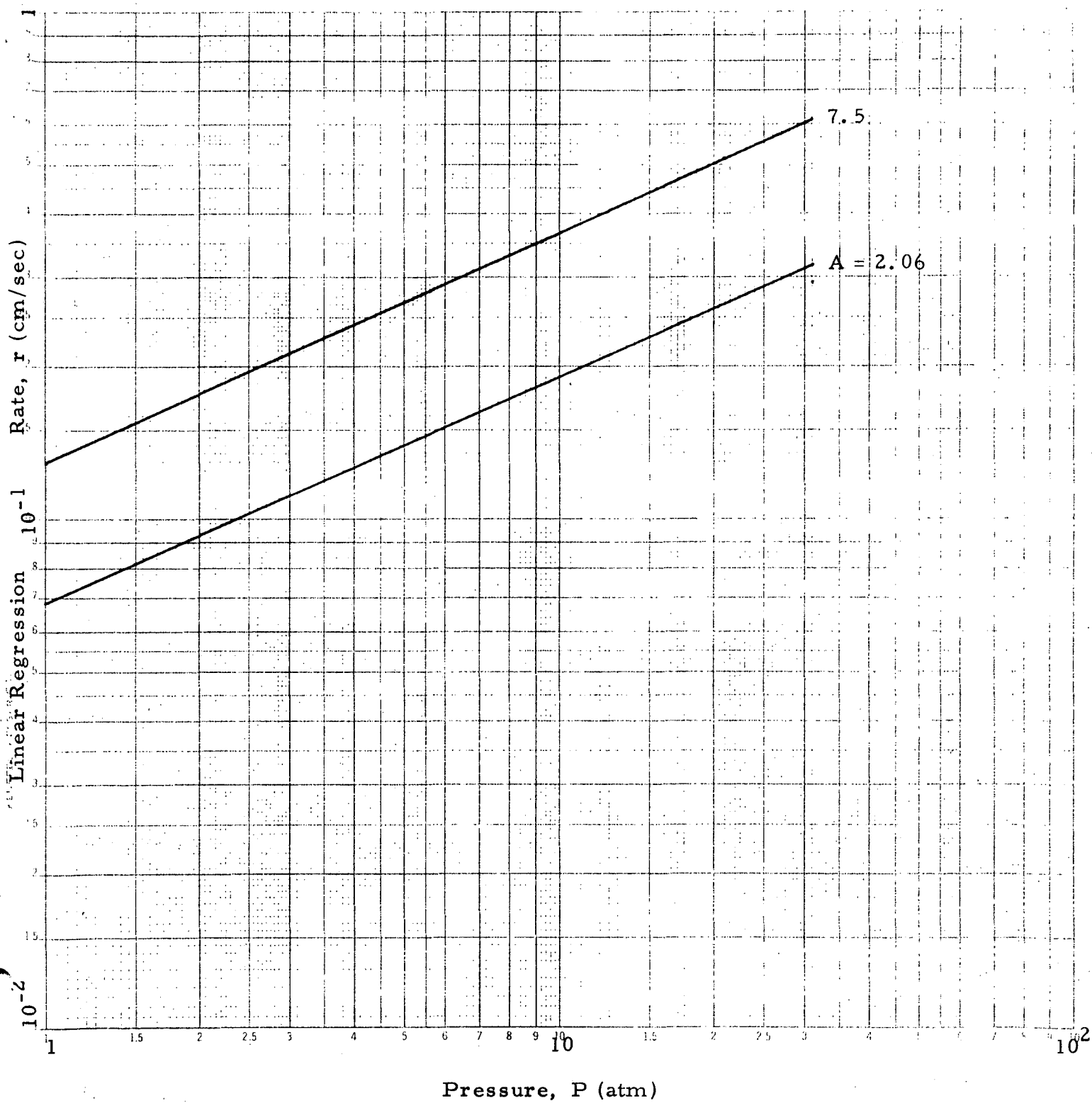

Figure 4(b).

04/29/72 20:22:36

Typical Composite Propellant. Surface Reactions in Melt Layer Augmenting Subsurface Reactions.

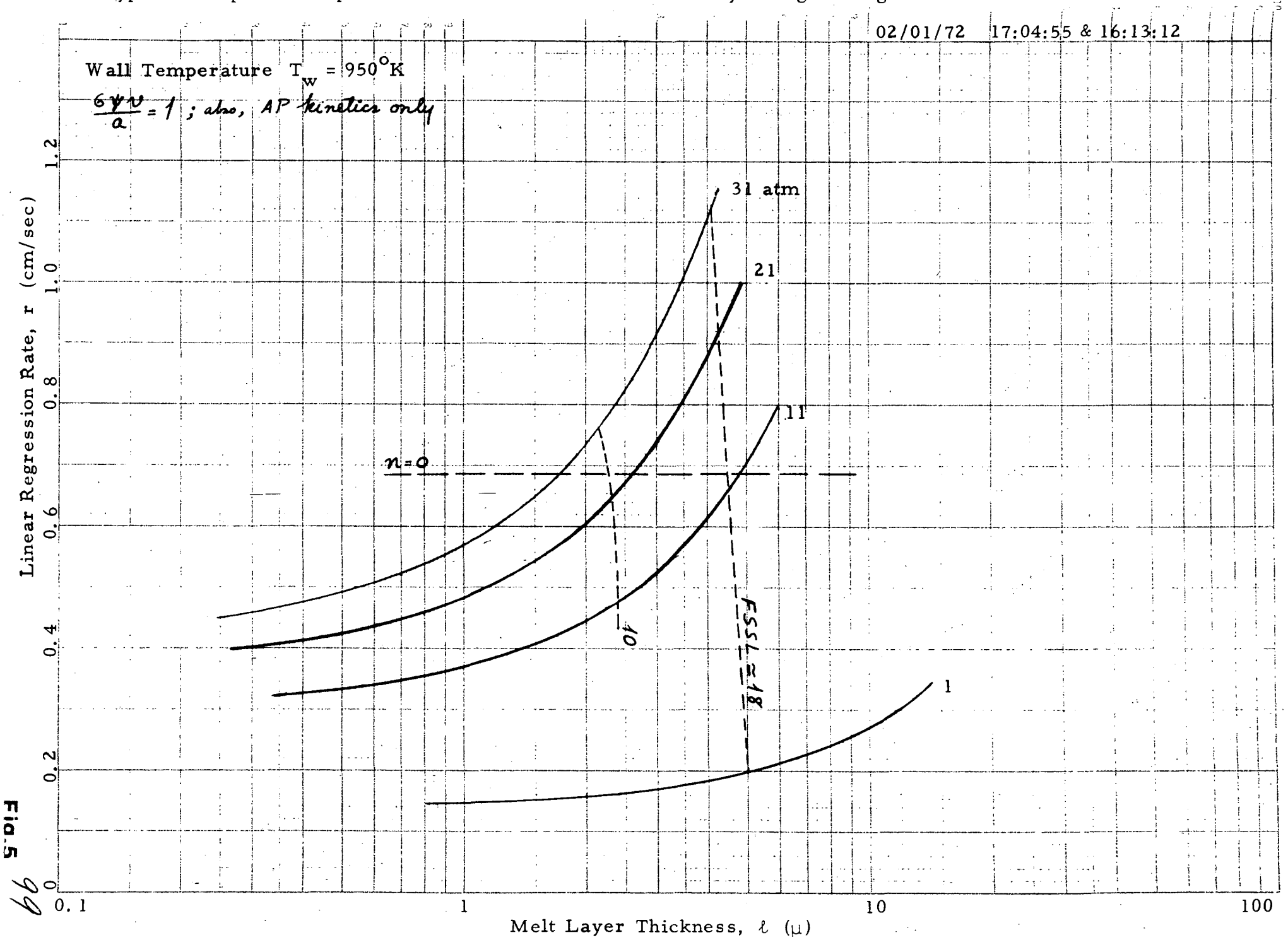

Fig. 5

Theoretical Predictions for a Typical AP Composite Propellant

Surface Reactions in the Melt Layer (Thickness ℓ)

Augmenting Subsurface Reactions

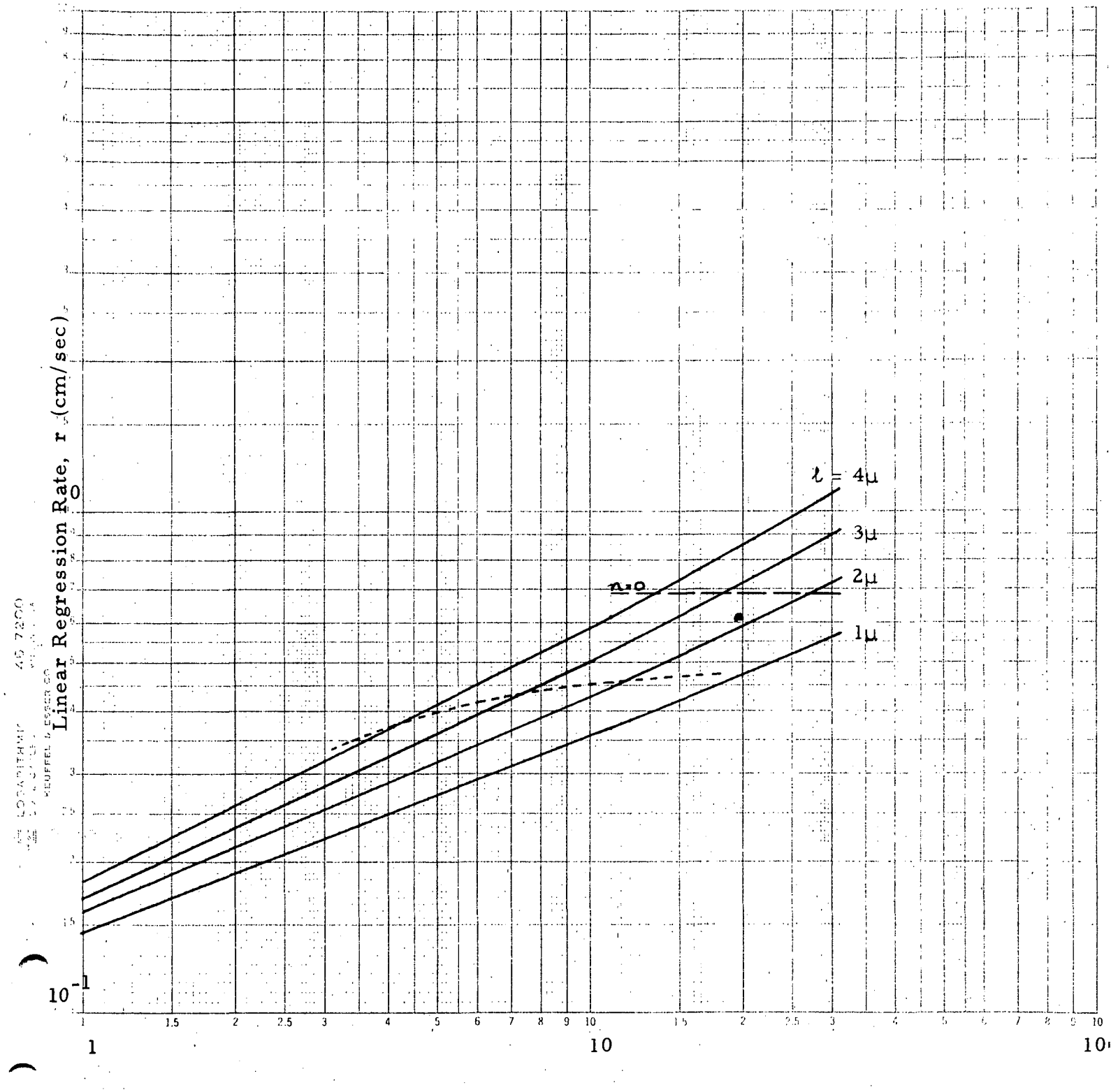

Pressure, atm.

Fig.6

100

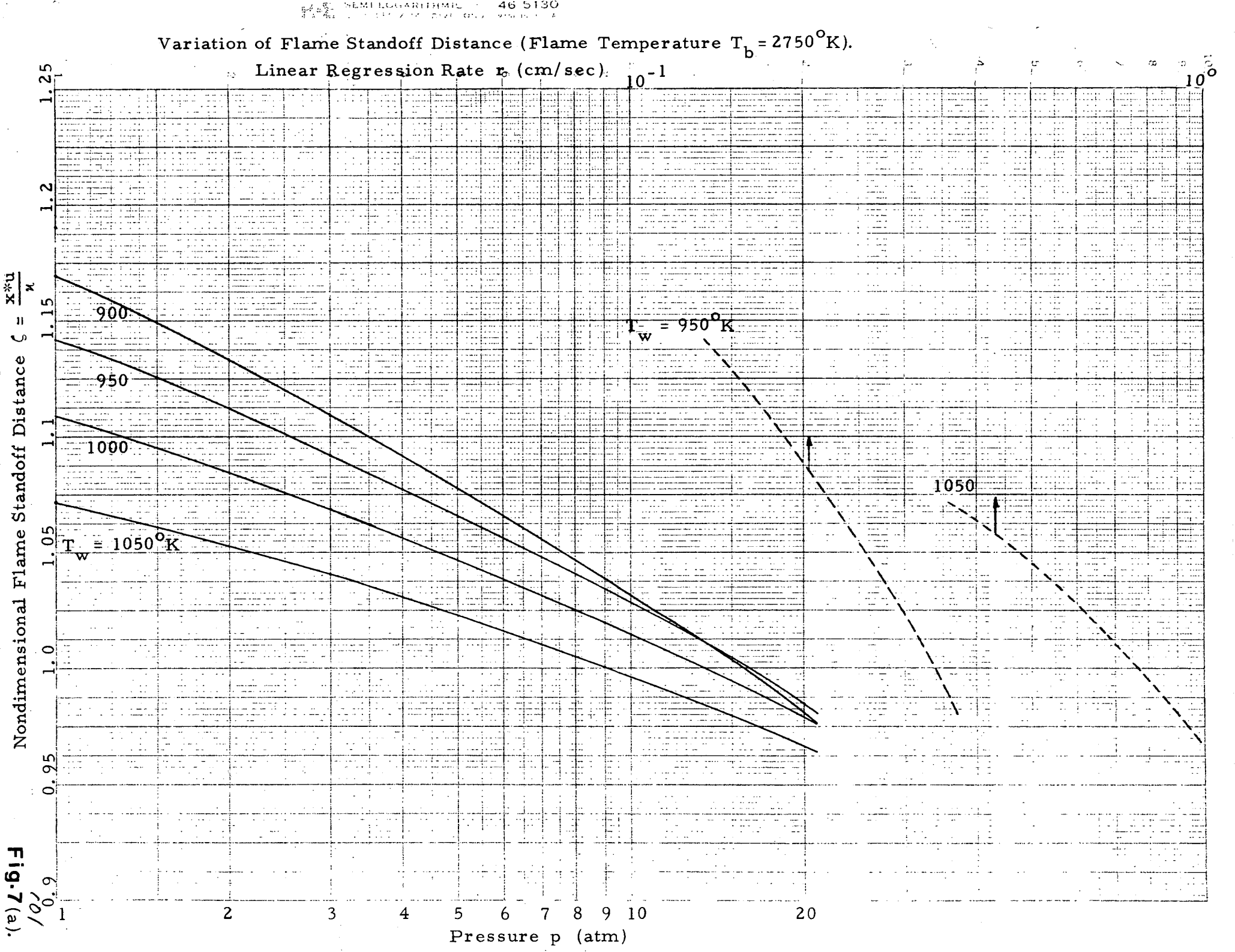
SEMILOGARITHMIC 46 5130
Variation of Flame Standoff Distance (Flame Temperature $T_b = 2750^\circ K$).
Linear Regression Rate r_b (cm/sec)
10^{-1}
10^0
Nondimensional Flame Standoff Distance $\zeta = \frac{x^* u}{\nu}$
1.25
1.2
1.15
1.1
1.05
1.0
0.95
0.9
900
950
1000
$T_w = 1050^\circ K$
$T_w = 950^\circ K$
1050
1
2
3
4
5
6
7
8
9
10
20
Pressure p (atm)

Fig. 7 (a).

Fig. 7(b). Variations of Wall Temperature and the Flame Standoff Distance under the Assumption of Uniform Combustion in the Gas Phase

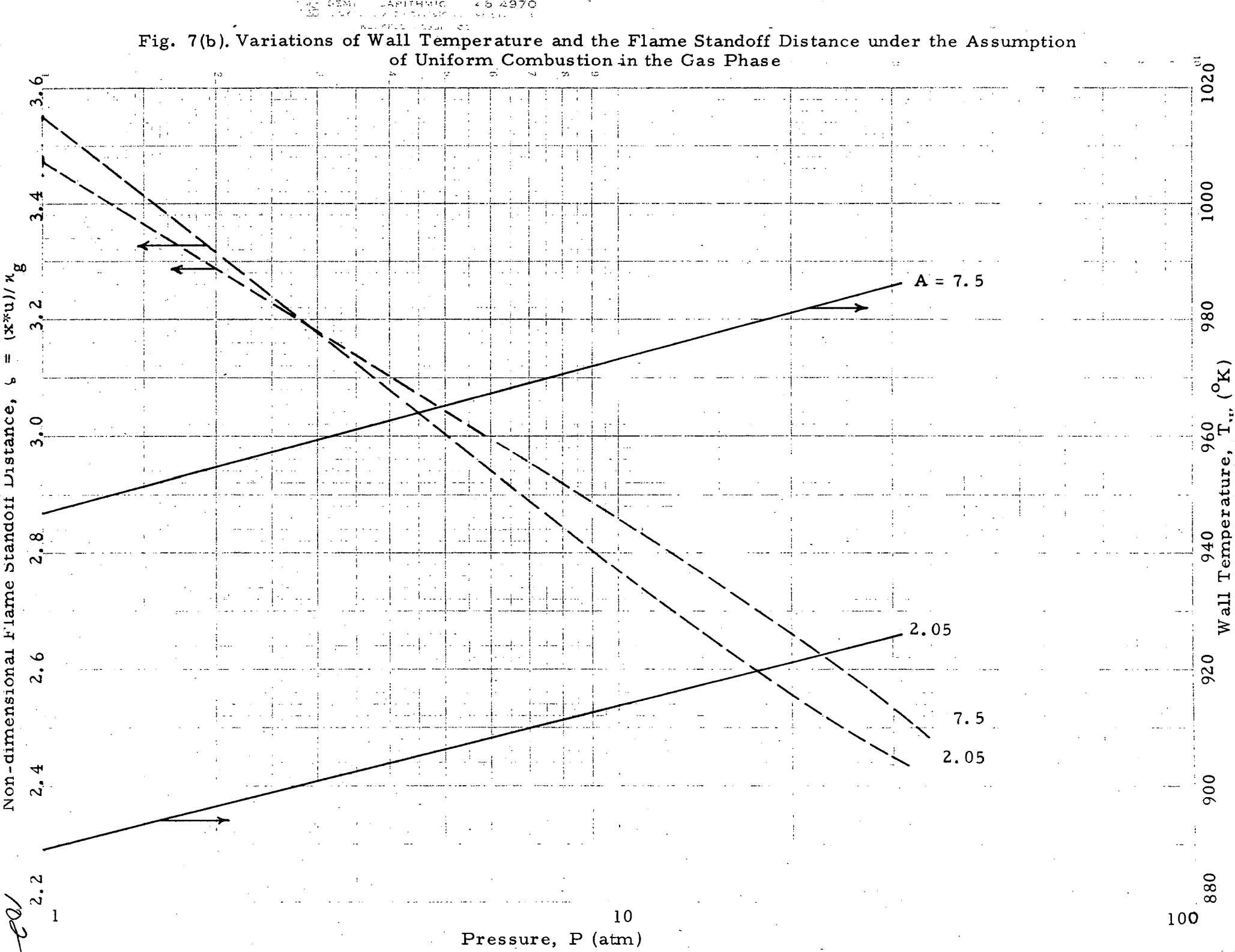

Fig. 7(c). Variations of Wall Temperature and the Flame Standoff Distance under the Assumption of Uniform Combustion in the Gas Phase

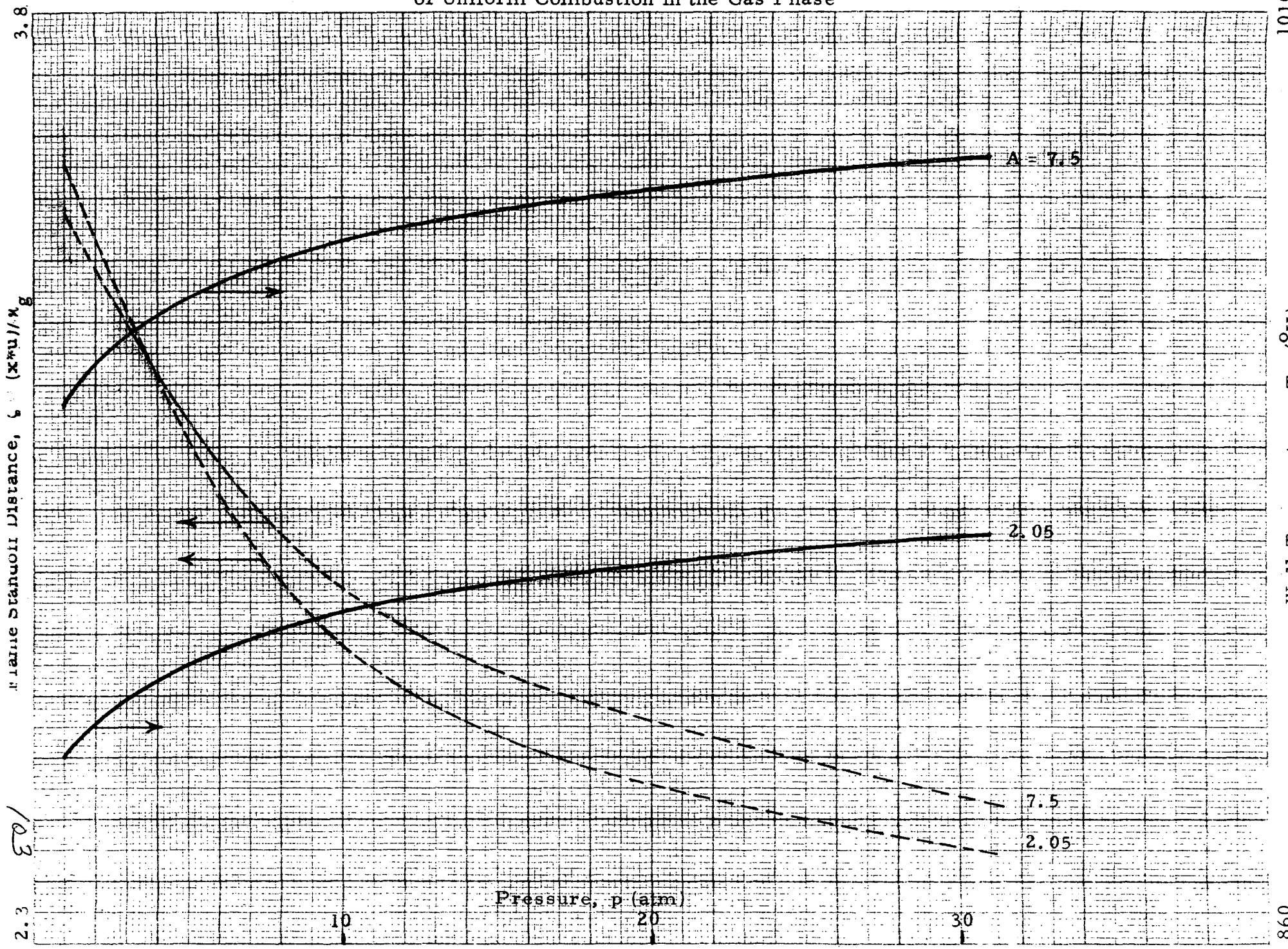

SEMI LOGARITHMIC 46 5490

Composite Propellant with Subsurface Reactions Only. Adiabatic Index for the Gases, $\gamma = 1.25$

02/10/72 06:09:26

31

21

11

P = 1 atm

$\frac{1}{n} \frac{dp}{dt} \left(\frac{r'}{r} \cdot \frac{\bar{p}}{p_T} \right)$

$\Omega \equiv \omega \kappa / \bar{r}^2$

0.025 0.25 2.5 25

1 2 3 4 5 6 7 8

Fig. 8(a).

K+E SEMI-LOGARITHMIC 46 6013
4 CYCLES X 70 DIVISIONS
KEUFFEL & ESSER CO.

Fig. 8(b). Composite Propellant with Subsurface Reactions Only. Uniform Combustion Model for the Gas Phase.

04/28/72 12:35:58

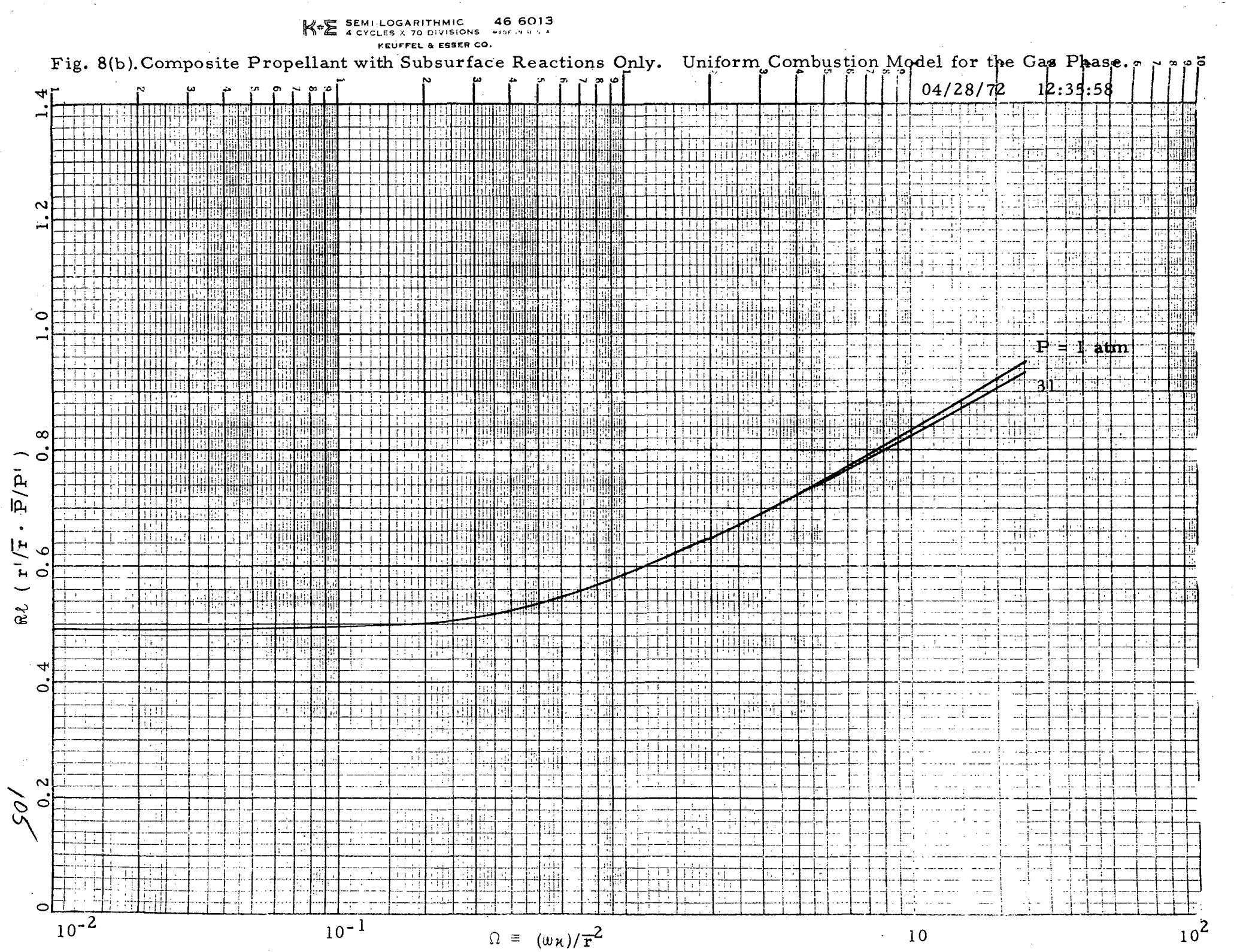

501

5 X 5 TO ½ INCH 46 0862
KEUFFEL & ESSER CO

Fig. 9. Response function for a composite propellant; case (i), constant thickness of melt layer (eq. 82). 12:48:52

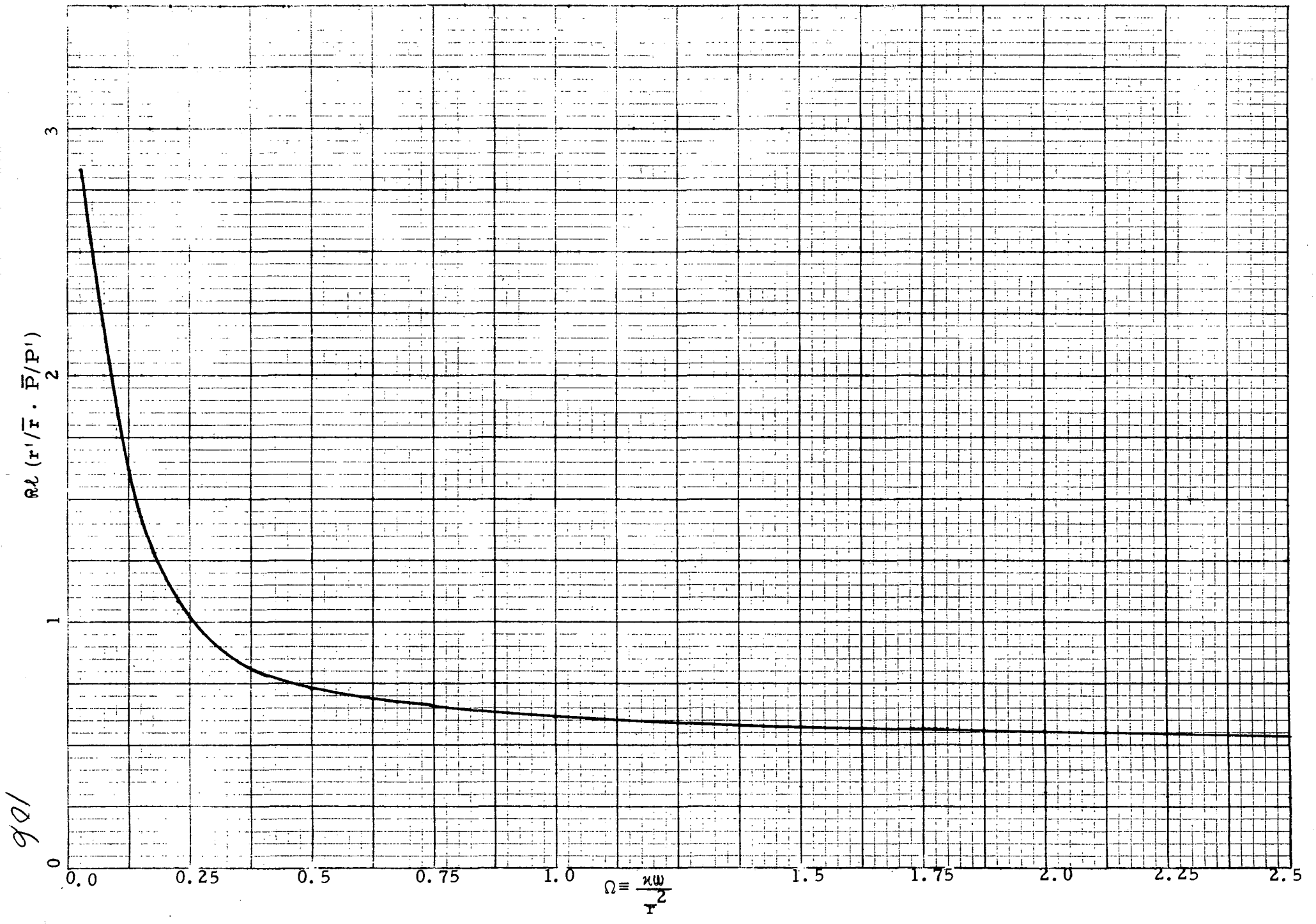

901

Fig.10(a) Response function for a propellant having n = 0 (eq. 89; see also Sec. VI).

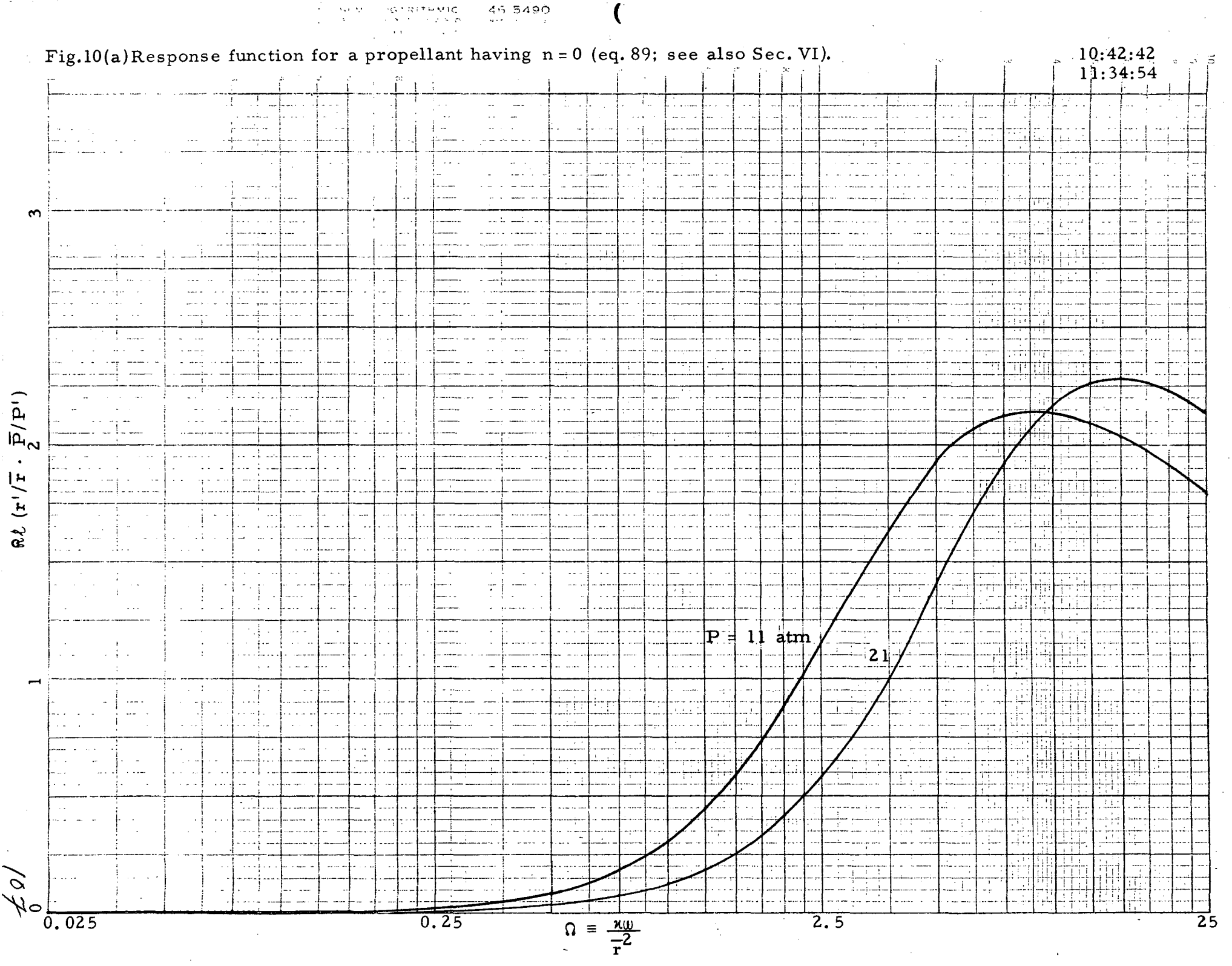

Fig.10(b). Response Function for a Propellant Having n = 0, Uniform Combustion in the Gas Phase.

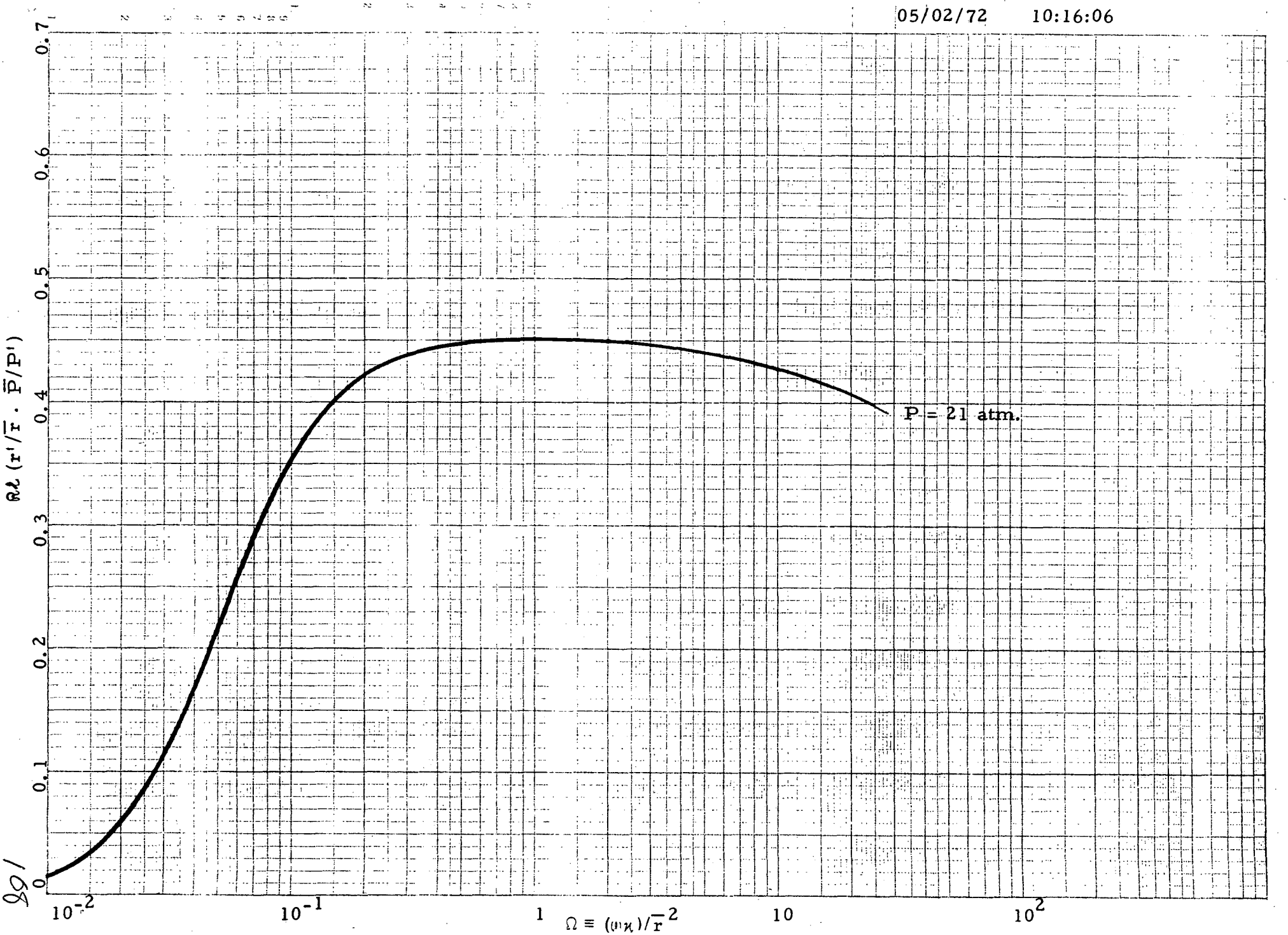

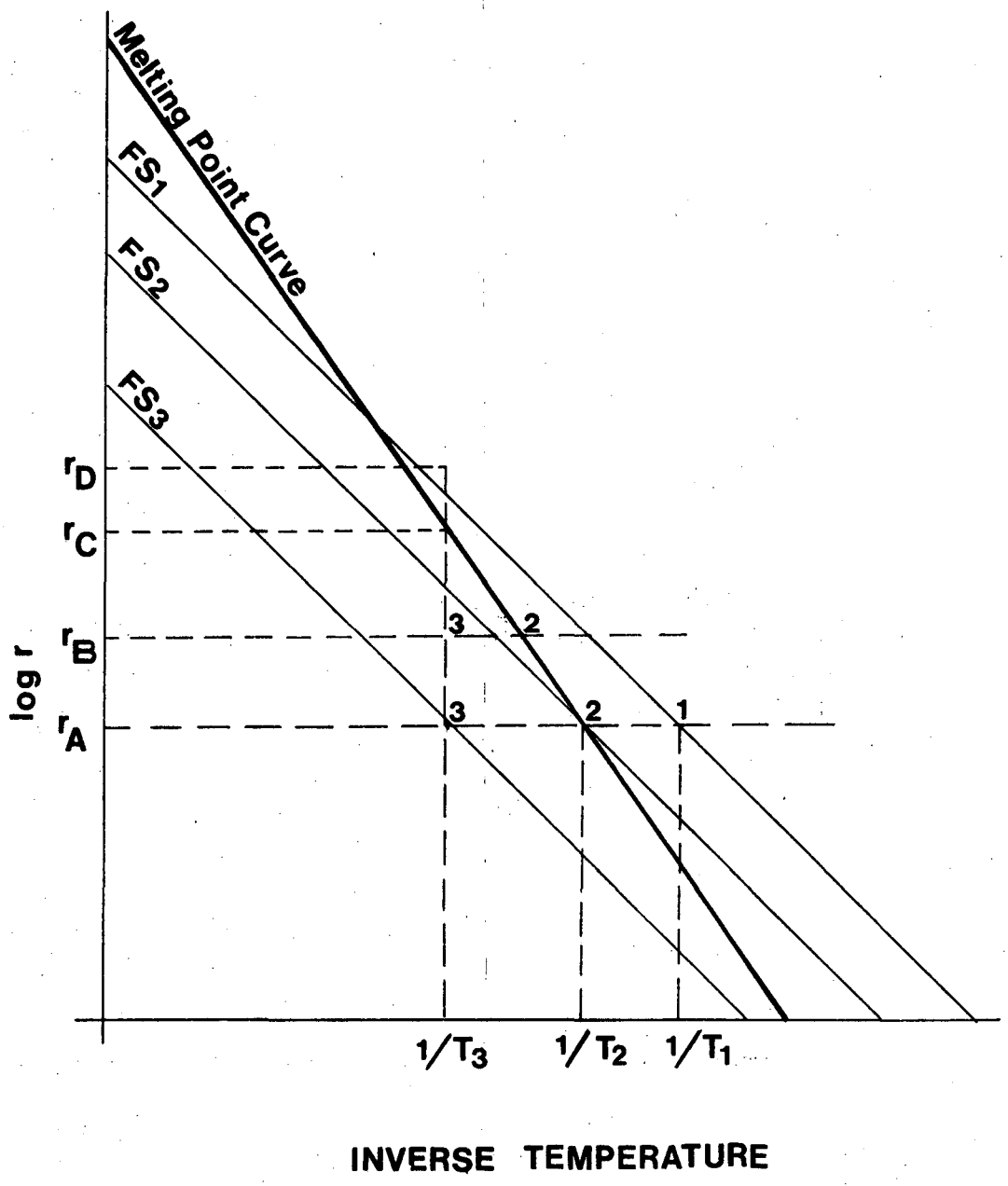
Melting Point Curve
FS1
FS2
FS3
r_D
r_C
r_B
r_A
log r
3
2
3
2
1
$1/T_3$
$1/T_2$
$1/T_1$
INVERSE TEMPERATURE

Fig. A–1